UNIVERSITY OF SILESIA

DOCTORAL THESIS

Identification and analysis of charged hadrons in p+p interactions from NA61/SHINE experiment at CERN SPS energies

mgr Szymon Puławski

Supervisor:

dr hab. Seweryn Kowalski

Katowice 2015

Contents

Introduction

The phase-transition of strongly interacting matter is a very interesting phenomena, which still is not fully understood. Significant contribution to improving knowledge about properties of the onset of deconfinement of strongly interacting matter might come from the NA61/SHINE experiment at CERN. The main goal of this fixed-target experiment is to discover the critical point and study the properties of the onset of deconfinement. This goal has been reached by the precise measurement of the hadron production in proton-proton, proton-nucleus and nucleus-nucleus interactions in a wide range of system sizes and collision energies.

The main goal of this thesis was to obtained two-dimensional spectra of positively and negatively charged pions, kaons and protons produced in $p + p$ interactions at SPS energy range (20, 30.9, 40, 80, 158 GeV/c). This studies are necessary for understanding of the onset of deconfinement. For this purpose, identification and correction techniques dedicated for analysis were developed.

This thesis consist of three main parts: description of the NA61/SHINE experiment and its physics program, introduction to identification methods, correction and error estimations techniques and discussion of the results.

At the beginning detailed introduce to the physics program as well as detector system of NA61/SHINE is described. The emphasis has been placed on the detectors used for the identification of charged particles. Detailed characterization of the experimental setup and the physics motivation are presented in Chapter 1 and 2, respectively.

The procedure of beam preparation and transportation is summarized in Chapter 3. The data preparation for the analysis is calibration and reconstruction. Description of this procedure is concluded in Chapter 4 together with the simulation chain of the experiment.

To ensure that only inelastic $p + p$ collisions are selected for the analysis, event selection criteria has been developed. Appropriate selections are described in Chapter 5.

Technique of charged hadron identification base on energy loss (dE/dx) and time of flight measurements (tof) consist of few steps and finally identification probability for each individual hadron is calculated. It is presented in Chapter 6. Obtained results are biased by the detector effects and contribution of the particles from weak decays. Therefore, appropriate corrections are calculated. Technique for determining these corrections is included in Chapter 7. In Chapter 8 statistical and systematic uncertainties are discussed.

The final results are presented in Chapter 9. Calculation of rapidity distributions as well as 4π multiplicities are also included. Moreover, particles multiplicities are compared with the NA49 experiment $p + p$ results.

Chapter 10 is devoted to study the energy and system size dependencies of particle production. Obtained results are an important step forward to study properties of the onset of deconfiment. Comparison with world data allow better understanding of $p + p$ interactions mechanism. Additionally, it is presented that even in $p + p$ collisions rapid changes of the variables assign to the phase transition are observed.

Chapter 1

NA61/SHINE experiment

The NA61/SHINE is a fixed target experiment situated in the North Area H2 beam-line of the CERN SPS [1]. The NA61/SHINE detector presented in Fig. 1.1 is a large acceptance hadron spectrometer [2].

The main components of the detection system are four large volume Time Projection Chambers (TPC). Two of them called Vertex TPCs (VTPC) are located inside superconducting magnets with maximum combined bending power of $9\ Tm$ downstream of the target. The TPCs are filled with $Ar : CO_2$ gas mixtures in proportions $90 : 10$ for the VTPCs and $95 : 5$ for the Main TPCs. MTPCs and two walls of pixel Time-of-Flight (ToF-L/R) detectors are placed symmetric to the beamline downstream of the magnets. In addition detector system consist of GAP-TPC (GTPC) between VTPCs, additional wall of strip ToF detector (ToF-F) in the middle of ToF-L/R and Projectile Spectator Detector (PSD). The detection system contains also a set of scintillation and Cherenkov counters, and as well as the beam position detectors (BPDs) placed upstream of the target. This counters provide timing reference, identification and position information of the incoming beam particles (more details are given in Chapter 2).

The NA61/SHINE experiment use primary (ions) and secondary (hadron and ions) beams with momentum from 13 to $158A\ GeV/c$ (see Chapter 3).

The particle identification capability of the TPCs based on measurements of the specific energy loss (dE/dx), is augmented by time-of-flight (tof) measurements using ToF detectors.
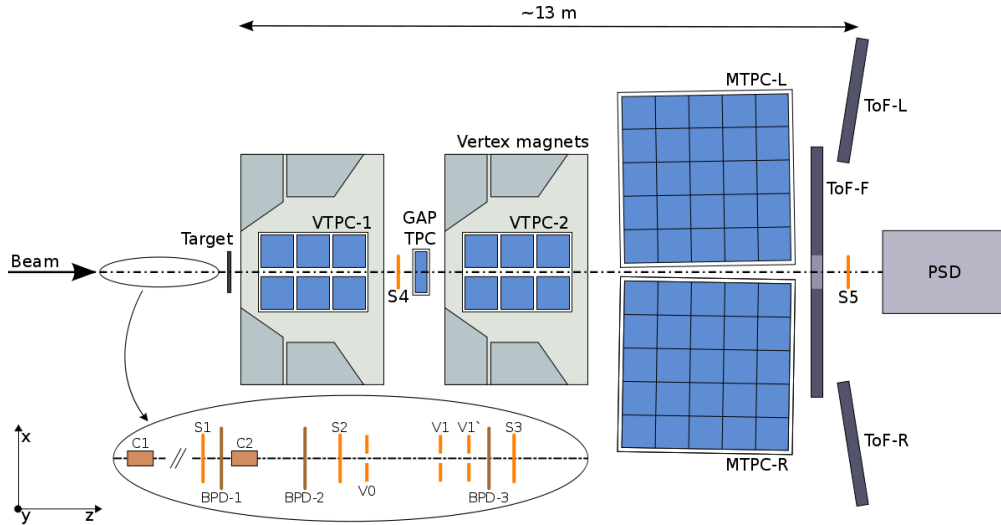
FIGURE 1.1: The NA61/SHINE experimental detection system.

Physics program of NA61/SHINE experiment comprises: heavy ion physics and measurements for neutrino (T2K [3]) and cosmic ray (Pierre Auger Observatory [4]) experiments. The main goal of strong interaction program is systematic measurement of hadron production in proton-proton, proton-nucleus and nucleus-nucleus collisions to study properties of onset of deconfinement and search for critical point of strong interacting matter.

The T2K is a neutrino oscillation experiment at JPARC, which uses neutrino beams produced indirectly by $p + C \rightarrow \pi, K + X$ reactions at proton beam momentum of 31 GeV/c and subsequent decay of pions and kaons. The neutrinos are detected in the Super-Kamiokande detector located 295 km from the production target. To predict neutrino fluxes with a required precision, initial cross section of π and K production in p+C interactions at 30.9 GeV/c were measured by NA61/SHINE experiment. For this purpose 1 cm graphite target and a 90 cm long T2K replica target were used. In future, this part of physics program will be extended by similar measurements for United States neutrino experiments [5].

Cosmic-ray experiment Pierre Auger Observatory investigates extensive air showers by large lateral coverage ground detector arrays. The particle type and energy of the incident particle is reconstructed by the simulation of the air shower. These simulations are very sensitive to $\mu^{\pm}$ production in cascades, which is related to the $p, \pi + C \rightarrow \pi, K + X$ production processes at SPS energies. The $\mu^{\pm}$ are produced by the weak decay of the π and K particles. By the precise measurement of π/K

production cross-sections, the model dependence of the air shower simulations can be largely reduced.

One of the most important issues of heavy ion collision physics is to explore the phase diagram of strongly interacting matter. It was predicted, that for large values of baryon chemical potential (μ_B) a first order phase transition between hadron matter and Quark Gluon Plasma (QGP) should be observed (Fig. 1.2). In contrast, for small μ_B values, the transition is expected to be a smooth crossover. The 1st-order phase transition line ends with a critical point of a 2nd-order phase transition.
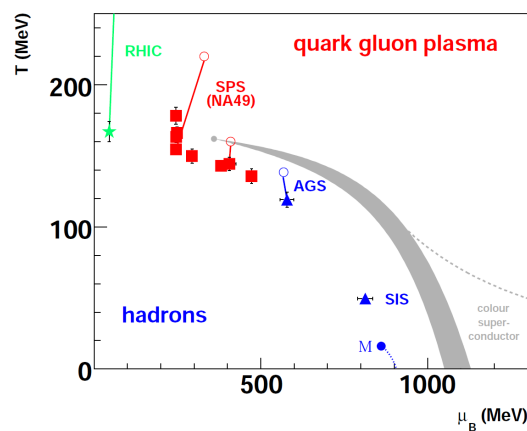
FIGURE 1.2: Quantum chromodynamics (QCD) phase diagram [6].

Main goal of NA61/SHINE experiment is to study the transition line and search for the critical point. Therefore, NA61/SHINE performs a 2-D scan (energy and system size) of the phase diagram (Fig. 1.3). The first part of the scan, i.e. collection of $p+p$ collisions was done in 2009–2011 and $Be+Be$ in 2011-2013. Measurements of $Ar + Sc$ and $Xe + La$ collisions are planned for 2015-2017. Moreover, one of the possible extension of 2-D scan is to measure $Pb + Pb$ collisions.

According to the Statistical Model of Eearly Stage (SMES) [7], when the early stage of nuclear matter is created, in the ion collisions, cross the transition line three signatures should be observed (called: kink, horn, step). SMES model assume 1st-order phase transition to QGP between top AGS and top SPS energies and predict:

- constant temperature and pressure in mixed phase (step),

- number of internal degrees of freedom increases in case of transition between Hadron Gas (HG) state and Quark Gluon Plasma (QGP) (kink),
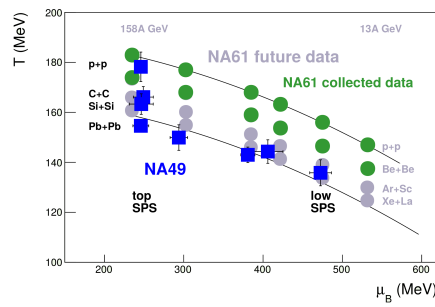
FIGURE 1.3: The NA61/SHINE experiment energy and system size scan.

- total entropy and strangeness are maintained before and after hadronization (horn).

This predictions are presented in Fig. 1.4.
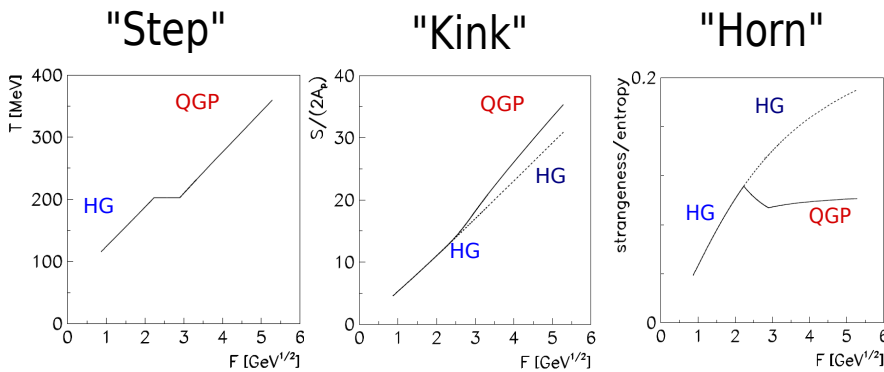
FIGURE 1.4: SMES model predictions for onset of deconfinement.

The critical point (CP) of the phase transition is predicted at energies accessible for SPS accelerator [8]. Assuming that hadronization and freeze-out take place near CP, the fluctuations in particles multiplicity and transverse momentum p_T should be enhanced [9]. Therefore, the NA61/SHINE experiment searches for a maximum of fluctuation by a 2-D scan (Fig. 1.3).

There are two very interesting phenomena in high transverse momentum (p_T) physics which are study by NA61/SHINE experiment:

- suppression of high p_T particles observed by RHIC experiments at $\sqrt{s_{NN}} = 62~GeV$ [10]. It is interesting to check whether such suppression appears already at SPS energies.

- modification of the shape of the near-side peak in the two-particle azimuthal angle correlation function with decreasing collision energy in the SPS regime, called Jet-Hole transition [11, 12].

Chapter 2

Charged particle identification - detectors

In this chapter detector used in NA61/SHINE experiment are described. Description is focused on detectors used for the identification of particle produced in $p+p$ interactions recorded in 2009. Moreover, beam counters and trigger system are presented.

2.1 Beam counters and trigger system

Beam counters provide information about properties and position of the beam upstream to the target. The properties (i.e. size, material type) of counters are selected to minimize beam interactions with them. A minimal set of plastic scintillator (BC-408) beam counters used during $p+p$ data taking in 2009 is presented in Fig. 2.1. The first detector S1 (thickness of 0.5 cm) is located upstream to the target. It is equipped with four photomultipliers (PMTs) directly coupled to the scintillator. The second beam counter S2 (0.2 cm thickness) has only one PMT. Downstream of the S2 detector, two 1 cm thick veto scintillator detectors V0 and V1 are positioned. The round V0 detector has outer diameter of 8 cm and in the center a hole of 1 cm diameter. The square ($10 \times 10 \ cm^2$) V1 detector also has a 0.8 cm diameter central hole. To remove interactions of the beam halo, one additional veto detector $V0^p$ is installed. The S4 detector (2 cm diameter, 0.5 cm thickness) is located downstream to the target. It is used to select interactions of

beam particles in the target indicated by the absence of the beam particle signal in S4 counter. The beam counter parameters are summarized in Table 2.1.
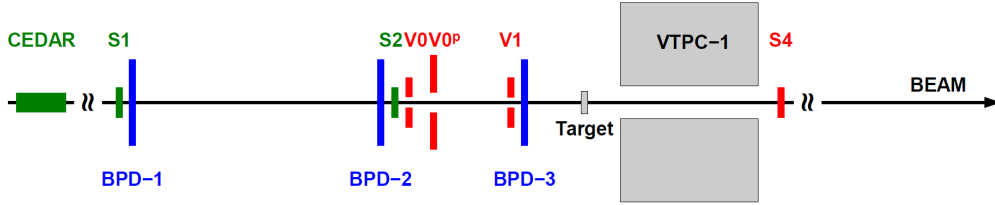
FIGURE 2.1: Schematic layout (horizontal cut in the beam plane, not to scale) of the beam detectors used in 2009 during $p + p$ data taking periods.

In the transverse plane to the beam direction (the $x - y$ plane) the detectors are centered at the maximum of the beam profile. The position of the incoming beam particles in the transverse plane is measured by a telescope of three Beam Position Detectors (BPDs) placed along the beamline upstream to the target. The NA61/SHINE BPDs are proportional chambers operated with Ar/CO_2 85/15 gas mixture with active areas of $48 \times 48 \ mm^2$. BPD measure the position of the trigger-selected beam particle in two orthogonal directions independently using two planes of orthogonal strips. On each strip plane a charge distribution is induced with a width of about 5 strips on average. To calculate vertex interaction in target beam path has to be known. The reconstruction algorithm first searches for a cluster in each plane. The cluster is defined as a set of adjacent strips with signal amplitudes above a threshold value (to remove signals from pedestal fluctuations). Then, an average of the strip positions weighted with the signal amplitudes on the strips is calculated for the cluster to estimate the position of the beam particle (centroid method). A position in 3 dimensions calculated by a given BPD is built from two transverse coordinates measured by the two strip planes and the position of the BPD along the beamline. In order to reconstruct a beam particle track, least squares fits of straight lines are performed to the positions measured by the three BPDs in $x - z$ and $y - z$ planes independently.

Detector	Dimensions [mm]	Hole [mm]	Position [m]
S1	$60 \times 60 \times 5$		-36.42
S2	$\phi = 28 \times 2$		-14.42
S4	$\phi = 20 \times 5$		-2.11
V0	$\phi = 80 \times 10$	$\phi = 10$	-14.16
$V0^p$	$300 \times 300 \times 10$	$\phi = 20$	≈ -14
V1	$100 \times 100 \times 10$	$\phi = 8$	-7.20
BPD-1	$48 \times 48 \times 32.6$		-36.20
BPD-2	$48 \times 48 \times 32.6$		-14.90
BPD-3	$48 \times 48 \times 32.6$		-6.93
Typical target position			-5.81

TABLE 2.1: Beam detector parameters: dimensions and positions along the beamline (z coordinates).

2.2 Time Projection Chamber

Time Projection Chambers (TPCs) are filled with the gas in detector active volume. Such construction allows for significant reduction of multiple scattering and photon conversion. Primary ionization generated by charged particles drift inside electric field which is typically parallel to magnetic field in the direction of the end plates of the chamber. The plates of TPC are in the most cases Multi-Wire Proportional Chambers (MWPC). The amplification of a signal in the gas of the primary ionization takes place at the anode wires. Schematic view of a TPC principle is presented in Fig. 2.2.
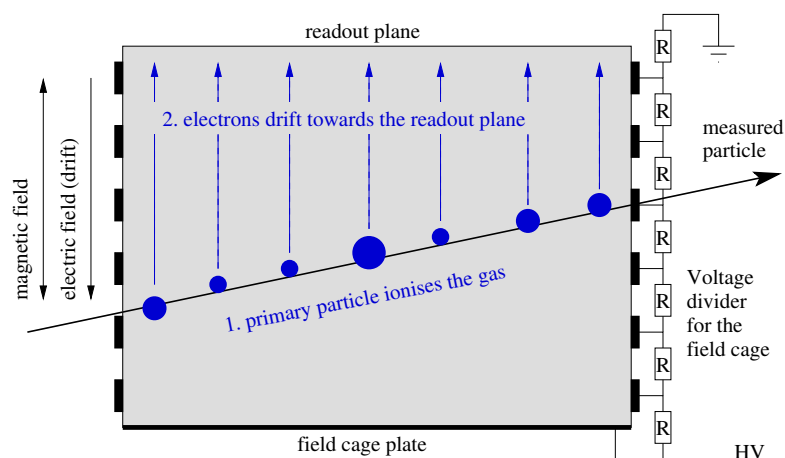
FIGURE 2.2: Schematic view of TPC principle [13].

The MWPCs are generally divided to segments structured as pads. When charged particle passes the gas volume interacts with it along the path length (ionization).

Electrons produced during thus process drift to Multi-Wire Proportional Chambers. The MWPCs readout for TPCs is typically build from gating, cathode, anode and pad planes as shown in Fig. 2.3. Gating grid plane is introduced to prevents positive ions from drifting back into the drift volume and prevent electrons from entering the amplification region. Then during the triggered event gate is open and electrons came to cathode plane. Between cathode and anode plane charge signal is amplified and finally collected.
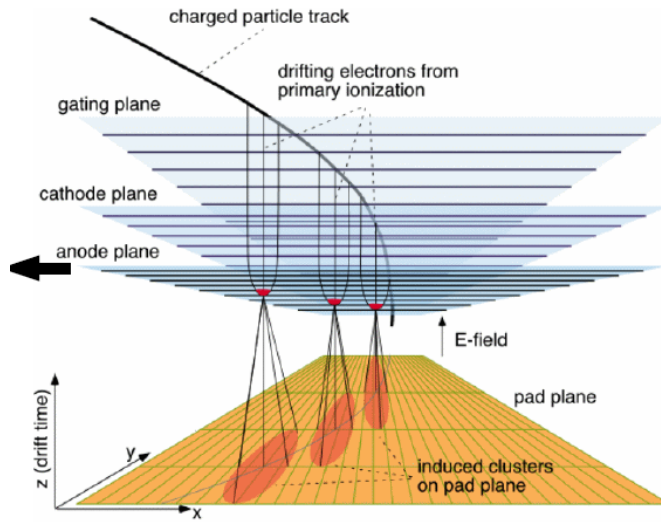
FIGURE 2.3: The MWPC readout of TPCs [14].

Such construction of TPC allows for both, particle identification and position measurement. The coordinates of an interaction point in three dimensions come from the measurement of drift time and position on clusters in the pad plane. This information allows to reconstruct particle path. Particle momentum can be calculated, by inserting the TPC in the magnetic field.

The energy loss per path length (dE/dx) of charged particle is approximately describe by the Bethe-Bloch formula [15, 16]:

$$-\frac{dE}{dx} = 4\pi N_A r_e^2 m_e c^2 z^2 \frac{Z}{A} \frac{1}{\beta^2} \left[\ln \frac{2mc^2\gamma^2\beta^2}{I} - \frac{\delta}{2} \right],$$ (2.1)

where:

$z, m :$ charge and mass of the incident particle,

$Z, A :$ atomic number and mass number of the active material,

m_e : electron mass, $m_e = 0.510998928 \pm 0.000000011 \ MeV$ [17],

r_e : classical electron radius, $r_e = e^2/4\pi\varepsilon_0 m_e c^2 = 2.8179403267(27) \times 10^{-5} \ m$ [17],

N_A : Avogadro constant, $N_A = 6.02214129(27) \times 10^{23} \ mol^{-1}$ [17],

I : mean excitation energy - characteristic of absorbed material (ionization potential),

δ : density correction describing how much the extended transverse electric field of incident relativistic particles is screened by the charged density of the atomic electrons,

β : ratio of the particle velocity to the speed of light (c).

Dependence on mass and velocity allows for particle identification based on TPC measurement. The average energy loss of electrons, muons, pions, kaons and protons in the momentum range between $10 \ keV/c$ and $100 \ GeV/c$ is shown in Fig. 2.4. It can be noticed that depending on the particle type and momentum range, the particle identification based only on the energy loss may not be sufficient for their identification. However pions, kaons and protons identification is achievable in momentum region beyond cross over of their Bethe-Bloch curves.
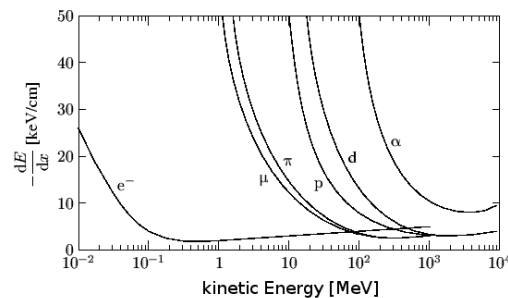
FIGURE 2.4: Average energy loss of electrons (e), muons (μ), pions (π), kaons (K) and protons (p) normalized to the minimum-ionization value [18].

Particle identification in NA61/SHINE inter alia is based on dE/dx measurement in all TPCs. An exemplary event measured by the NA61/SHINE collaboration is presented in Fig. 2.5. Each MTPC of NA61/SHINE experiment has a readout surface at the top of $3.9 \times 3.9 \ m^2$ and a length of the field cage of about $1.1 \ m$. It is filled with a gas mixture of Ar/CO_2 in the proportion 95/5. The track signals are readout by 25 proportional chambers providing up to 90 measured points along

particle trajectory. The accuracy of the measurement of the average ionization energy loss for is about 4% [2].
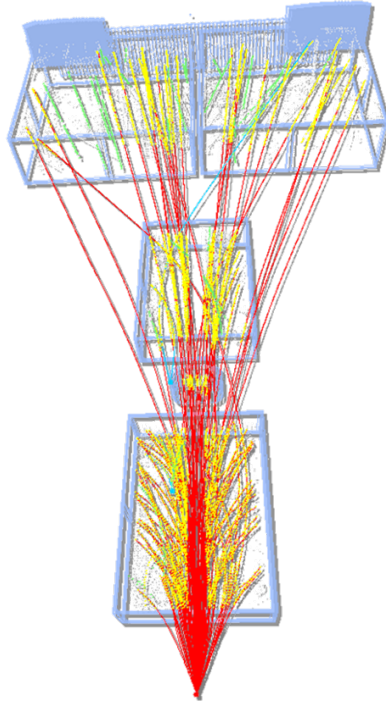
FIGURE 2.5: Example of reconstructed event measured in $Be + Be$ at $150A\ GeV/c$ interaction. Red line corresponds to tracks reconstructed in primary vertex, yellow points - measured clusters in TPCs matched to primary tracks, green points - measured clusters in TPCs without matching.

Each VTPC consists of a gas box with $2.0 \times 2.5\ m^2$ top surface area and $0.67\ m$ depth. The inserted field-cage structures exclude the region of $0.12\ m$ on either side of the beamline in which the particle density in $Pb + Pb$ reactions is so high that particles trajectories cannot be resolved. A gas mixture of Ar/CO_2 in the proportion 90/10 is applied. The readout is performed by 6 proportional chambers on the top which provide up to 72 measurements along particle trajectories [2].

Between VTPC-1 and VTPC-2, an additional tracking device, the GAP-TPC is located directly on the beamline. It covers the gap between the sensitive volumes of the VTPCs and MTPCs. High momentum particle tracks can be better extrapolated to the primary vertex using the additional points measured in the GAP-TPC. Since the beam passes this detector its material was minimized to 0.15% of a radiation length and 0.05% of an interaction length. The drift volume is enclosed in a gas box made of a single layer of $125\ mm$ Mylar. The readout

plane consists of 7 padrows with 96 pads each and pad dimensions of $28 \times 4\ mm^2$. The gas composition is Ar/CO_2 (90/10) like in the VTPCs.

The parameters of NA61/SHINE Time Projections Chambers are summarized in Table 2.2 [2].

	VTPC-1	VTPC-2	MTPC-L/R	GAP-TPC
Size ($L \times W \times H$) [cm]	$250 \times 200 \times 98$	$250 \times 200 \times 98$	$390 \times 390 \times 180$	$30 \times 81.5 \times 70$
No. of pads/TPC	26 886	27 648	63 360	672
Pad size [mm]	$3.5 \times 28(16)$	3.5×28	$3.6 \times 40, 5.5 \times 40$	4×28
Drift length [cm]	66.60	66.60	111.74	58.97
Drift velocity [cm/ms]	1.4	1.4	2.3	1.3
Drift field [V/cm]	195	195	170	173
Drift voltage [kV]	13	13	19	10.2
Gas mixture	Ar/CO_2 (90/10)	Ar/CO_2 (90/10)	Ar/CO_2 (95/5)	Ar/CO_2 (90/10)
No. of sectors	2×3	2×3	5×5	1
No. of padrows	72	72	90	7
No. of pads/padrow	192	192	192, 128	96

TABLE 2.2: Parameters of the VTPCs, MTPCs and GTPC.

2.3   Time of Flight detector

Identification of a particle is also possible by the measurement of its time of flight and path length L between "start" and "stop" signals provided by two counters or by the moment of particle production and "stop" counter. Difference of time of flight (Δt) between two particles of masses m_1 and m_2 with the same momentum p and flight distance L can be calculated as:

$$\Delta t = L \left(\frac{1}{v_1} - \frac{1}{v_2} \right) = \frac{L}{c} \left(\frac{1}{\beta_1} - \frac{1}{\beta_2} \right), \tag{2.2}$$

or, substituting $pc = \beta E$ as

$$\Delta t = \frac{L}{pc^2} (E_1 - E_2) = \frac{L}{pc^2} \left(\sqrt{p^2c^2 + m_1^2 c^4} - \sqrt{p^2 c^2 + m_2^2 c^4} \right). \tag{2.3}$$

Relativistic approximation $p^2 c^4 \gg m_{1,2}^2 c^4$ leads to:

$$\Delta t = \frac{Lc}{2p^2} \left(m_1^2 - m_2^2 \right). \tag{2.4}$$

With high time resolution counters and sufficiently long particle path length, better particle identification by the ToF detectors can be achieved.

One of the particle identification methods in NA61/SHINE experiment are based on time of flight measurements by two ToF walls: ToF-L (Left) and ToF-R (Right) placed

behind the MTPCs. Each of it contains 891 rectangular scintillation detectors with a single photomultiplier tube (PMT) glued to the short side. The scintillators have 23 *mm* thickness matched to the photocathode diameter, 34 *mm* height and horizontal width of 60, 70 or 80 *mm*, with the shortest scintillators positioned closest to the beamline and the longest on the opposite side (Fig. 2.6).
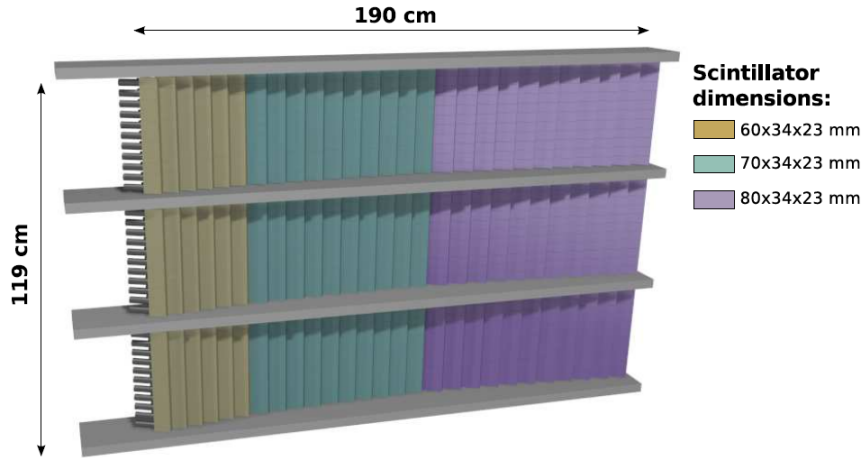
FIGURE 2.6: Schematic layout of scintillators in the ToF-R detector.

The start signal for the TDCs (Time to Digital Converters) is provided by the PMT of the S1 beam counter. If ToF signal is above a threshold, it provides a stop signal. The calibration procedure is based on the tracks extrapolation reconstructed in the MTPCs into the area of the ToF walls. Based on this extrapolation, corresponding scintillator is identified and checked if signals in TDC and ADC (Analog to Digital Converters) channels are above threshold. Afterwards detailed corrections are performed depending on charge deposition and relative position of the incident particle in each scintillator. Position corrections of the main interaction and position of the beam particle in the S1 counter are also performed.
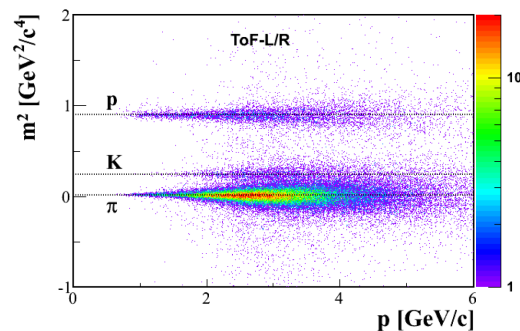
FIGURE 2.7: Mass squared (m^2) versus momentum measured by ToF-L/R.

The estimation of time resolution of the ToF-L/R system is based on the distribution of the differences between the measured time of flight for particles identified as pions and prediction from the measured momentum and trajectory assuming the pion mass. This distribution can be described by a Gaussian function. In $p + p$ and $Be + Be$ collisions, a standard deviation for ToF-L equals 95 ps, while a standard deviation for ToF-R of 80 ps was calculated. These values of the time resolution include all contributions to the tof measurement, i.e. the intrinsic ToF detector resolution, the start detector resolution, uncertainties in tracking, etc.. This resolution allows to separate pions from kaons for momenta up to 3 GeV/c (up to 6 GeV/c if tof is used together with dE/dx) and pions from protons for even higher momenta. Fig. 2.7 shows mass squared as a function of particle momentum for $p + p$ interactions at 80 GeV/c measured by NA61/SHINE detector.

Chapter 3

Beams and target

In this chapter procedure of the proton beam preparation and short introduction to the proton target used during 2009 measurements is presented.

As was already mentioned in the previous chapter, the NA61/SHINE experiment uses secondary beams of positively charged hadrons at momenta of 20, 31, 40, 80 and 158 GeV/c. This beams are produced from 400 GeV/c protons extracted from the SPS in a slow extraction mode with a flat-top of 10 seconds. The beam momentum and intensity is adjusted by proper setting of the H2 beamline magnets and collimators (see Fig. 3.1). The precision of the setting of the beam magnet currents is approximately 0.5%. It was verified by the direct measurement of the beam momentum at 31 GeV/c by bending the incoming beam particles into the TPCs with the maximum magnetic field. The selected beam properties are given in Table 3.1.

Beam detectors set-up of NA61/SHINE experiment was described in Chapter 2 and illustrated in Fig. 1.1. For measurements of $p+p$ interactions, protons from the secondary hadron beam are identified by two Cherenkov counters, a gas ring imaging CEDAR [19] and a threshold counter (THC). The CEDAR counter, based on a coincidence of six out of the eight photomultipliers placed radially along the Cherenkov ring, provides identification of protons, while the THC, operated at pressure lower than the proton threshold, is used in anti-coincidence in the trigger logic. Due to their limited range of operation two different CEDAR counters were used: for beams momenta of 20, 31 and 40 GeV/c the CEDAR-W counter, whereas for beams at 80 and 158 GeV/c the CEDAR-N counter. The threshold counter was used for all beam energies. A selection based on signals from the Cherenkov counters allowed to identify beam protons with a purity of about 99%. A consistent value for the purity was found by bending the beam into the TPCs with the full magnetic field and using the dE/dx identification method [20].
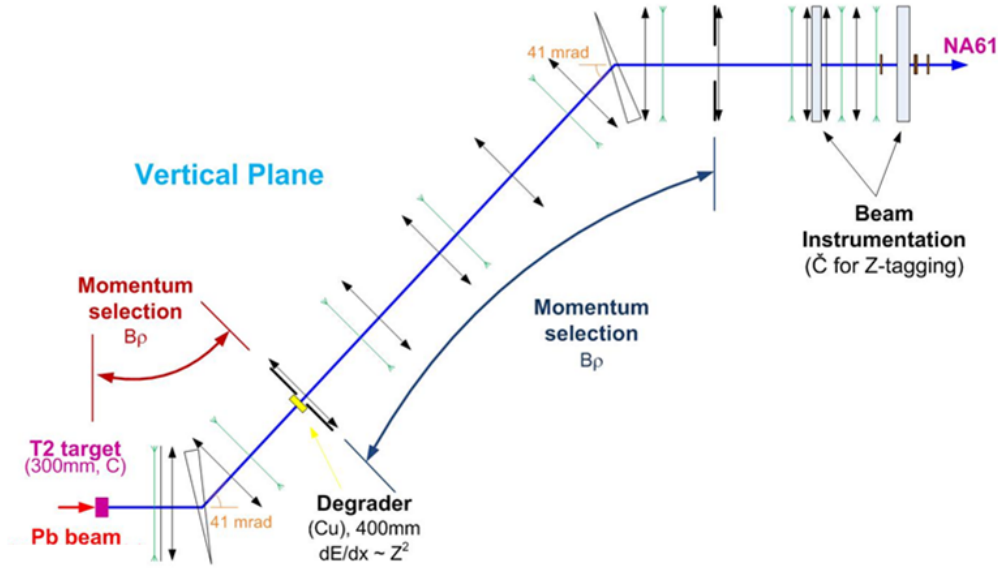
FIGURE 3.1: Schema of H2 beam line for fragmented ion beam.

p_{beam} $[GeV/c]$	$\sqrt{s}$ $[GeV]$	Particles per spill $\times 10^3$	Proton fraction	Number of recorded events
20	6.2	1000	12%	$1.3 \cdot 10^6$
31	7.7	1000	14%	$3.1 \cdot 10^6$
40	8.8	1200	14%	$5.2 \cdot 10^6$
80	12.3	460	28%	$4.3 \cdot 10^6$
158	17.3	250	58%	$3.5 \cdot 10^6$

TABLE 3.1: Basic beam properties and number of events recorded for $p + p$ interactions at incident proton momentum of 20, 31, 40, 80 and 158 GeV/c.

For data taking of $p+p$ interactions a Liquid Hydrogen Target (LHT) of 20.29 cm length (2.8% interaction length) and 3 cm diameter placed 88.4 cm upstream of VTPC-1 was used. The LHT facility filled the target cell with para-hydrogen obtained in a closed-loop liquefaction system which was operated at 75 $mbar$ overpressure with respect to the atmospheric pressure. For the atmospheric pressure of 965 $mbar$ the liquid hydrogen density ρ_{LH} is equal to 0.07 g/cm^3.

Chapter 4

Data processing and simulation

Before the identification of the particles calibration and reconstruction of the data and appropriate simulation has to be performed. These procedures are shortly presented in this chapter.

4.1   Data calibration and reconstruction

Detector parameters were optimised by a data-based calibration procedure which also took into account their time dependences. Small adjustments were determined in consecutive steps for:

1. detector geometry, drift velocities in TPCs and distortions due to the inhomogeneities of the magnetic field in the corners of the VTPC detectors,

2. magnetic field settings,

3. specific energy loss measurements,

4. time-of-flight measurements.

Each step required reconstruction of the data in order to optimize a set of calibration constants and time dependent corrections followed by verification procedures.

Data reconstruction was performed accordingly to the following steps:

1. extraction of the cluster in the TPC raw data, calculation of its center-of-gravity and total charge,

2. reconstruction of track segments sections in each TPC separately,

3. matching track segments into global TPCs tracks,

4. fitting track through the magnetic field and determination of its parameters at the first measured TPC cluster,

5. determination of the interaction vertex using the beam trajectory (x and y coordinates) fitted in the BPDs and the trajectories of tracks reconstructed in the TPCs (z coordinate),

6. refitting the particle trajectory using the interaction vertex as an additional point and determination of the particle momentum at the interaction vertex,

7. matching of ToF hits with the TPC tracks.

4.2 Monte-Carlo Simulation

A simulation of the NA61/SHINE detector response is used to correct the reconstructed data. Several Monte-Carlo (MC) models predictions were compared with the NA61/SHINE experimental results on $p + p$, $p + C$ and $\pi + C$ interactions: FLUKA 2008 [21, 22], URQMD 1.3.1 [23, 24], VENUS 4.12 [25], EPOS 1.99 [26], GHEISHA 2002 [27], QGSJetII-3 [28] and Sibyll 2.1 [29–31]. Based on these comparisons and taking into account continuous support and documentation from the developers the EPOS model was selected.

The simulation consists of the following steps (for more details see Ref. [32]):

1. generation of inelastic interactions,

2. propagation of outgoing particles through the detector material using the GEANT 3.21 package [33], taking into account the magnetic field and relevant physics processes, such as particle interactions and decays,

3. simulation of the detector response using dedicated NA61/SHINE packages which introduce distortions corresponding to all corrections applied to the physical data,

4. storage of the simulated events in a file which has the same format as the raw data,

5. reconstruction of the simulated events with the reconstruction chain used for the reconstruction of experimental data,

6. matching of the reconstructed tracks to the simulated ones based on the cluster positions.

Only inelastic $p + p$ interactions in the hydrogen in the target cell were simulated and reconstructed. Therefore, the corrections based on Monte Carlo can be applied only for inelastic events. The contribution of elastic events is eliminated by the event selection cuts, whereas the contribution of off-target interactions is subtracted using procedure described in Chapter 7.

Chapter 5

Event and track selection

The selection of inelastic $p + p$ interactions from collected data and correctly reconstructed tracks are described in this chapter.

5.1 Event selection

Inelastic $p + p$ events are selected using the following criteria applied to the events recorded with interaction trigger:

- no off-time beam particle detected within the time window of $\pm\ 2\ ms$,

- the beam particle trajectory is measured in at least three planes of BPD-1 and BPD-2 and in both planes of BPD-3,

- at least one track reconstructed in the TPCs and fitted to the interaction vertex is required,

- the vertex z position (fitted using the interaction vertex from beam and TPC tracks) is not farther away than 20 cm from the center of the LHT,

- events with a single, positively charged track with absolute momentum close to the beam momentum are removed.

The online trigger was setup during data taking to register at the same time four sets of data:

T1: $S1 \times S2 \times \bar{V}0 \times \bar{V}1 \times Ce\bar{d}ar$ - proton beam trigger with prescale factor 1000,

T2: $S1 \times S2 \times \bar{V}0 \times \bar{V}1 \times Ce\bar{d}ar \times \bar{S}4$ - proton interaction trigger with prescale factor 1,

T3: $S1 \times S2 \times \bar{V}0 \times \bar{V}1$ - hadron beam trigger with prescale factor 4000,

T4: $S1 \times S2 \times \bar{V}0 \times \bar{V}1 \times \bar{S}4$ - hadron interaction trigger with prescale factor 40,

where for example S1 is the requirement of the signal from S1 counter and $\bar{V}0$ corresponds to the absents of signal from $V0$ detector.

First step of the offline analysis is cut out events with second (off-time) beam particle during acquisition time, for this purpose one of photomultiplier (S1 PMT) is connected to Wave Form Analyzer (WFA) which register signals coming close in the time. This measurement allows to select only interactions with no off-time beam particle. Proton beam have small probability to observed second beam particle in time of $\pm$ 2 ms around the trigger particle. Time distribution measured between trigger particle and next particles is presented in Fig. 5.1.
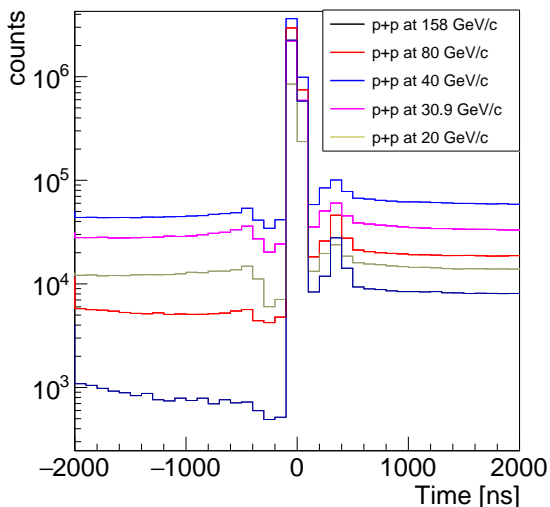
FIGURE 5.1: Time between trigger particle and other beam particles measured by Wave Form Analyzer (WFA) before the cut.

Therefore for each event, information from the Beam Particle Detectors has to be verified. The minimum requirement was to measured a signal in BPD3 and atleast three planes of other BPDs. This is needed to establish the beam particle path and position of the interaction vertex in the target.

The next selection criteria refers to the reconstructed data. It is checked whether the tracks (at least one) in an event points to the main vertex. Thus the vertex fit position can be checked. Since, the length of the Liquid Hydrogen Target is of 20 cm length along the beam direction, fitted vertex need to be in a range $\pm$ 20 cm from its center. The distribution of fitted vertex z position measured in $p+p$ interactions by NA61/SHINE experiment is shown in Fig. 5.2.

In addition to remove events with a single proton from elastic interactions, all measured events with only one positive reconstructed track with momentum close to the beam
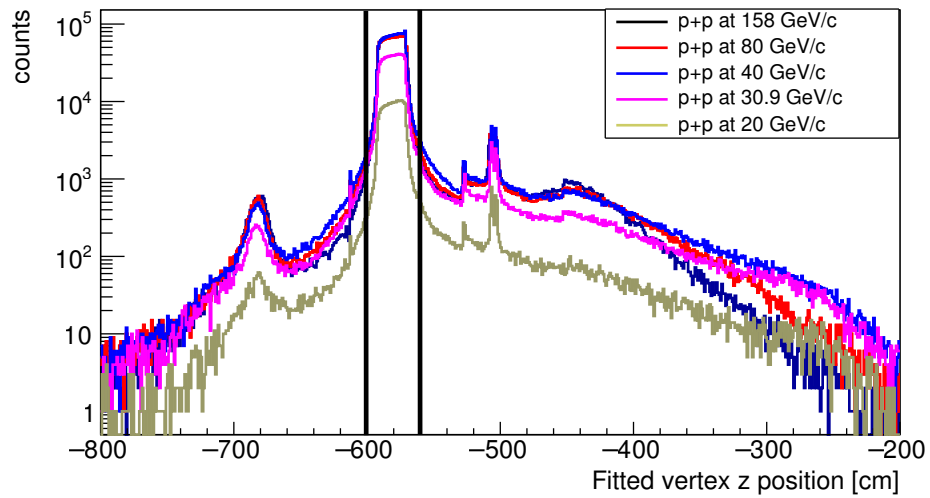
FIGURE 5.2: Fitted vertex z position measured in $p + p$ interactions at 20, 30.9, 40, 80 and 158 GeV/c. Target interaction are in range from -600 cm to -560 cm in NA61/SHINE coordinate system.

momentum are cut out. Distribution of reconstructed track momentum is presented in Fig. 5.3.
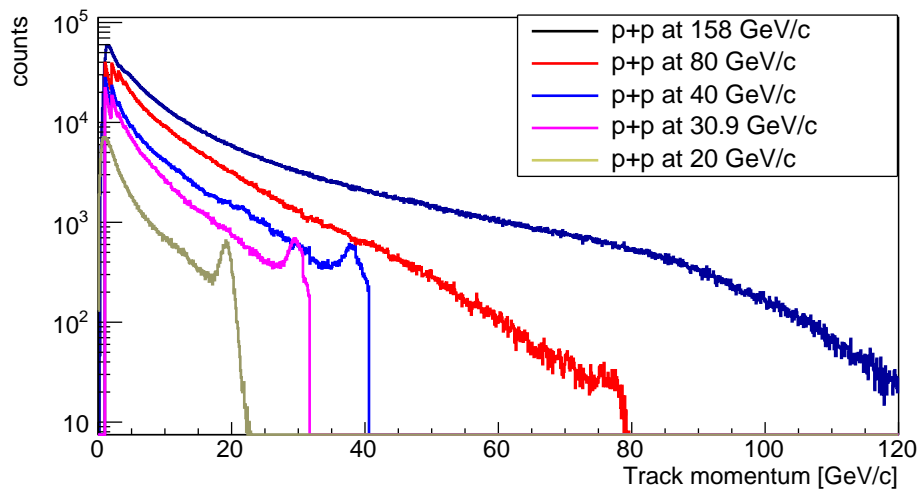
FIGURE 5.3: Distribution of reconstructed track momentum in $p + p$ interactions. Peaks around beam momentum are from protons interacting elastically.

Statistic of events after each cut is shown in Fig. 5.4.
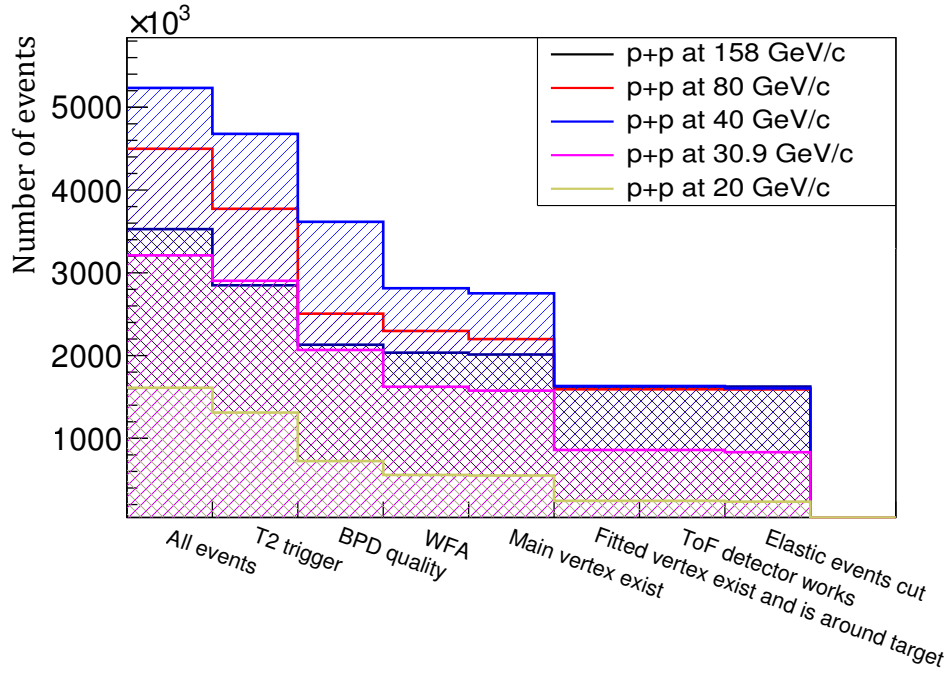
FIGURE 5.4: Events statistic reduction due to the selection criteria.

5.2 Track selection

In order to select tracks of primary charged hadrons and to reduce the contamination of tracks from secondary interactions, weak decays and off-time interactions, the following track selection criteria were applied:

- track momentum fit at the interaction vertex should converged,

- fitted track momentum component ($p_x \times charge$) is positive. This selection minimises the angle between the track trajectory and the TPC pad direction for the chosen magnetic field direction. This reduces statistical and systematic uncertainties of the cluster position, energy deposition and track parameters,

- total number of reconstructed points on the track should be greater than 30 (Fig. 5.5),

- sum of the number of reconstructed points in VTPC-1 and VTPC-2 should be greater than 15 or the number of reconstructed points in the GAP-TPC should be greater than 4,

- the distance between the track extrapolated to the interaction plane and the interaction point (impact parameter) should be smaller than 4 *cm* in the horizontal (bending) plane and 2 *cm* in the vertical (drift) plane (Fig. 5.6),
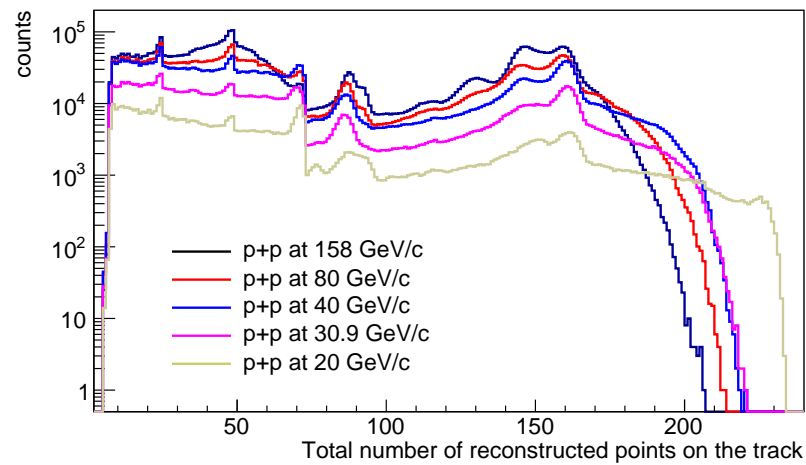
FIGURE 5.5: Total number of reconstructed points on the track.
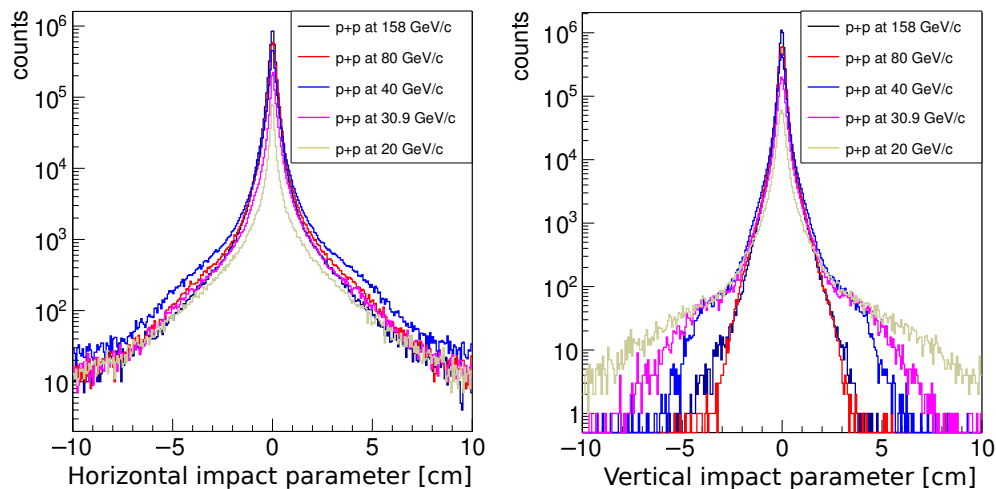
FIGURE 5.6: Distance between the track extrapolated to the interaction plane and the interaction point (impact parameter) in the horizontal (left panel) and vertical (right panel) planes.

- the total number of reconstructed dE/dx points on the track should be greater than 30,

- in case of $tof - dE/dx$ identification, three additional selection criteria were used:

  - the hit in the ToF pixel should be matched only with one TPC track,

  - the Charge Digital Converters (QDC) and Time to Digital Converters (TDC) measurements of the hit are required,

  - last point in MTPC should to be in 2 last padrows, to ensure good matching between TPC and ToF walls.

The number of measured tracks after application of selection criteria is presented in Fig. 5.7. The largest reduction result after applying the first cut, which is caused by neutral V^0 tracks fitted to main vertex. Final number of events and tracks used in both identifications are summarized in Table. 5.1.

Target inserted			
Energy [GeV/c]	Number of events	Number of dE/dx tracks	Number of $tof - dE/dx$ tracks
158	1625578	4464269	158520
80	1591076	1592538	214316
40	1604483	1625595	199775
30.9	832608	859573	44228
20	234758	244813	17023
Target removed			
Energy [GeV/c]	Number of events	Number of dE/dx tracks	Number of $tof - dE/dx$ tracks
158	26837	41234	3373
80	51588	38132	8003
40	42115	39893	4745
30.9	12618	10080	691
20	3184	2175	402

TABLE 5.1: Statistic of inelastic events and tracks used in dE/dx and $tof - dE/dx$ identification methods for target inserted and removed. Events with removed target were used for corrections of interactions outside the target - for more details see Chapter 7.
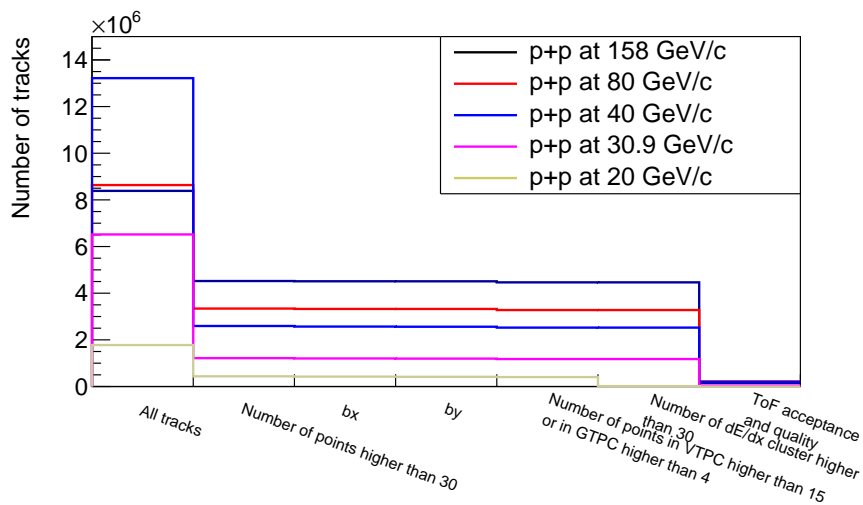
FIGURE 5.7: Number of tracks after implementation of selection criteria.

Chapter 6

Identification methods

In this chapter two identification methods used in the NA61/SHINE experiment based on the energy loss measurement (dE/dx) and combined time of flight and energy loss information ($tof - dE/dx$) are described. New developed method based on the identification probabilities used for calculation of the particle yields is also presented.

6.1 Identification based on energy loss measurement (dE/dx)

As described in Chapter 2, time projection chambers allow to measure particles energy loss along their path. On this basis different particles type can be identified. As an example, the energy loss measurement for $p + p$ interactions at 80 GeV/c, for positively and negatively charged particles, as a function of their momenta is presented in Fig. 6.1.

The identities of being e^+, e^-, π^+, π^-, K^+, K^-, p and $\bar{p}$ are defined by fitting the binned inclusive dE/dx spectra with the multiple-Gaussian function in the relativistic rise region. In order to keep a sufficient statistics of particles in high momentum bins 19 logarithmic bins in total momentum (p_{tot}) in the momentum range $1 - 100$ GeV/c are chosen. The ratio of produced particle types varies for the different charges and transverse momenta. Thus, there are 2 bins in charge (q), and 19 equal bins in transverse momentum (p_T) in the range $0 - 2$ GeV/c.

The inclusive dE/dx fit considers five particle types ($i = d$, p, K, π, e). The signal's shape for a given particles type is assumed as the sum of asymmetric Gaussians with the widths $\sigma_{i,l}$ depending on the particle type i and track length l, defined as number of
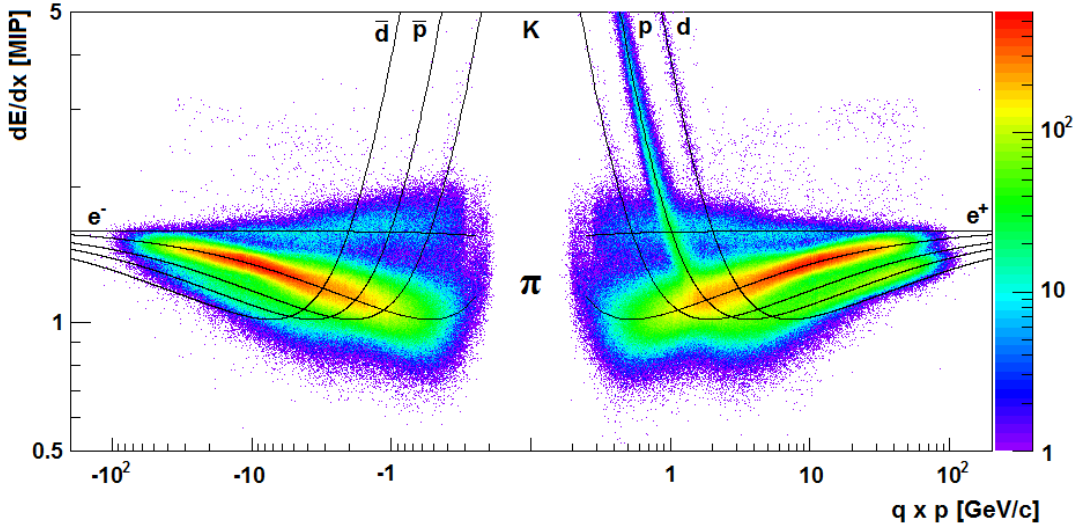
FIGURE 6.1: The energy loss in the TPCs for different charged particles as a function of momentum p measured for $p + p$ interactions at 80 GeV/c. Theoretical curves are also plotted.

points measured in TPC. Simplifying the notation in the fit formulas, peak position of dE/dx distribution for a particle types i is denoted as x_i. Hence, the width of a single Gaussian distribution is equal to:

$$\sigma_{i,l} = \sigma_0 \left(\frac{x_i}{x_\pi} \right)^{0.625} / \sqrt{l}. \tag{6.1}$$

The width parameter σ_0 is assumed to be common for all particle types and bins. The $1/\sqrt{l}$ dependence on path-length is assumed. The Gaussian peaks are allowed to be asymmetric to reflect the tail of the Landau distribution which still may be present after truncation. The fitted function for a given dE/dx track x reads

$$\rho(x) = \sum_i \rho_i(x) = \sum_{i=d,p,K,\pi,e} A_i \frac{1}{\sum_l n_l} \sum_l \frac{n_l}{\sqrt{2\pi}\sigma_{i,l}} exp \left[-0.5 \left(\frac{x - x_i}{(1 \pm \delta)\sigma_{i,l}} \right)^2 \right], \tag{6.2}$$

where n_l is the number of tracks with length (l) and A_i is the amplitude of each peak. The second sum is the weighted average of the line-shape from the different track-lengths in the sample.

The main goal of the fitting-procedure is application of Eq. 6.2 to the dE/dx distribution for each of the selected bin. The fitting function has 12 parameters (5 amplitudes, 5 positions, width and asymmetry) and therefore it is very difficult to fit all these parameters in each bin independently. However:
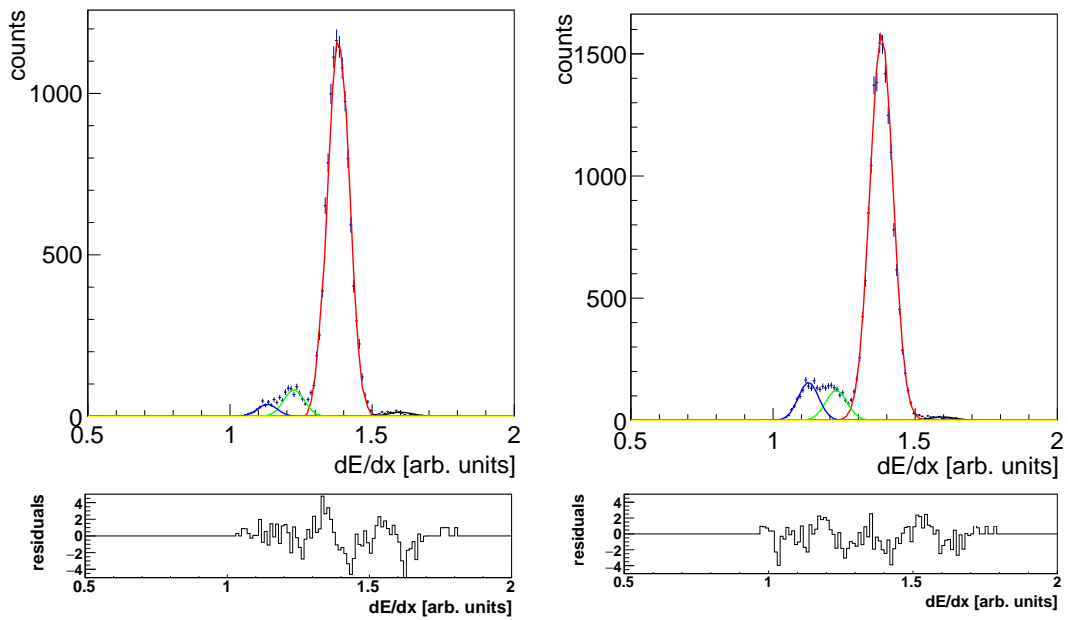
FIGURE 6.2: Typical dE/dx fit obtained in a single phase-space bin $12.6 < p_{tot} \leq 15.8\ GeV/c$ and $0.2 < p_T \leq 0.3\ GeV/c$ (top panel) and residuals (bottom panel) for negatively (left panel) and positively (right panel) charged particles in $p + p$ interactions at $158\ GeV/c$.

- relative positions of electrons, kaons and protons to pion are assumed to be p_T-independent,

- remove deuterons from the fit (not visible in $p + p$ interaction),

- in the analysed data, the asymmetry parameter δ is smaller than 0.001 and thus fixed to 0,

- the fitted amplitudes are required to be greater than or equal to 0,

- the electron amplitude is set to 0 for the total momentum, $p_{tot} > 23.4\ GeV/c$ (i.e. starting from the 13th bin), as the electron contribution vanishes at high p_{tot},

- if possible, the relative position of kaon peak is determined from the negatively charged bin for a given p_{tot} and p_T, then fixed for a positively charged kaons. This procedure is a consequence of the large overlap between kaons and protons in the dE/dx distributions.

These approximations reduce the number of independently fitted parameters in each bin from 12 to 5: the amplitudes of four particle types and a pion peak position.

An exemplary fits and its parameters (x_i, σ) for $p + p$ interactions at $158\ GeV/c$ are presented in Figs. 6.2, 6.3 and 6.4.
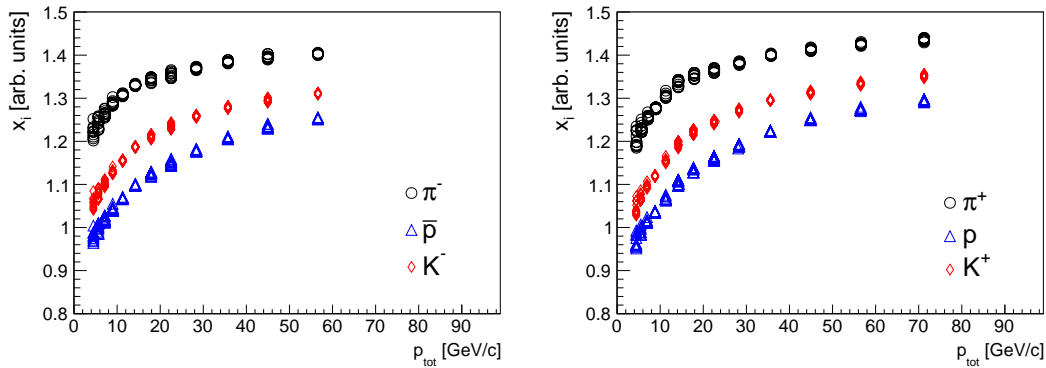
FIGURE 6.3: Fitted peak positions in $p + p$ interactions at 158 GeV/c for different particles as a function of p_{tot}. Different points for the one value of p_{tot} corresponds to the different transverse momentum bins.
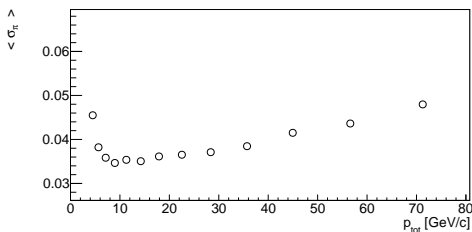
FIGURE 6.4: The fitted width to the pion dE/dx distribution, σ_π (Eq. 6.1) in $p + p$ interactions at 158 GeV/c as a function of the total momentum.

In order to ensure a good fit quality, only bins with the number of tracks grater than 300 are selected. Fitting procedure works until the p_{tot} and p_T with a low statistics has been reached or the fit cannot coverage. The Bethe-Bloch curves for different particle types cross each other at a low values of the total momentum. Thus, the separation is not sufficient for particle identification at low p_{tot} and therefore bins up to 5th ($p_{tot} < 3.98$ GeV/c) are excluded from the analysis. The worst separation occurs between kaon and proton peaks.

6.2 Identification based on time of flight and energy loss measurements ($tof - dE/dx$)

Identification of π^+, π^-, K^+, K^-, p at low momenta (from $2 - 10$ GeV/c) is possible when dE/dx information is combined together with the time of flight (tof) measurement. Based on tof information for each track m^2 variable is calculated. Example of m^2 versus dE/dx distribution in $p + p$ interactions at 40 GeV/c measured by the NA61/SHINE experiment is presented in Fig. 6.5. This combined method gives excellent identification of π^+, π^-, K^+, K^- and p.
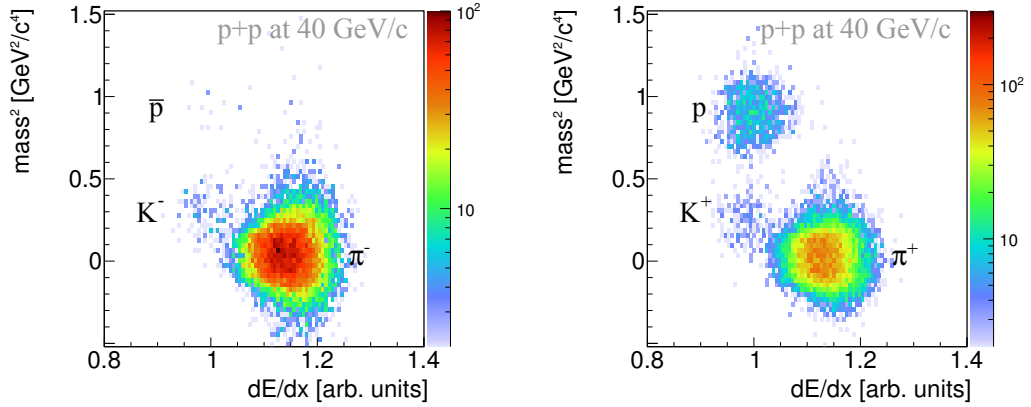
FIGURE 6.5: Distributions of m^2 versus dE/dx for particles with momenta close to 4 GeV/c measured in $p + p$ interactions at 40 GeV/c.

This identification method is very similar to the dE/dx technique. Analysis is perform in 10 equal linear momentum bins from $1 - 10\ GeV/c$ and 19 equal bins in transverse momentum (p_T) range $0 - 2\ GeV/c$.

The inclusive $tof - dE/dx$ fit considers four particle types (p, K, π, e). Fitting function in case of $tof - dE/dx$ is assumed to be the sum of two weighted two dimensional Gaussians with three standard deviations. For the simplicity of notation like in Chapter 6.1 in the fit formulas, dE/dx is denoted as x and m^2 for a given track is denoted as y. The fitted function reads

$$
\begin{aligned}
\rho(x, y) &= \sum_i \rho_i(x, y) \\
&= \sum_{i=\pi,K,p,e} A_i \left(f e^{-\left(\frac{(x-x_i)^2}{2\sigma_x^2} + \frac{(y-y_i)^2}{2\sigma_y^2} \right)} + (1-f)\, e^{-\left(\frac{(x-x_i)^2}{2\sigma_x^2} + \frac{(y-y_i)^2}{2\sigma_{2y}^2} \right)} \right),
\end{aligned}
\tag{6.3}
$$

where f is a weighting factor, A_i is the amplitude of each peak and σ_{2y} is the standard deviation of the function used to described tail of the mass distribution.

To reduce the number of independent fitted parameters from 15 to 5, three additional assumptions to those applied in case of dE/dx identification were used:

- mass of the particles is well measured so m^2 can be fixed,

- σ_{2y} is used to described only tails of m^2 measurements, so its value should be bigger than σ_y,

- amplitude of the second Gauss (tail one) need to be smaller than 30% of the first one.

Example of the $tof-dE/dx$ fit obtained in a single phase-space bin for positively charged particles in $p+p$ interactions at 158 GeV/c is shown in Fig. 6.6.
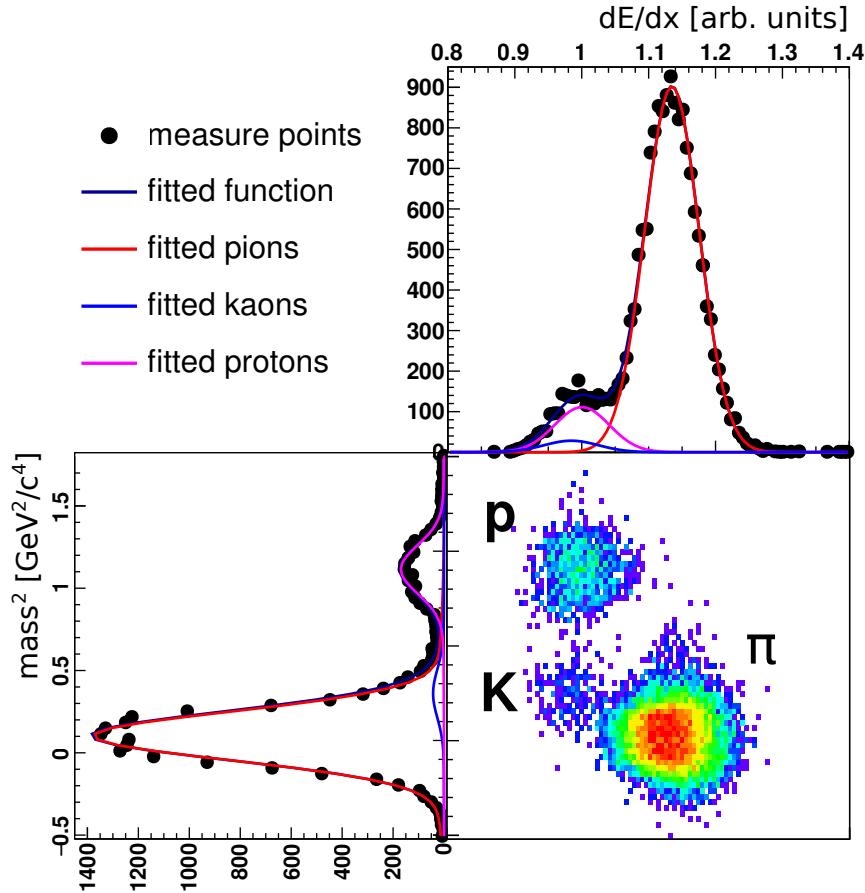
FIGURE 6.6: Example of the $tof - dE/dx$ fit (Eq. 6.3) obtained in a single phase-space bin ($3 < p_{tot} < 4$ GeV/c and $0.2 < p_T < 0.3 GeV/c$ for positively charged particles in $p+p$ interactions at 158 GeV/c.

The inclusive $tof-dE/dx$ fit allow to cover acceptance region close to the mid-rapidity of kaons not accessible for the dE/dx analysis and enlarge acceptance of pions and protons.

6.3 Probability method

Identification method based on energy loss measurement (dE/dx) and combination of time of flight and energy loss measurements ($tof-dE/dx$) described above are performed in momentum vs transverse momentum bins thanks to energy loss dependence from

particle momenta. Due to the fact that transformation between momentum and rapidity bins is ambiguous, therefore the identification based on probabilities was developed.

Proposed method of calculating particle yields requires to estimate probability of being proton, pion, kaon or electron for each track. This probability for dE/dx measurement can be described by the following formula:

$$P_i(p_{tot}, p_T, dE/dx) = \frac{\rho_i(p_{tot}, p_T, dE/dx)}{\sum\limits_{i=\pi,K,p,e} \rho_i(p_{tot}, p_T, dE/dx)}, \quad (6.4)$$

where P_i is a probability for a given track to be identified as i particle type ($i = \pi, K, p, e$), ρ_i is a value of fitted function (Eq. 6.2) in particular p_{tot} and p_T bin for the corresponding value of energy loss (dE/dx) of each particle.
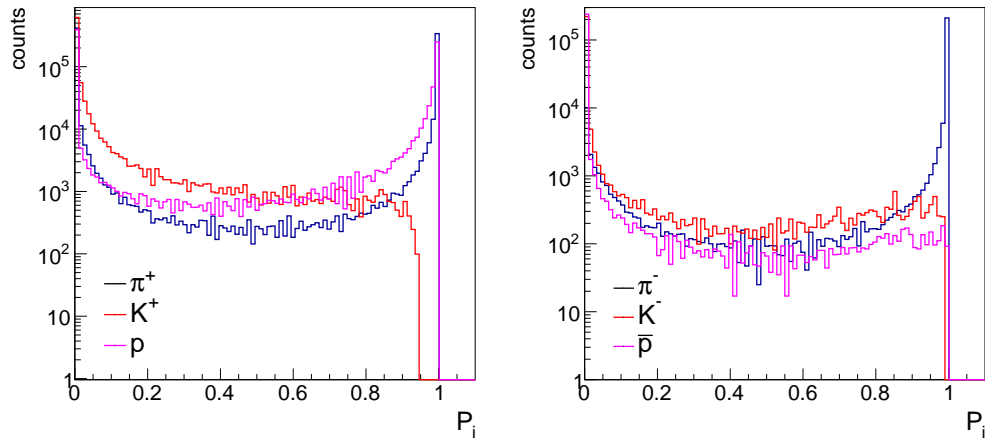
FIGURE 6.7: Probability of track identification as pion, kaon, proton for positively (left panel) and negatively (right panel) charged tracks from dE/dx measured in $p + p$ interactions at 40 GeV/c.

The same technique was used for the $tof - dE/dx$ identification based on the fitted function (Eq. 6.3). In this case the probability of a track being a particular particle type is calculated from:

$$P_i(p_{tot}, p_T, m^2, dE/dx) = \frac{\rho_i(p_{tot}, p_T, m^2, dE/dx)}{\sum\limits_{i=\pi,K,p,e} \rho_i(p_{tot}, p_T, m^2, dEd/x)}. \quad (6.5)$$

A probability distributions for dE/dx and $tof - dE/dx$ methods are very similar. The only difference is the additional variable (m^2) for each track in the $tof - dE/dx$ identification method.

Results of the probability method for positively and negatively charged particles are presented in Fig. 6.7 for dE/dx identification measured in $p+p$ interactions at 40 GeV/c and in Fig. 6.8 in $p+p$ collisions at 158 GeV/c for $tof - dE/dx$ technique.
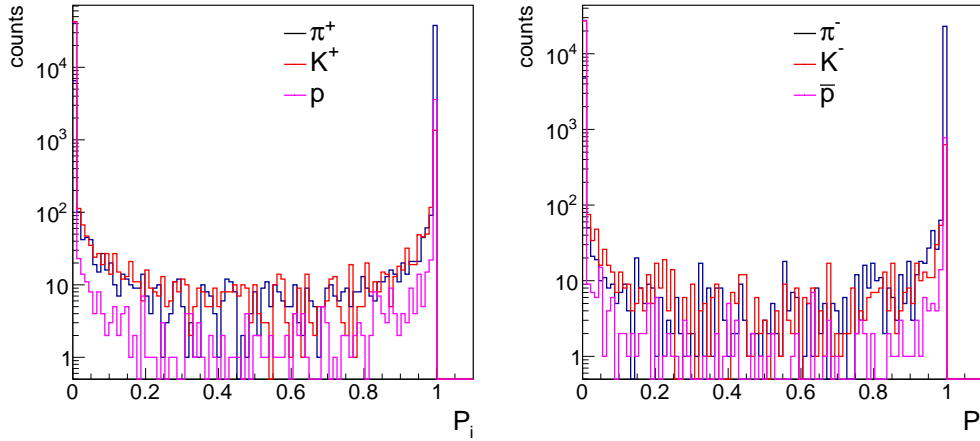
FIGURE 6.8: Probability of track identification as pion, kaon, proton for positively (left panel) and negatively (right panel) charged tracks from $tof - dE/dx$ measured in $p+p$ interactions at 158 GeV/c.

This method allows to describe yield of particular particles (π^+, π^-, K^+, K^-, p, $\bar{p}$) in the different ranges of rapidity and transverse momentum as the sum of the probabilities described by Eqs. 6.4 and 6.5 [34]:

$$n_{i=\pi,K,p} = \sum_{j=1}^{j=n'} P_i, \tag{6.6}$$

where n is number of particles type i, whereas n' represents number of tracks.

Described method not only allows for transformation from momentum to rapidity, but also for the conversion to any variable connected with the measured track. Results of such transformation (not corrected) for yields of positively and negatively charged pions, kaons and protons measured in $p+p$ interaction at 158 GeV/c is shown in Fig. 6.9.
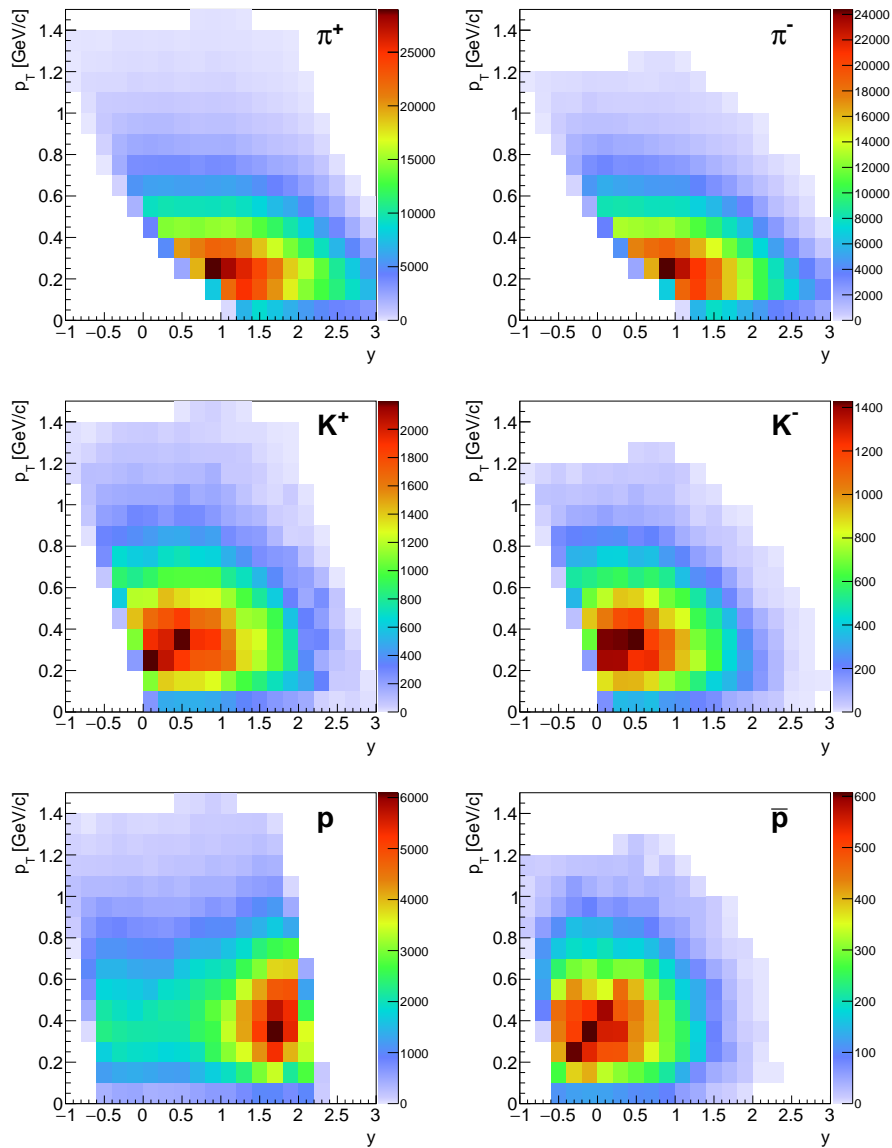
FIGURE 6.9: Yields of positively and negatively charged pions (top panel), kaons (middle panel) and protons (bottom panel) measured in $p + p$ interaction at 158 GeV/c (not corrected).

Chapter 7

Corrections

Results obtained from the identification methods described in Chapter 6 are biased by out of the target interactions, detector effects (acceptance, inefficiency etc.) and particles originating from weak decays. Thus, it is necessary to develop technique that will allow to estimate these effects and next, correct for them. In this chapter, corrections to several effects based on collected data and Monte-Carlo (MC) models will be presented.

7.1   Correction for out of target interactions

Out of target interactions are collected during the whole period of data taking. To estimate this effect dedicated runs with removed target were performed. Statistic of such runs is around 10% of collected data with inserted target.

This correction is implemented on the level of fits described in Chapter 6. Corrections concerning out of target interactions are performed for each bin of total momentum and transverse momentum variables. Then fitting procedure is applied and probabilities are calculated. In this case the same probability can be used for target in/out data.

Normalization of target removed data are based on the fitted vertex z distribution. The yield of the fitted vertex outside the target is calculated (in range from -400 cm to -200 cm) for target inserted and removed and used as a normalization ratio between them.

For $p + p$ interactions at 158 GeV/c, normalized vertex z distribution for target inserted and removed is shown in Fig. 7.1. This method allows to subtract proton interactions with windows of target aquarium ($z = -600$ cm and $z = -580$ cm), VTPC1 ($z =$
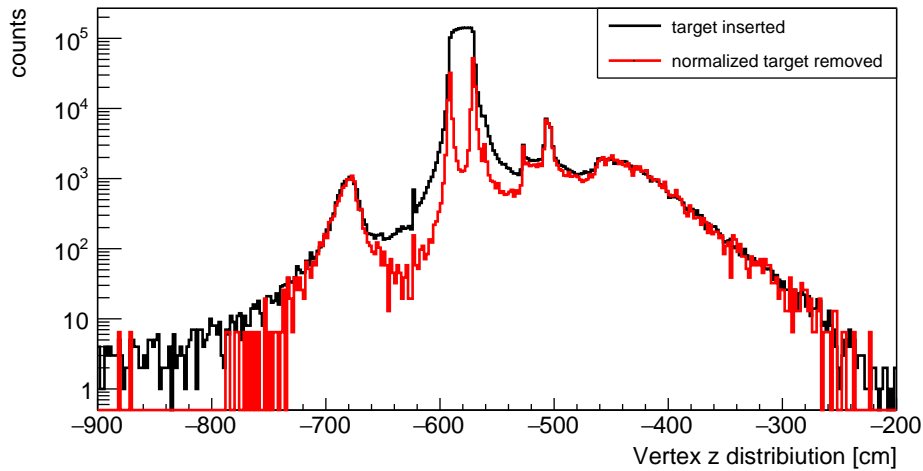
FIGURE 7.1: Fitted vertex z distribution for target inserted and normalized target removed.

Beam momentum $[GeV/c]$	Normalization factor
20	5.65
30.9	4.27
40	3.77
80	3.57
158	6.46

TABLE 7.1: Normalization factor for removed target for measured $p + p$ interactions at SPS energies range.

$-500\ cm$) and interactions with air inside VTPC hat (z in range from $-460\ cm$ to $-300\ cm$). The subtracted data consist only interactions with LHT.

Normalization factors for target removed for $p + p$ interactions at 20, 30.9, 40, 80 and 158 GeV/c are given in Table 7.1.

7.2   Corrections for detector effects and particles from weak decays

Corrections for detector effects and particles originating from weak decays are based on the Monte-Carlo model and data measurement. The NA61/SHINE simulation chain described in Chapter 4 takes into account time projection chambers parameters obtained from data. The time of flight parameters are obtained for each energy and then propagated to simulation chain. In this chapter, description of procedure used to estimate

and correct raw data for identification methods (dE/dx and $tof - dE/dx$) characterized in Chapter 6, is presented.

7.2.1   Correction method for energy loss (dE/dx)

A direct result of dE/dx analysis method is improved by single Monte-Carlo correction. For this purpose EPOS model [26] was selected. Correction factor C is defined as:

$$C = \frac{n_{gen}^{MC}}{N_{gen}^{MC}} \Big/ \frac{n_{rec}^{MC}}{N_{rec}^{MC}},\tag{7.1}$$

where:

- n_{gen}^{MC} - number of negatively or positively charged pions, kaons or protons generated by EPOS model,

- n_{rec}^{MC} - number of the same particle type after applying selection criteria described in Chapter 5,

- N_{gen}^{MC} - number of generated inelastic events in MC sample,

- N_{rec}^{MC} - number of events after applying selection criteria (the exception are WFA and BPD cuts which are not simulated).

The correction factor C includes both, the detector effects and particles originating from weak decays. It is calculated in same bins of y and p_T as particle spectra. Example of generated Monte-Carlo particles spectra, spectra after selection criteria and correction factors for $p + p$ interactions at 30.9 GeV/c are presented in Fig. 7.2. Correction factor range is from 0 to 2. Bins with correction factor lower than 0.5 and higher than 1.5 are rejected from final results due to low acceptance or high contamination of particles from weak decays. Statistical error of the correction factor is calculated from binomial distribution.

7.2.2   Correction method for $tof - dE/dx$

Correction of $tof - dE/dx$ results are more complicated than one for dE/dx. It is due to the lack of ToF detector geometry in the simulation and detector response simulator. Corrections are calculated in small bins of momentum and transverse momentum. To
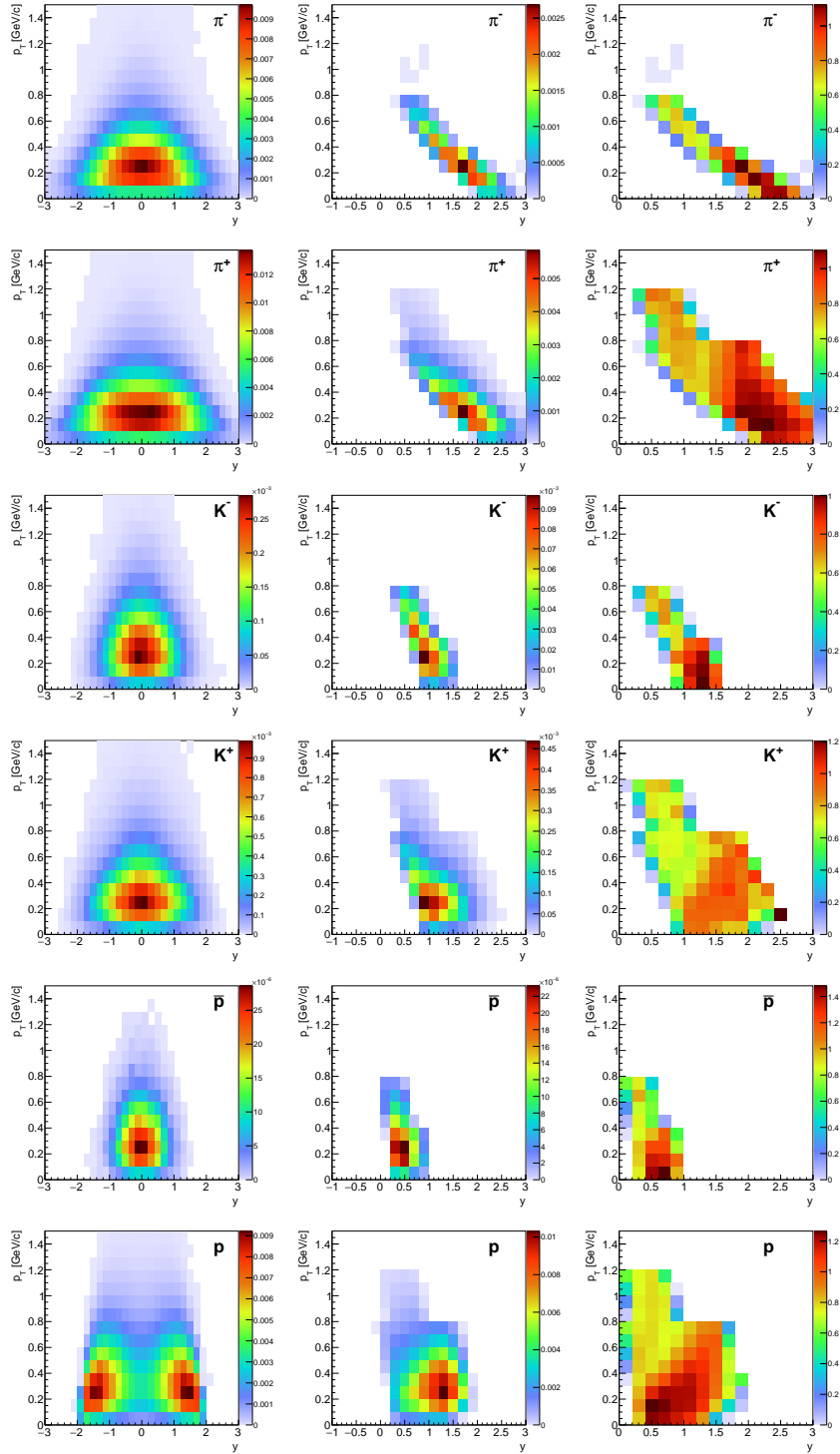
FIGURE 7.2: Example of generated Monte-Carlo particles spectra (left panels), spectra after selection criteria (middle panels) and correction factor (right panels) for $p + p$ interactions at 30.9 GeV/c for positively and negatively charged pions, kaons and protons.

obtain correction, each simulated and reconstructed track was extrapolated to the ToF walls and if cross one of the ToF pixels was taken into account as the ToF hit.

Corrections for the $tof - dE/dx$ identification method comprise several components. The efficiency of geometrical acceptance based on simulation introduced ϵ_{geo} factor:

$$\epsilon_{geo} = \frac{(n_i)_{geo}^{MCrec}}{(n_i)^{MCgen}}, \tag{7.2}$$

where $(n_i)_{geo}^{MCrec}$ is multiplicity of particle type $i = \pi^-$, π^+, K^-, K^+, p, $\bar{p}$ after the TPC selection criteria and track extrapolation to the ToF wall within Time of Flight detector geometrical limits, and $(n_i)^{MCgen}$ is multiplicity of particle type i generated by the Monte-Carlo model. Such correction takes into account geometrical acceptance of TPCs and ToF detectors. In addition, the extrapolation requirement of last point in MTPC in last two padrows is implemented. Hence, this requirement in the same time corrects for particle decays and interactions with the material of the TPCs. Estimation of geometrical correction for $p + p$ interactions at 158 GeV/c is presented in Fig. 7.3. Difference between efficiency for pions, kaons and protons is due to different mean free path length.
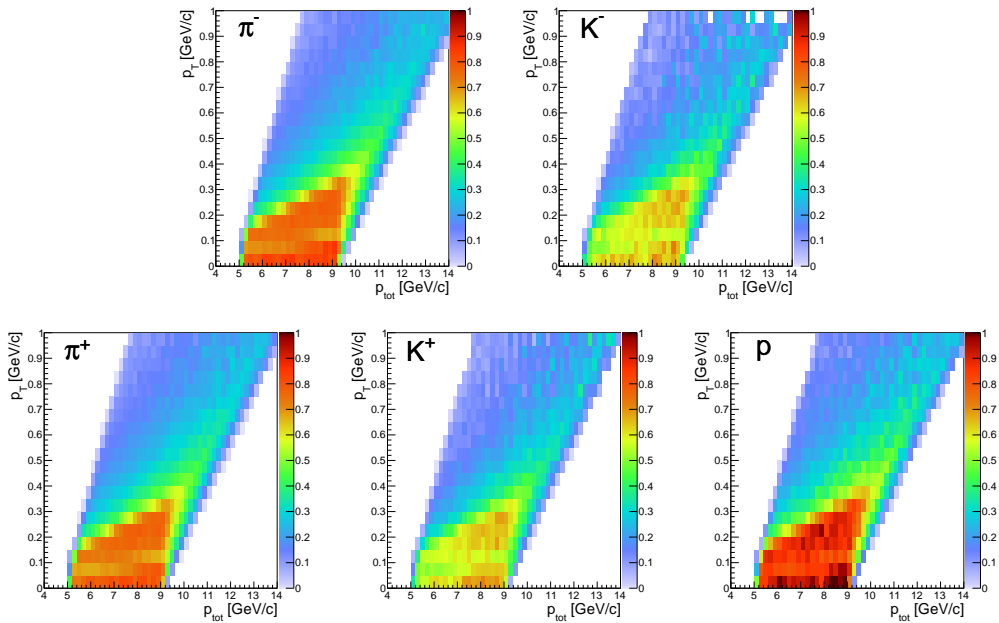
FIGURE 7.3: Correction for geometrical acceptance and decays before two last padrows of MTPC for $p + p$ collisions at 158 GeV/c.

The second correction is based on collected data and reconstructed Monte-Carlo. The pixel efficiency is calculated as ratio between ToF hits with correct TDC and QDC measurements and all tracks which extrapolation to ToFs is in theirs acceptance. Pixel efficiency during 2009 data taking for $p + p$ at 158 GeV/c is presented in Fig. 7.4.
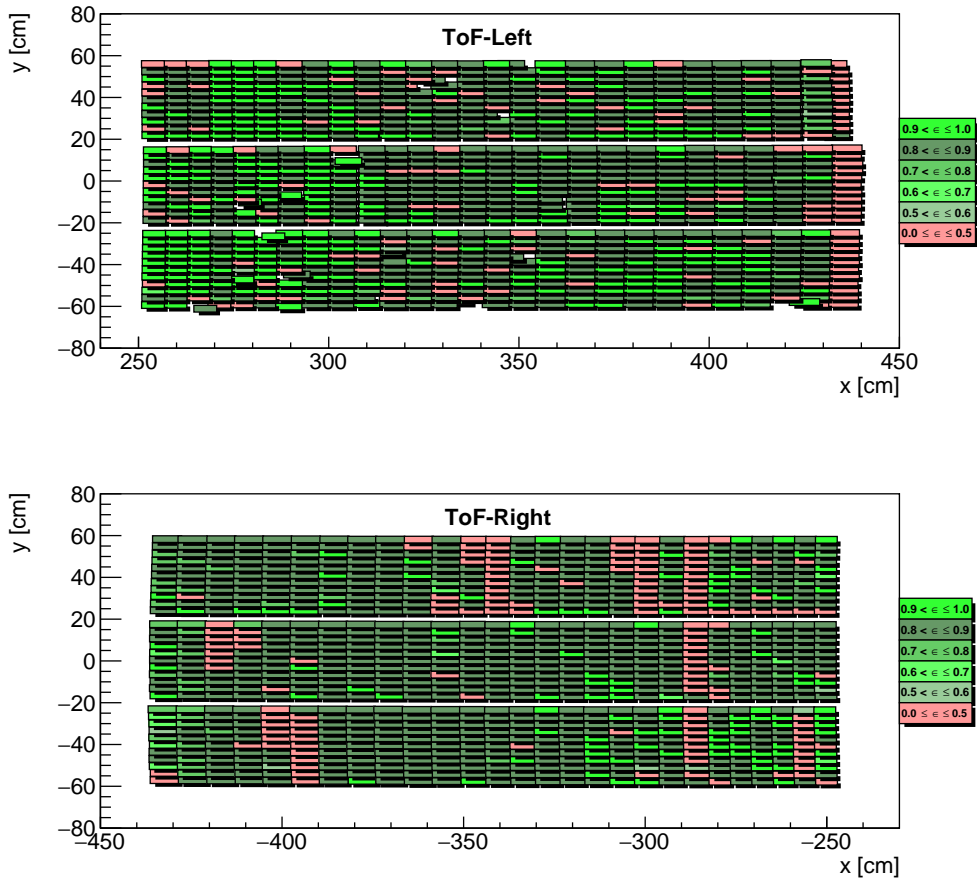
FIGURE 7.4: Pixel efficiency extracted from $p + p$ at 158 GeV/c in $x - y$ plane for ToF-L (top panel) and ToF-R (bottom panel).

Monte-Carlo efficiency ϵ_{dead} for not operating pixels is calculated as the ratio of the $(n_i)^{MCrec}_{dead\ pixel}$ defined as the multiplicity of the tracks with hit in the working pixel (pixel efficiency from data higher than 50%) and multiplicity of all tracks with hits in ToF geometry $(n_i)^{MCrec}_{geo}$. It can be defined as:

$$\epsilon_{dead} = \frac{(n_i)^{MCrec}_{dead\ pixel}}{(n_i)^{MCrec}_{geo}}. \tag{7.3}$$

This correction is the same for all particles with the same charge. Efficiency obtained for $p + p$ at 158 GeV/c is presented in Fig. 7.5.

In the next step, each MC hit is weighted with corresponding pixel efficiency in case of working ToF parts. Weighting factor — pixel efficiency is taken from data and presented
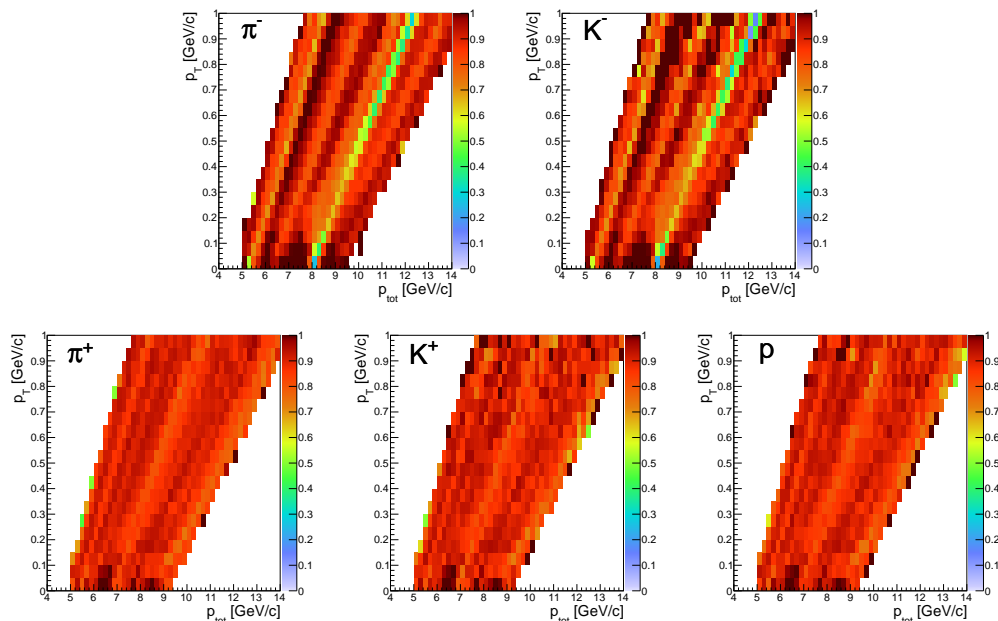
FIGURE 7.5: Monte-Carlo correction for not active pixels. Visible strips with lower value are due to groups of not working pixels.

in Fig. 7.4. The Monte-Carlo correction $\epsilon_{efficiency}$ can be written as:

$$\epsilon_{efficiency} = \frac{(n_i)_{efficiency}^{MCrec}}{(n_i)_{dead\ pixel}^{MCrec}}, \tag{7.4}$$

where $(n_i)_{efficiency}^{MCrec}$ are the multiplicities of the particles with hit in working ToF pixel weighted by the efficiency factor obtained from data. Correction is the same for particles with the same charge as predicted. It is shown in Fig. 7.6.

Moreover, decays and interactions between last measured point in the MTPC and ToF detectors are consider. This effects are included based on Monte-Carlo calculations. The decay correction factor ϵ_{decay} is defined in the following way:

$$\epsilon_{decay} = \frac{(n_i)_{decay}^{MCrec}}{(n_i)_{efficiency}^{MCrec}}, \tag{7.5}$$

where $(n_i)_{decay}^{MCrec}$ are particles with hit in the working ToF pixel weighted by its efficiency from data which do not decayed or interact in the Monte-Carlo between last measured point in MTPC and ToF walls. ϵ_{decay} is presented in Fig. 7.7. Low efficiency is caused by the interactions with Forward Time of Flight detector.
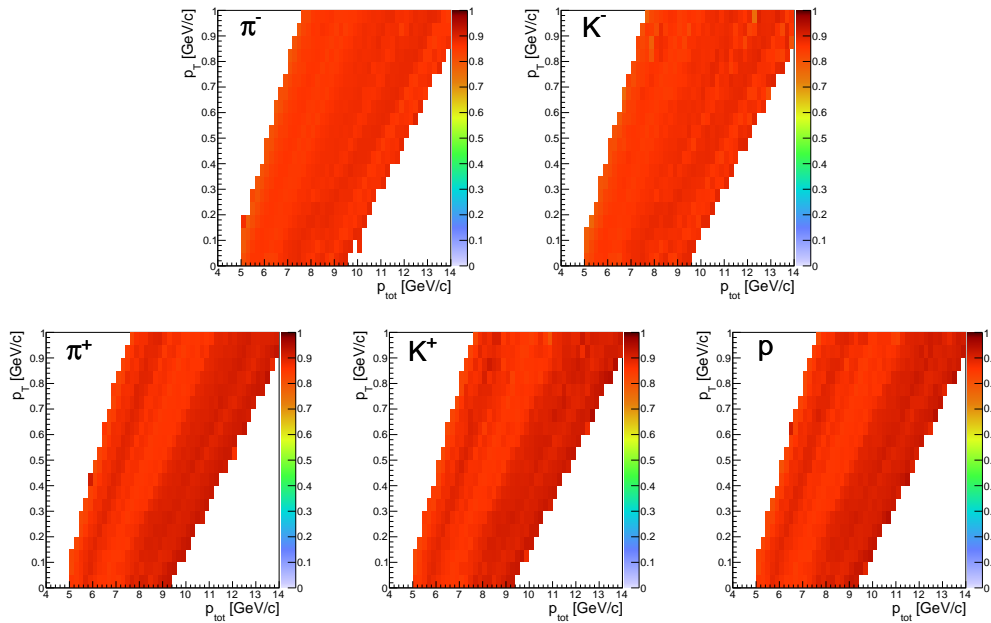
FIGURE 7.6: Correction for pixel efficiency from $p + p$ at 158 GeV/c.
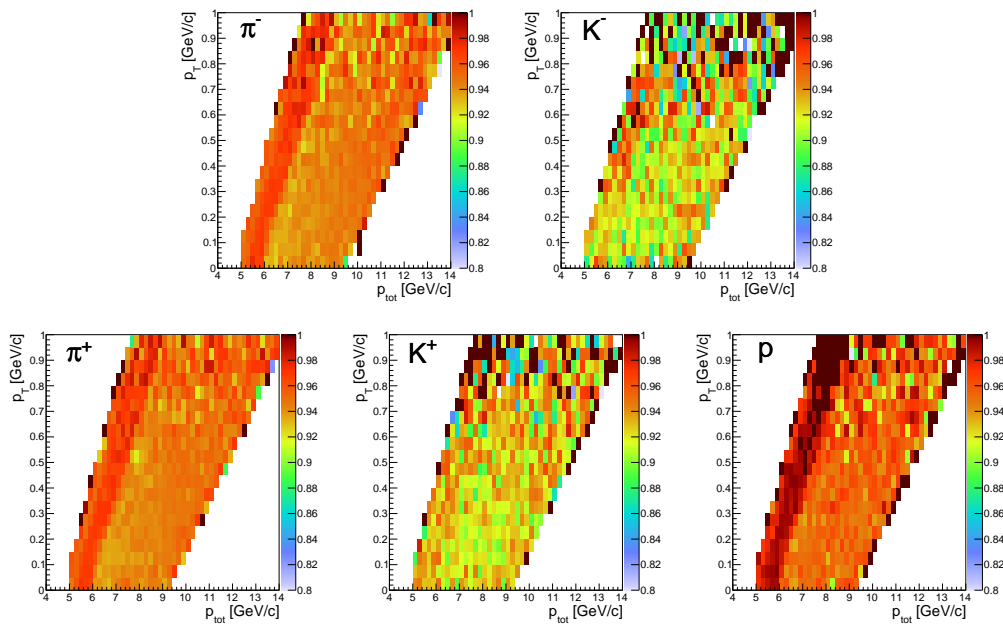
FIGURE 7.7: Correction for decays and interactions between last measured point in the MTPC and ToF-L or ToF-R walls for $p + p$ interactions at 158 GeV/c.

The final correction can be calculated as:

$$
\begin{aligned}
\epsilon &= \epsilon_{geo} \times \epsilon_{dead} \times \epsilon_{efficiency} \times \epsilon_{decay} \\
&= \frac{(n_i)_{geo}^{MCrec}}{(n_i)^{MCgen}} \times \frac{(n_i)_{dead\ pixel}^{MCrec}}{(n_i)_{geo}^{MCrec}} \times \frac{(n_i)_{efficiency}^{MCrec}}{(n_i)_{dead\ pixel}^{MCrec}} \times \frac{(n_i)_{decay}^{MCrec}}{(n_i)_{efficiency}^{MCrec}} \\
&= \frac{(n_i)_{decay}^{MCrec}}{(n_i)^{MCgen}}.
\end{aligned}
\tag{7.6}
$$

Chapter 8

Corrected spectra and uncertainties

Multiplicities calculation of positively and negatively charged π, K and p based on identification described in Chapter 6 and correction methods from Chapter 7 are presented in this chapter. Estimation of statistical and systematic uncertainties is also discussed.

8.1 Final multiplicities calculations and statistical uncertainties

Multiplicity of different hadrons from inelastic $p+p$ interactions measured by the dE/dx technique is defined as a sum of probabilities divided by the number of events corrected for detector effects, feed-down and out of target contamination. For particle type $i = \pi^-,\ \pi^+,\ K^-,\ K^+,\ \bar{p},\ p$, it is defined as:

$$\frac{n_i}{N} = \frac{1}{C} \frac{\sum\limits_{I} P_i(p_{tot}, p_T, dE/dx) - B \sum\limits_{R} P_i(p_{tot}, p_T, dE/dx)}{N_I - BN_R},$$ (8.1)

where:

- C - correction factor defined in Eq. 7.1,

- $\sum\limits_{I} P_i(p_{tot}, p_T, dE/dx) \equiv \sum\limits_{I} P_i$ - sum over probabilities P_i defined in Eq. 6.4 of all tracks for inserted target (abbreviated as "I"),

- $\sum_R P_i(p_{tot}, p_T, dE/dx) \equiv \sum_R P_i$ - sum over probabilities P_i defined in Eq. 6.4 for all tracks for removed target (abbreviated as "R"),

- B - the normalization factor (see Chapter 7.1),

- N_I and N_R - the number of events of target inserted and removed, respectively.

Statistical error of multiplicities obtained by dE/dx method has been calculated in the following way:

$$
\left(\Delta \frac{n_i}{N}\right)^2 = \left(\left|\frac{-1}{C^2} \frac{\sum_I P_i - B \sum_R P_i}{N_I - BN_R}\right| \Delta C\right)^2 +
$$
$$
\left(\left|\frac{1}{C} \frac{1}{N_I - BN_R}\right| \sqrt{\sum_I P_i}\right)^2 + \qquad (8.2)
$$
$$
\left(\left|\frac{1}{C} \frac{-B}{N_I - BN_R}\right| \sqrt{\sum_R P_i}\right)^2 ,
$$

where: Δ devote statistical uncertainty of the variables used to calculate particle multiplicity. Uncertainty of normalization factor (B) as well as number of events (N_I and N_R) are not taken into account during this calculation due to their negligible influence on the uncertainty value.

Example of obtained by dE/dx identification and corrected spectra in $p+p$ interactions at 40 GeV/c is presented in Fig. 8.1

Particle multiplicities for $tof - dE/dx$ technique can be calculated in a similar way (exception are corrections factors). In this case, particle yields are defined as:

$$
\frac{n_i}{N} = \frac{1}{C_{tof}} \frac{\sum_I \frac{P_i(p_{tot}, p_T, dE/dx, tof)}{\epsilon} - B \sum_R \frac{P_i(p_{tot}, p_T, dE/dx, tof)}{\epsilon}}{N_I - BN_R}, \qquad (8.3)
$$

where: P_i are the probabilities defined in Eq. 6.5, ϵ - efficiency described by Eq. 7.6 and C_{tof} - the correction for the losses due to the momentum acceptance of the fitting procedure.

Statistical error estimation of the multiplicities calculated by the $tof - dE/dx$ technique is more complicated. It was assumed that ϵ statistical error is equal to the mean statistical uncertainty in full $y - p_T$ bin, and therefore it can be moved in front of the sums.
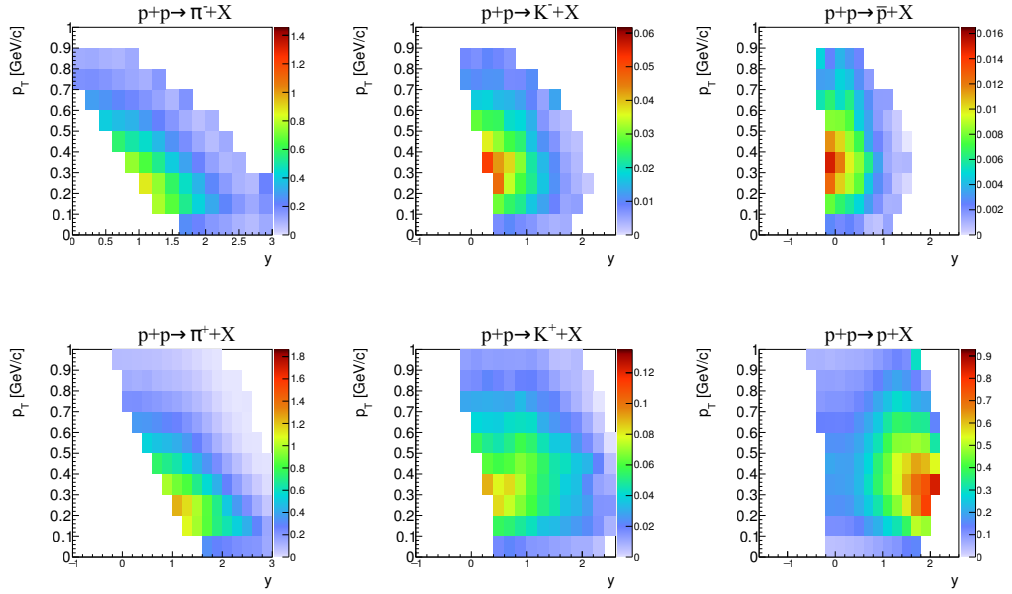
FIGURE 8.1: Multiplicity of π^+, π^-, K^+, K^-, p and $\bar{p}$ from $p + p$ inelastic interactions at 40 GeV/c from dE/dx method.

Finally, statistical error can be calculated according to the following formula

$$
\left(\Delta \frac{n_i}{N}\right)^2 = \left(\left|\frac{-1}{C_{tof}^2} \frac{\sum\limits_I \frac{P_i}{\epsilon} - B \sum\limits_R \frac{P_i}{\epsilon}}{N_I - BN_R}\right| \Delta C_{tof}\right)^2 +
$$

$$
\left(\left|\frac{1}{C_{tof}} \frac{\sum\limits_I \frac{1}{\epsilon}}{N_I - BN_R}\right| \sqrt{\sum\limits_I P_i}\right)^2 +
$$

$$
\left(\left|\frac{1}{C_{tof}} \frac{\sum\limits_R \frac{-B}{\epsilon}}{N_I - BN_R}\right| \sqrt{\sum\limits_R P_i}\right)^2 +
$$

$$
\left(\left|\frac{-1}{C_{tof}\langle\epsilon\rangle^2} \frac{\sum\limits_I P_i - B \sum\limits_R P_i}{N_I - BN_R}\right| \langle\Delta\epsilon\rangle\right)^2 . \tag{8.4}
$$

Spectra of π^+, π^-, K^+, K^- and p produced in inelastic $p + p$ at 40 GeV/c obtained by $tof - dEdx$ method are shown in Fig. 8.2.
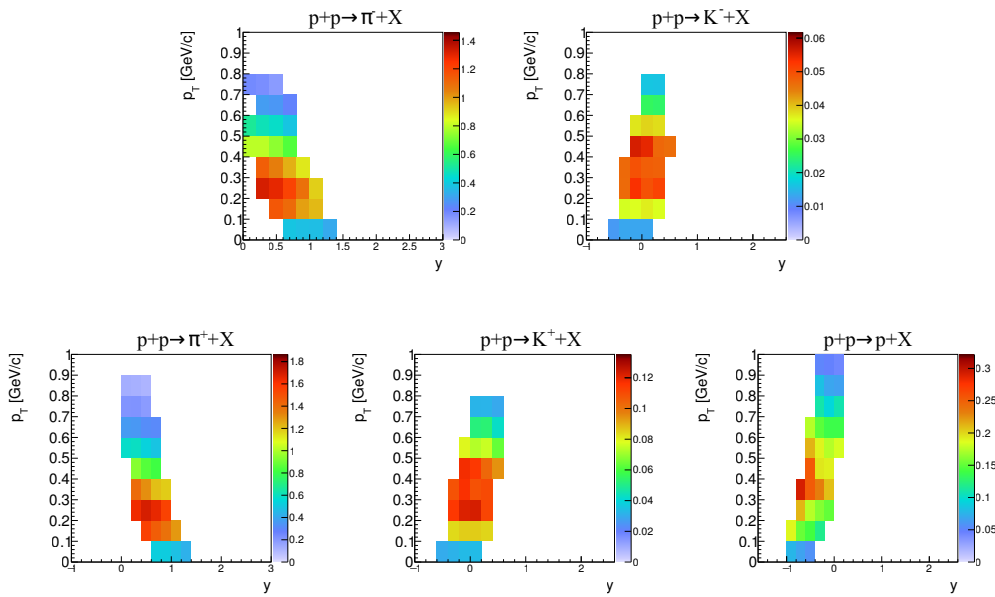
FIGURE 8.2: Multiplicity of π^+, π^-, K^+, K^- and p from $p + p$ inelastic interactions at 158 GeV/c from $tof - dE/dx$ method.

8.2 Systematic uncertainty of measured multiplicities

The main systematic biases to the measurement could come from:

- event and track cuts which are not corrected,

- event losses due to trigger settings,

- methods of track and event selection,

- used identification techniques.

The first possible uncertainty is related to the event and track cuts for which are not corrected for. The main source of such bias can be assign to the off-time particles. Therefore, to estimate this systematic uncertainty, selections criteria has been changed. The analysis was performed with different time windows in which second beam particle can be observed in the same event (WFA $\pm$ 1 ms over nominal one). This results were compered with the nominal one and maximum difference between them was assign as the systematic uncertainty of the measurement.

Second source of the systematic bias are the event losses connected to the trigger settings. During the data taking, in the trigger system, the S4 detector was used to remove from

the data elastic events. However, such configuration can also result in losses of the inelastic events. To take into account this effect, identification procedure has to be done with Monte-Carlo correction calculated with and without S4 counter. Difference between this two results allow to estimate this systematic error.

The next source of the systematic bias are track and event selection methods. To calculate the effect of the selection criteria for the results, following variations of them were performed independently:

- number of requested points of track in all TPCs was changed by ± 5,

- number of requested points of track in VTPCs was reduced or enlarge by 5,

- position of fitted vertex was checked in the range of $\pm 10\ cm$ around the nominal value.

Moreover, additional biases of the dE/dx method have been studied and estimated by the 10% variation of the parameter limits for function used for particle identification. In case of $tof - dE/dx$ identification source of the possible uncertainty were found by changing the selection criteria related to this technique. The systematic uncertainties for the dE/dx method, for selected p_T interval and beam momentum of 40 GeV/c are presented in Fig. 8.3.
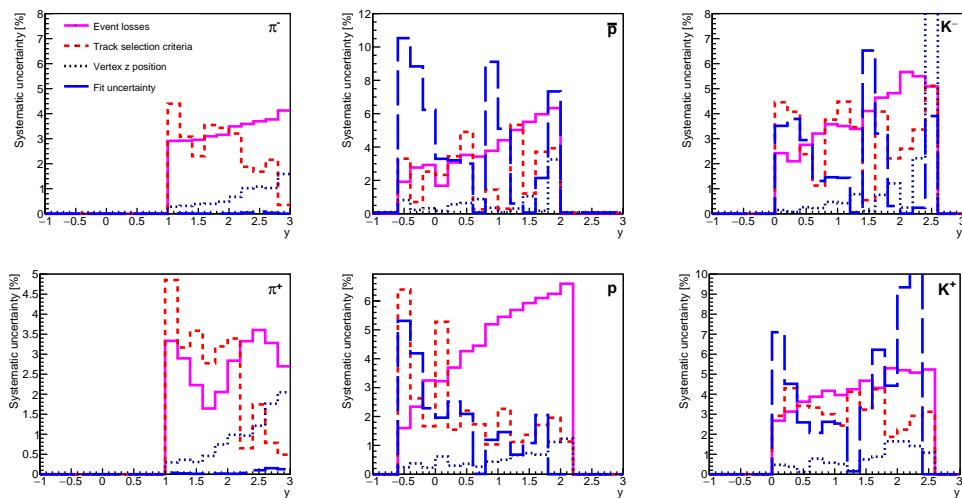
FIGURE 8.3: Systematic uncertainty components in $p + p$ interaction at 40 GeV/c as the function of rapidity for transverse momentum interval between 0.3 and 0.4 GeV/c.

Assuming the independence of all systematic error sources, the final systematic uncertainty has been calculated as a square root of sum squares of the above described components.

Chapter 9

Final particle spectra

Two dimensional spectra of negatively and positively charged pions, kaons and protons in rapidity versus transverse momentum phase space, obtained with dE/dx and $tof - dE/dx$ methods are presented in this chapter.

9.1 Particle production in y vs p_T phase space

One of the main goal of analysis presented in this thesis is calculation of the particle yields as function of the rapidity and transverse momentum. Two dimensional spectra (y vs. p_T) of π^-, π^+, K^-, K^+, p and $\bar{p}$ produced in inelastic $p+p$ collisions at different SPS energies are presented in Fig 9.1. The anti-protons at 20 GeV/c were not identified due to limited statistics of collected data. It can be noticed that, the particles production increases with collision energy. That behavior is observed for all particles types. Empty bins in the phase-space (mostly for lower energies) are caused by missing acceptance of the methods used for analysis.

Multiplicities presented in Fig. 9.1 can be studied as a function of rapidity (y) or transverse momentum (p_T). Transverse mass distributions of K^-, K^+ produced in $p + p$ interactions at 20, 30.9, 40, 80, 158 GeV/c as the function of rapidity are presented in Figs. 9.2, 9.3 , 9.4, 9.5 and 9.6, respectively. Additionally, double differential p_T spectra of π^- and π^+ are shown in Figs. 9.7, 9.8 , 9.9, 9.10 and 9.11 for five SPS energies. Spectra are scaled by appropriate factors for better separation. Shadow band in the figures correspond to systematic uncertainties of double differential spectra.
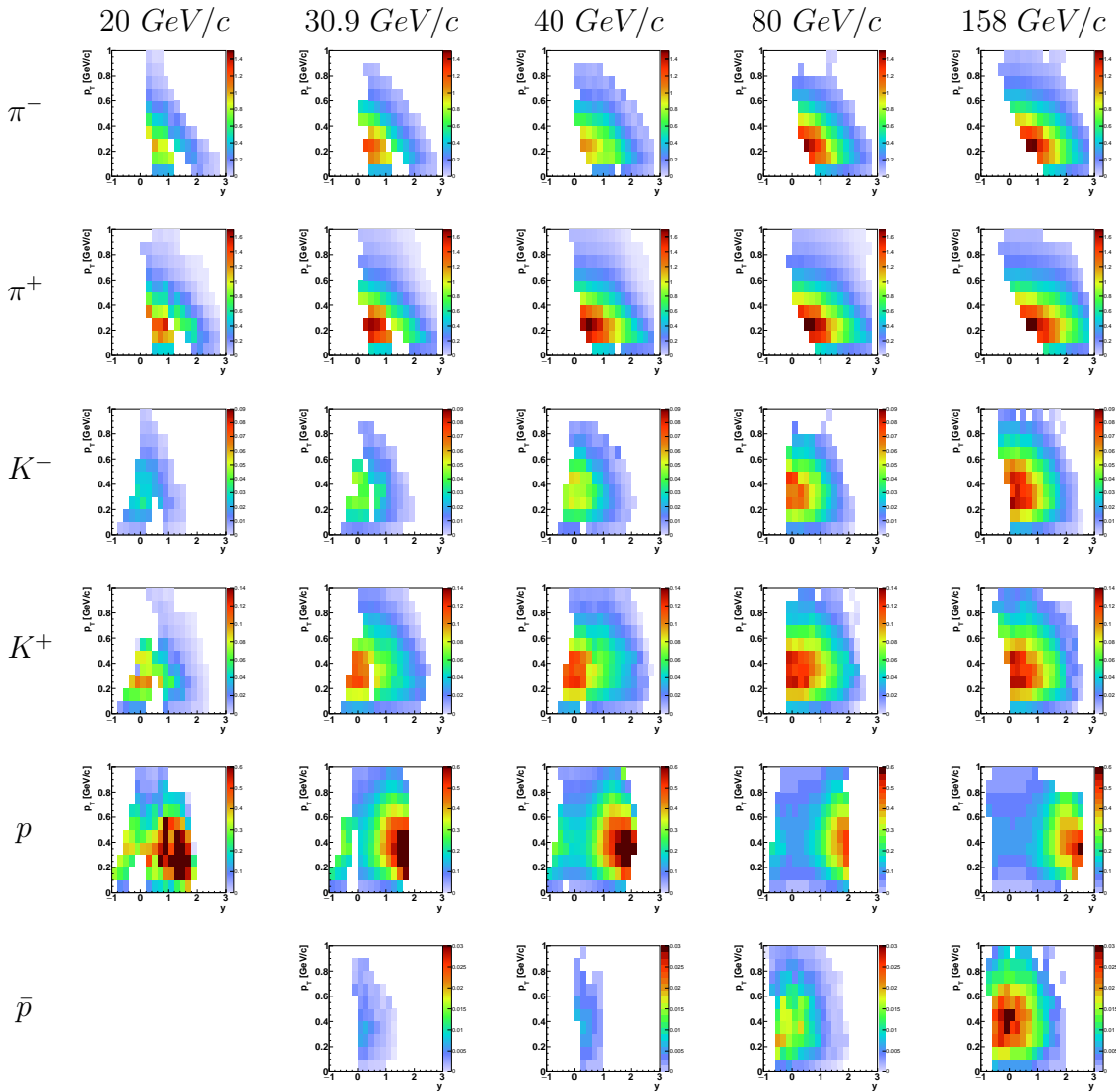
FIGURE 9.1: Two dimensional spectra of π^-, π^+, K^-, K^+, p and $\bar{p}$ produced in inelastic $p+p$ collisions at 20, 30.9, 40, 80 and 158 GeV/c. Color scale represents particle multiplicities normalized to the phase-space bin size ($\frac{dn}{dydp_T}$).
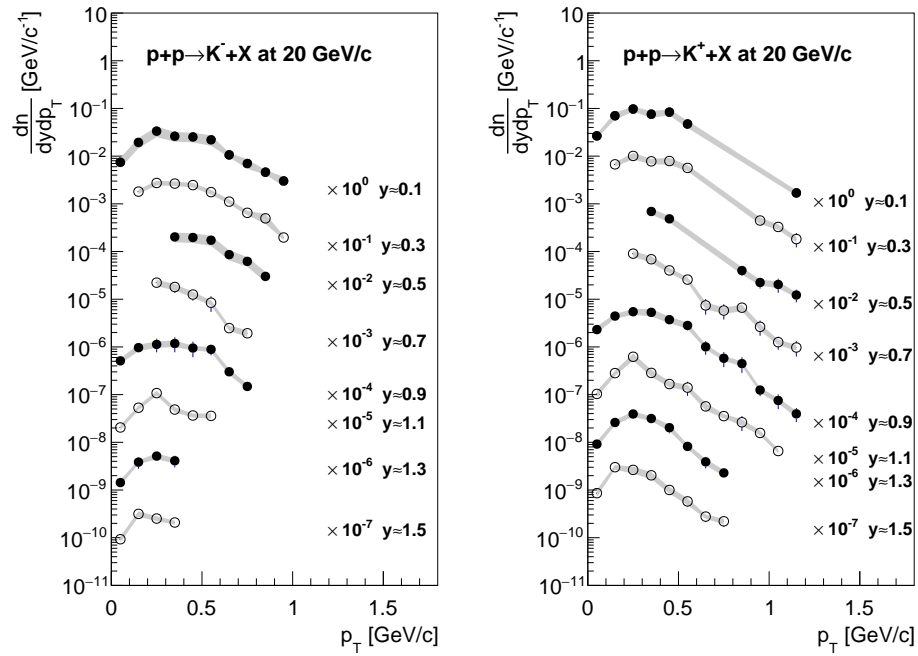
FIGURE 9.2: K^- and K^+ spectra produced in inelastic $p + p$ collisions at 20 GeV/c beam momentum. Rapidity values on the figure correspond to the middle of the presented bin.
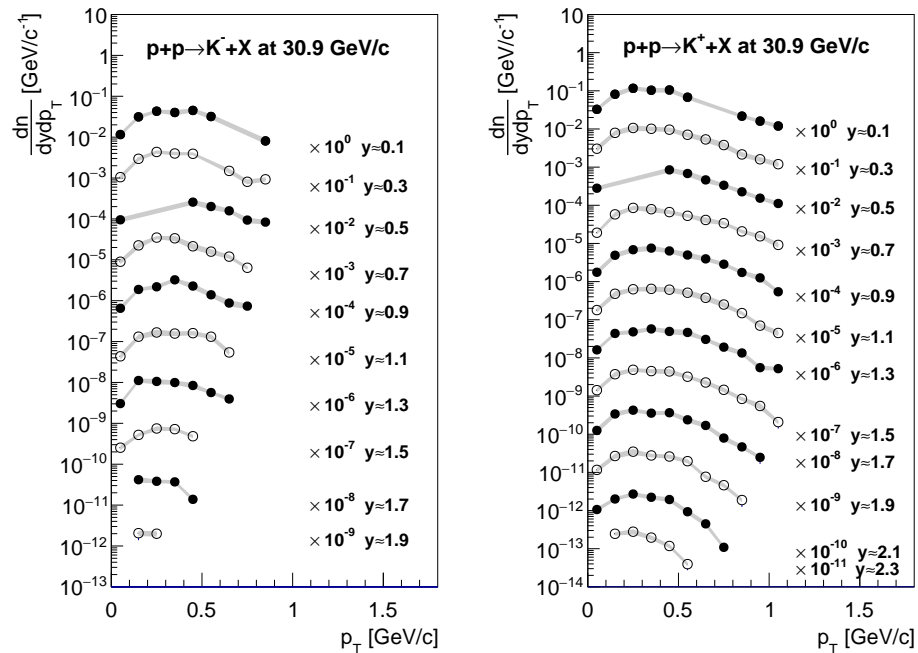
FIGURE 9.3: K^- and K^+ spectra produced in inelastic $p + p$ collisions at 30.9 GeV/c beam momentum. Rapidity values on the figure correspond to the middle of the presented bin.
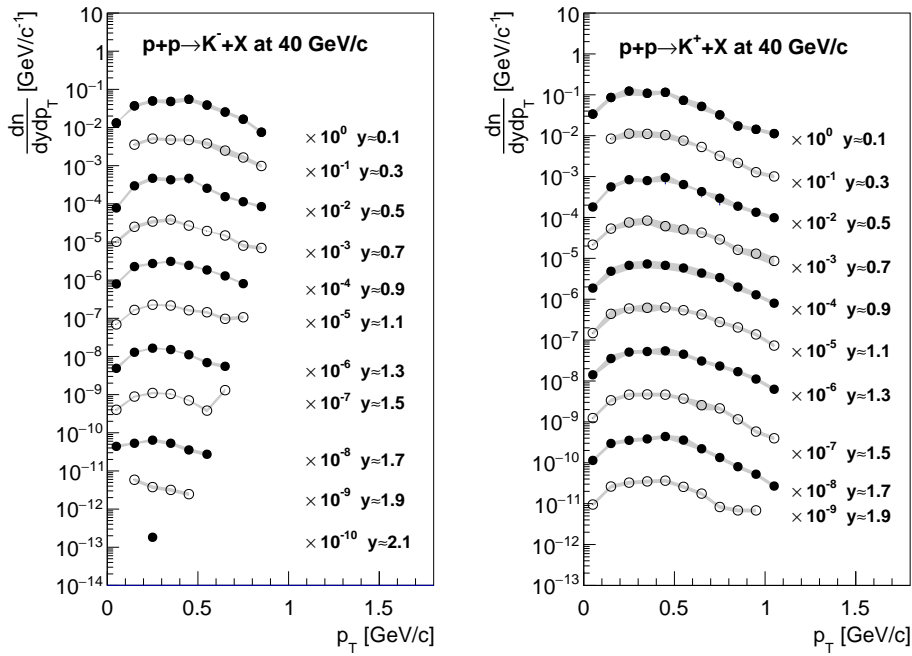
FIGURE 9.4: K^- and K^+ spectra produced in inelastic $p + p$ collisions at 40 GeV/c beam momentum. Rapidity values on the figure correspond to the middle of the presented bin.
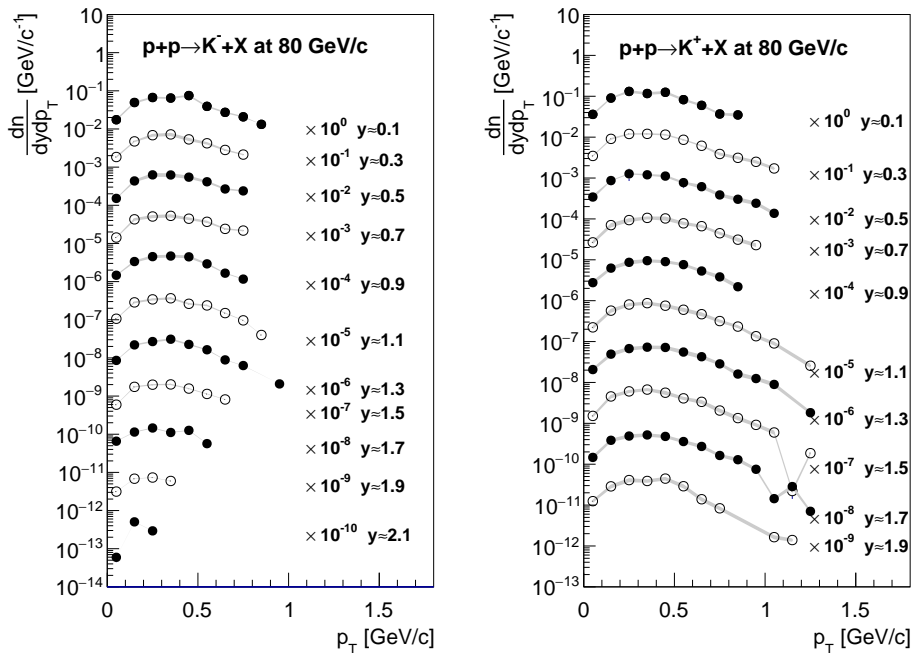
FIGURE 9.5: K^- and K^+ spectra produced in inelastic $p + p$ collisions at 80 GeV/c beam momentum. Rapidity values on the figure correspond to the middle of the presented bin.
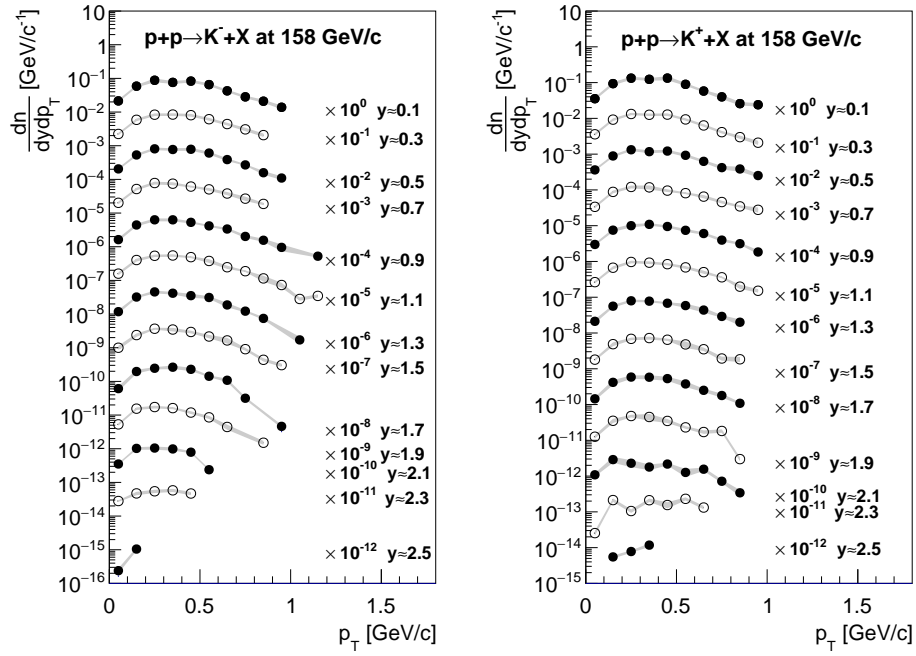
FIGURE 9.6: K^- and K^+ spectra produced in inelastic $p + p$ collisions at 158 GeV/c beam momentum. Rapidity values on the figure correspond to the middle of the presented bin.
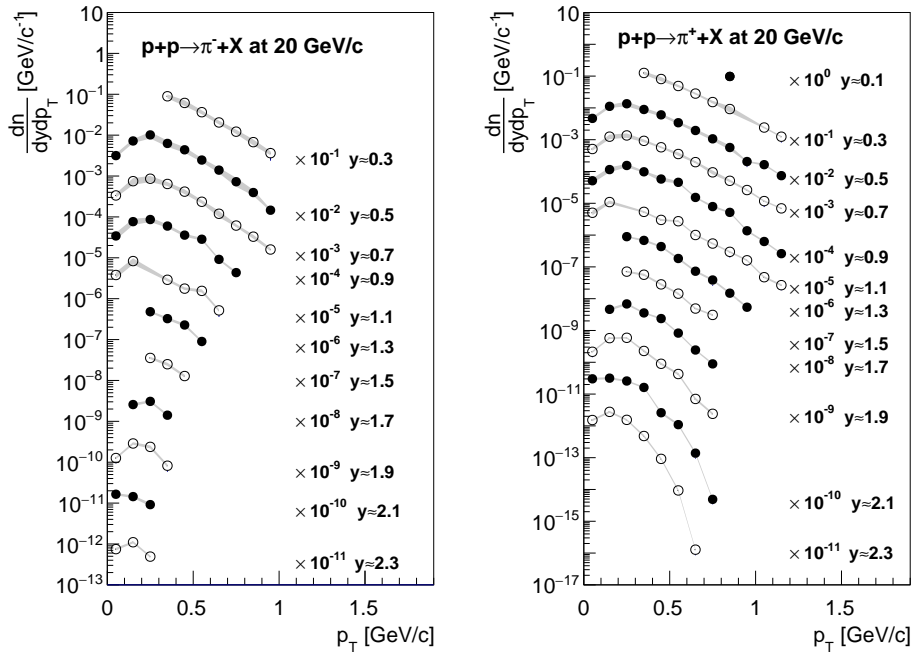
FIGURE 9.7: Double differential spectra of positively and negatively charged pions produced in inelastic $p + p$ collisions at 20 GeV/c beam momentum. Rapidity values on the figure correspond to the middle of the presented bin.
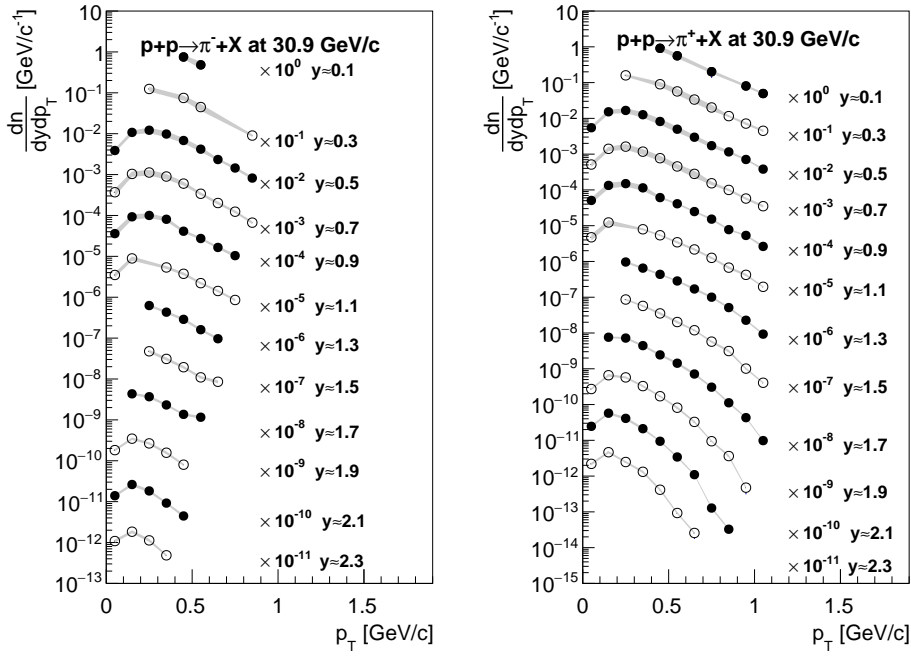
FIGURE 9.8: Double differential spectra of positively and negatively charged pions produced in inelastic $p + p$ collisions at 30.9 GeV/c beam momentum. Rapidity values on the figure correspond to the middle of the presented bin.
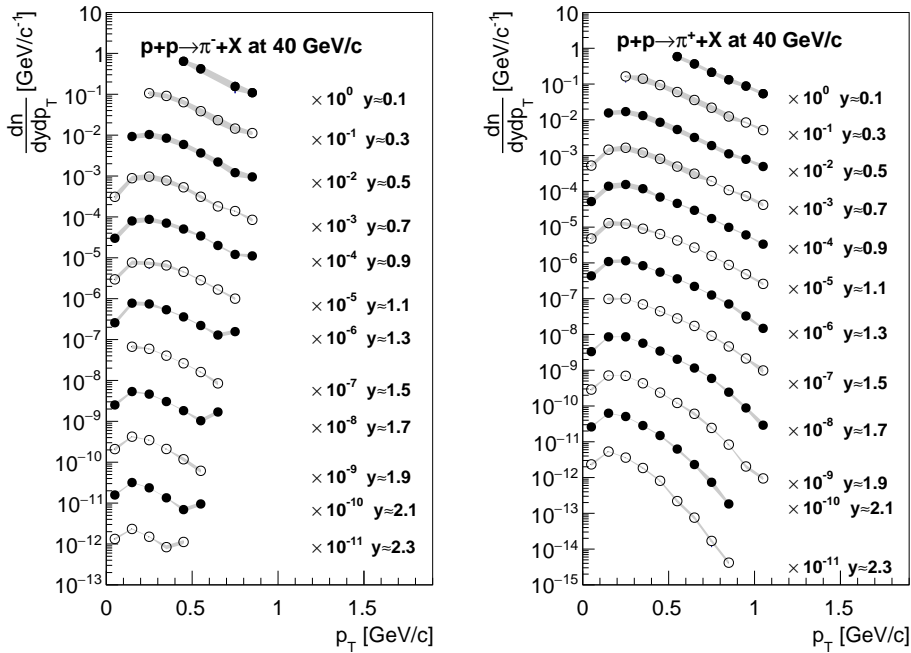
FIGURE 9.9: Double differential spectra of positively and negatively charged pions produced in inelastic $p + p$ collisions at 40 GeV/c beam momentum. Rapidity values on the figure correspond to the middle of the presented bin.
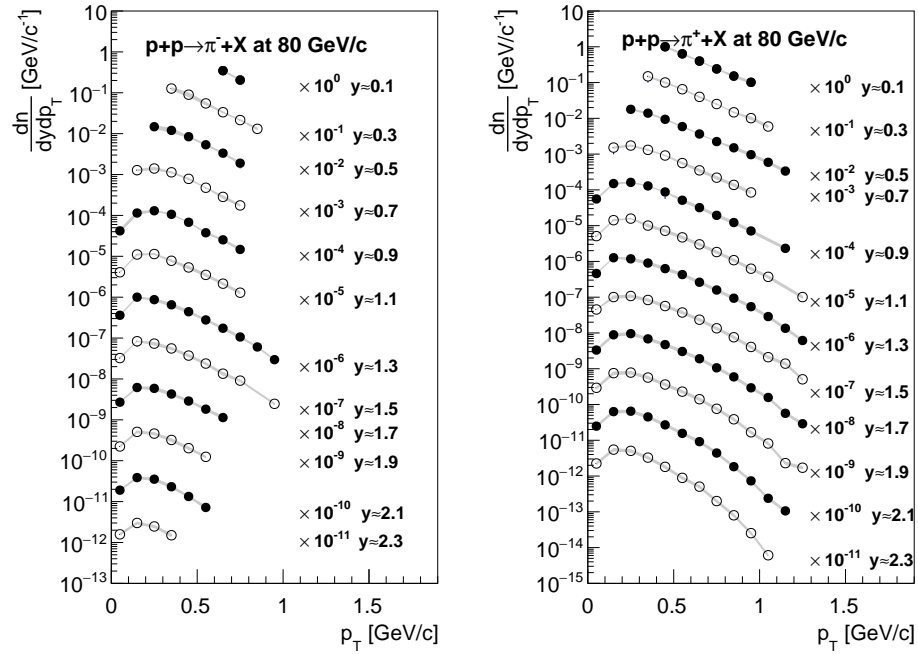
FIGURE 9.10: Double differential spectra of positively and negatively charged pions produced in inelastic $p + p$ collisions at 80 GeV/c beam momentum. Rapidity values on the figure correspond to the middle of the presented bin.
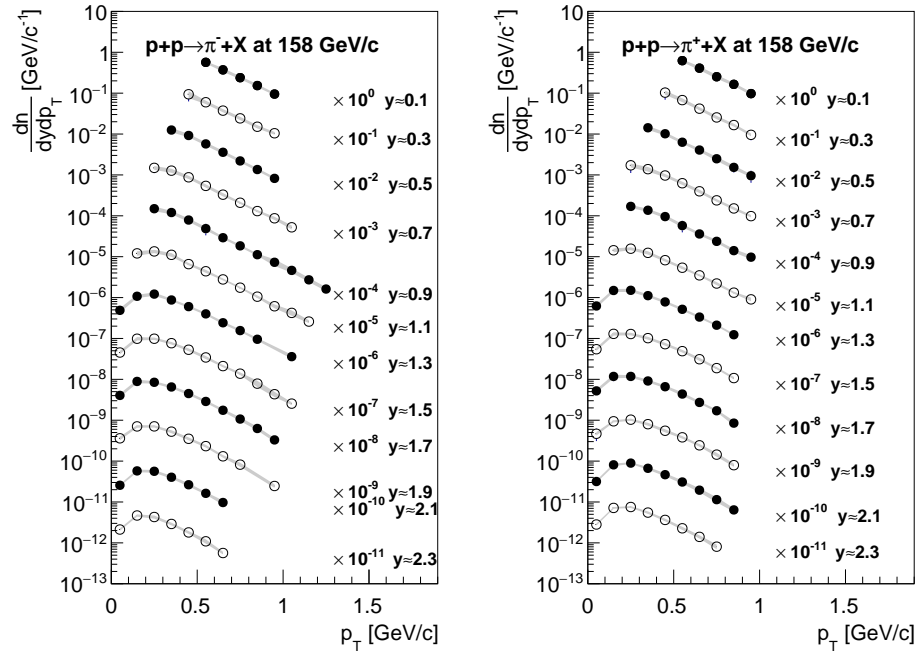
FIGURE 9.11: Double differential spectra of positively and negatively charged pions spectra produced in inelastic $p + p$ collisions at 158 GeV/c beam momentum. Rapidity values on the figure correspond to the middle of the presented bin.

It was mentioned that the particle production can be presented as the function of the transverse momentum. The rapidity distribution of protons and anti-protons produced in inelastic $p + p$ collisions at 30.9, 40, 80 and 158 GeV/c for transverse momentum intervals are shown in Figs. 9.12, 9.13, 9.14, 9.15. The spectra are symmetrical around the mid-rapidity ($y = 0$).
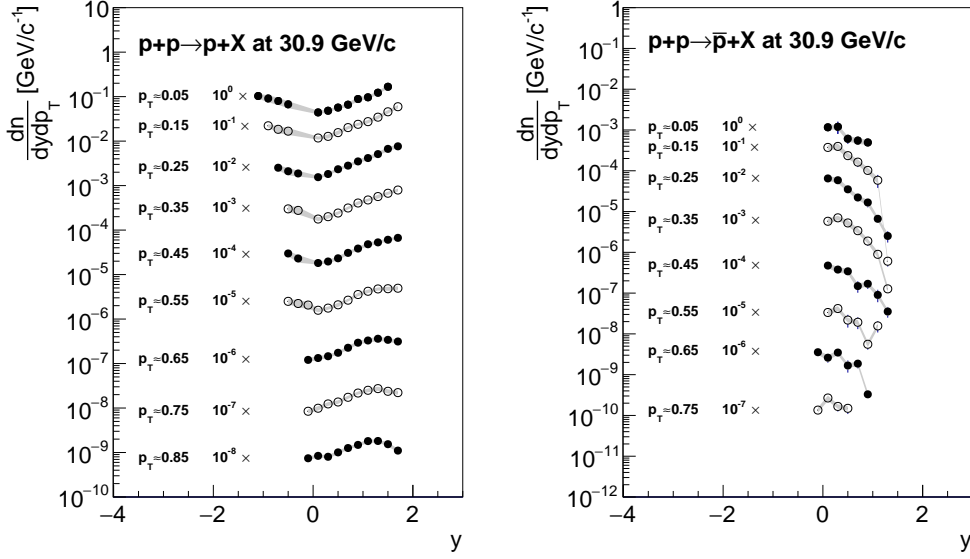
FIGURE 9.12: Double differential rapidity spectra of protons and anti-protons from $p + p$ at 30.9 GeV/c for different transverse momentum intervals.
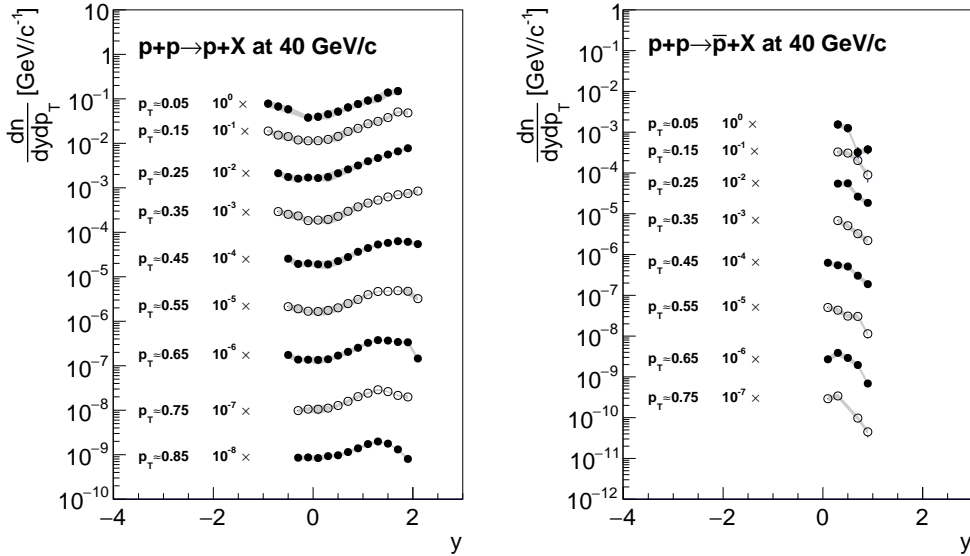
FIGURE 9.13: Double differential rapidity spectra of protons and anti-protons from $p + p$ at 40 GeV/c for different transverse momentum intervals.
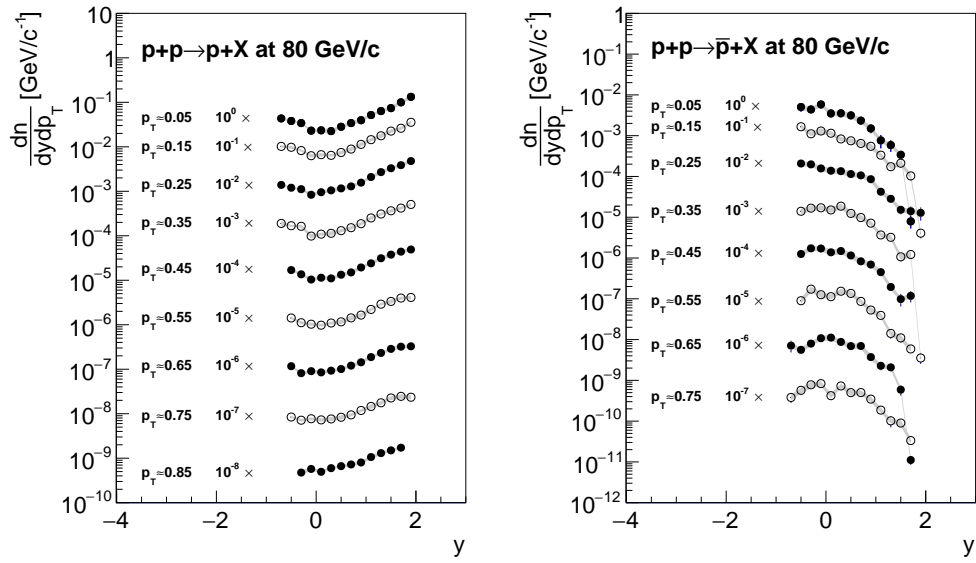
FIGURE 9.14: Double differential rapidity spectra of protons and anti-protons from $p + p$ at 80 GeV/c for different transverse momentum intervals.
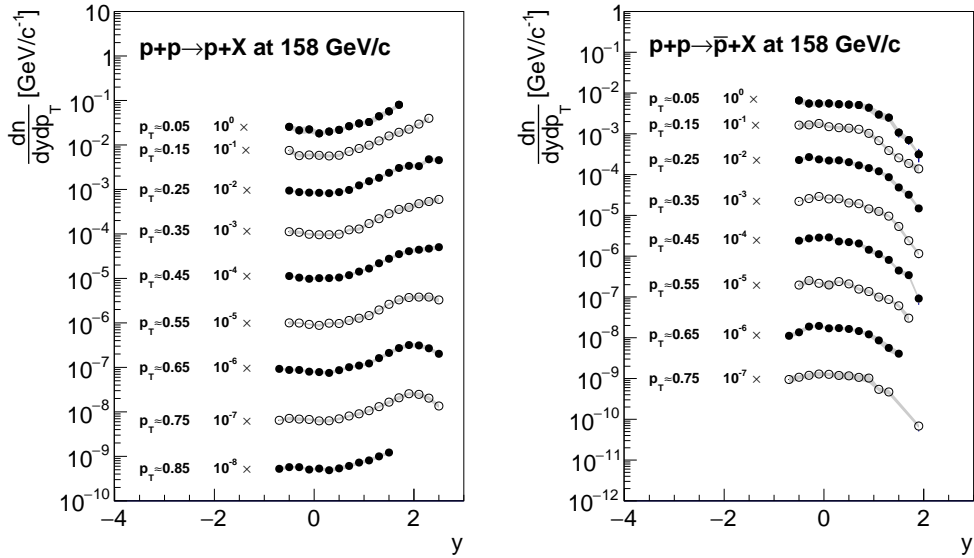
FIGURE 9.15: Double differential rapidity spectra of protons and anti-protons from $p + p$ at 158 GeV/c for different transverse momentum intervals.

9.2 4π multiplicities

Calculation of 4π multiplicities have been also performed. Firstly, the extrapolation to not measure phase-space region in p_T by the exponential function fit and then reflection of the result around mid-rapidity ($y = 0$) to the backward hemisphere was done. The

reflection can be done thanks to the symmetrical collision system. Thus, calculations for the backward rapidity region for some bins of transverse momentum can be performed.

Next, 4π multiplicities distribution for positive hemisphere of particle production are integrated and extrapolated over transverse momentum. Results of this procedure are presented in Fig. 9.16. Statistical error, visible as a bars, are calculated as the square root of sum of the squares statistical errors of measured point and exponential fit. The systematic uncertainty (shadow bands) is a square root of sum of the squares measured systematic uncertainty and half of the extrapolated yield. Visible lines corresponds to the fits with sum of two identical Gaussian functions with mean position symmetrically displaced around mid-rapidity. Such function was selected, hence it gives the best description of the data.
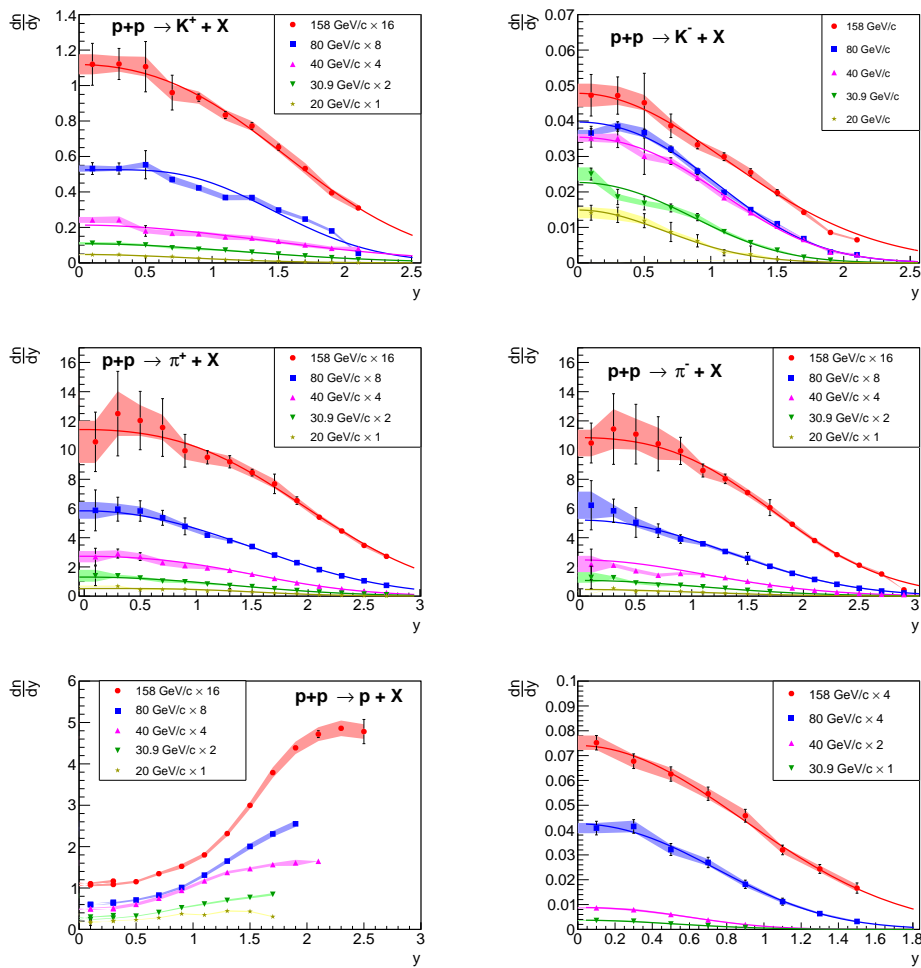
FIGURE 9.16: Rapidity spectra of different particles at SPS energies range, scaled by appropriate factors for better separation.

Study of the proton production in $p + p$ collisions by the NA49 experiment [35] and it's comparison to theoretical model excluded possibility to calculate 4π proton multiplicity based on the Monte-Carlo models. Comparison of presented NA61/SHINE results, NA49 measurement and theoretical models: UrQMD [23, 24], EPOS [26] is presented in Fig. 9.17. It can be observed that models do not described well high momentum (rapidity) region for protons at 158 GeV/c.
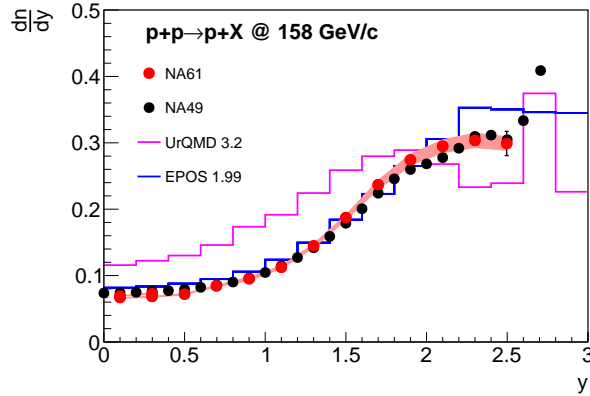
FIGURE 9.17: Proton rapidity distribution at 158 GeV/c compered with NA49 measurement and Monte-Carlo models.

The multiplicity of π^+, π^-, K^+, K^- and $\bar{p}$ per inelastic event were calculated using results presented in Fig. 9.16. The mean number of produced particles with the statistical and systematical uncertainties is summarized in Tables 9.1 and 9.2, for positively and negatively charged particles, respectively.

	K^+	π^+
20 GeV/c	$0.097 \pm 0.014 \pm 0.0062$	$1.582 \pm 0.122 \pm 0.197$
30.9 GeV/c	$0.157 \pm 0.010 \pm 0.015$	$1.985 \pm 0.210 \pm 0.197$
40 GeV/c	$0.170 \pm 0.009 \pm 0.023$	$2.221 \pm 0.220 \pm 0.164$
80 GeV/c	$0.201 \pm 0.010 \pm 0.010$	$2.556 \pm 0.220 \pm 0.140$
158 GeV/c	$0.234 \pm 0.014 \pm 0.017$	$2.991 \pm 0.305 \pm 0.250$

TABLE 9.1: Mean multiplicity of positive particles at SPS energies with statistical and systematic uncertainties.

	K^-	π^-	$\bar{p}$
20 GeV/c	$0.024 \pm 0.006 \pm 0.002$	$1.067 \pm 0.053 \pm 0.196$	—
30.9 GeV/c	$0.045 \pm 0.004 \pm 0.003$	$1.438 \pm 0.219 \pm 0.187$	$0.0047 \pm 0.0007 \pm 0.0003$
40 GeV/c	$0.084 \pm 0.006 \pm 0.003$	$1.703 \pm 0.192 \pm 0.213$	$0.0059 \pm 0.0006 \pm 0.0004$
80 GeV/c	$0.095 \pm 0.004 \pm 0.005$	$2.030 \pm 0.248 \pm 0.132$	$0.0183 \pm 0.0015 \pm 0.0011$
158 GeV/c	$0.132 \pm 0.011 \pm 0.009$	$2.494 \pm 0.259 \pm 0.179$	$0.0402 \pm 0.0020 \pm 0.0026$

TABLE 9.2: Mean multiplicity of negative particles at SPS energies with statistical and systematic uncertainties.

9.3 NA61/SHINE results and world data

Production of positive and negative pions, kaons and protons in $p + p$ collisions at 158 GeV/c was measured only by the NA49 experiment [36–38]. Comparison of NA61/SHINE and NA49 rapidity distributions is presented in Fig 9.18.
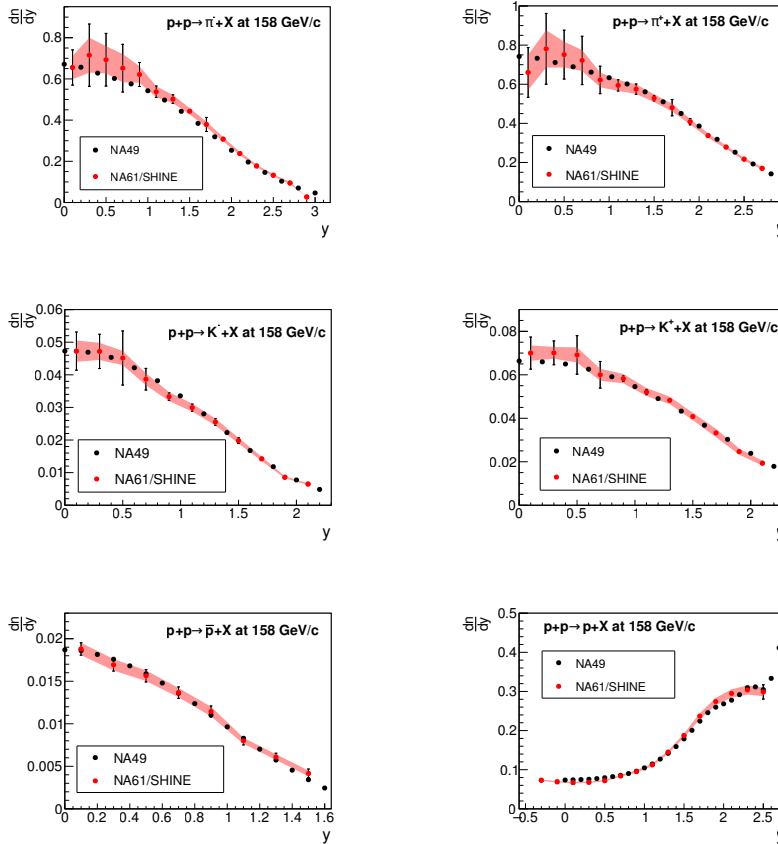
FIGURE 9.18: Comparison of rapidity distributions of pions, kaons and protons produced in $p + p$ collisions at 158 GeV/c. The NA49 results were published without quotation of uncertainties.

The NA61/SHINE experiment published also π^- spectra at all presented energies obtained by method so-called h^- [39]. This technique is based on the fact that the majority of negatively charged particles are π^- mesons. Contribution of the other particles is subtracted using EPOS model. Comparison of h^- method results with the results presented in this thesis is shown in Fig 9.19. All methods give results which are in agreement within statistical errors.
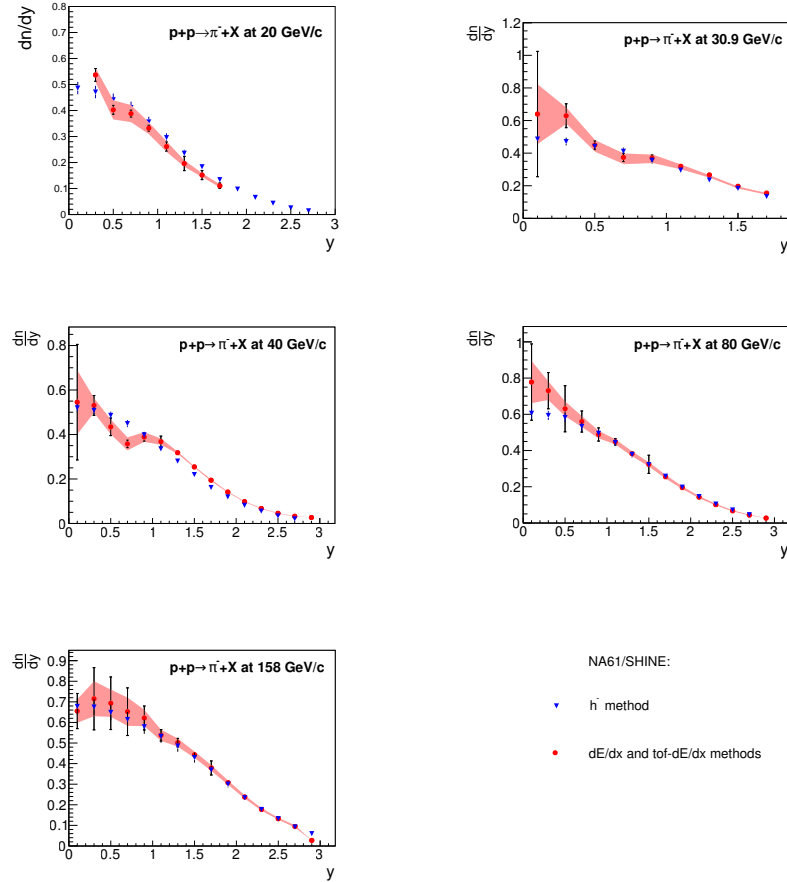
FIGURE 9.19: Comparison of π^- rapidity distribution obtained by dE/dx and $tof - dE/dx$ methods (this thesis) with h^- technique.

Chapter 10

Energy and system size dependencies of the particle production

In this chapter study of the energy and system size dependencies on the particle production is presented. These investigations represent an important step forward to study properties of the onset of deconfinement. The results of the NA61/SHINE experiment described in this section are compared with results from other experiments, and with theoretical predictions.

10.1 Energy dependence of mean particle production in $p + p$ collisions

Investigation of $p + p$ collisions for mean multiplicity of positive and negative kaons exhibit different trends. It increases with the collision energy ($\sqrt{S_{NN}}$). This dependence is presented in Fig. 10.1. The NA61/SHINE results are presented together with the existing world data [36, 40–47]. The most of the world data points came from bubble chambers experiments and they are presented without the error bars (statistical uncertainty of $20 - 70\%$).

Ratio of mean multiplicities of positive and negative kaons produced in protons interactions decreases with the collision energy, and around $40 \ GeV/c$ ($\sqrt{S_{NN}} = 8.8 \ GeV$) stabilize to the constant value. It is presented in Fig. 10.2 together with the available world data [36].
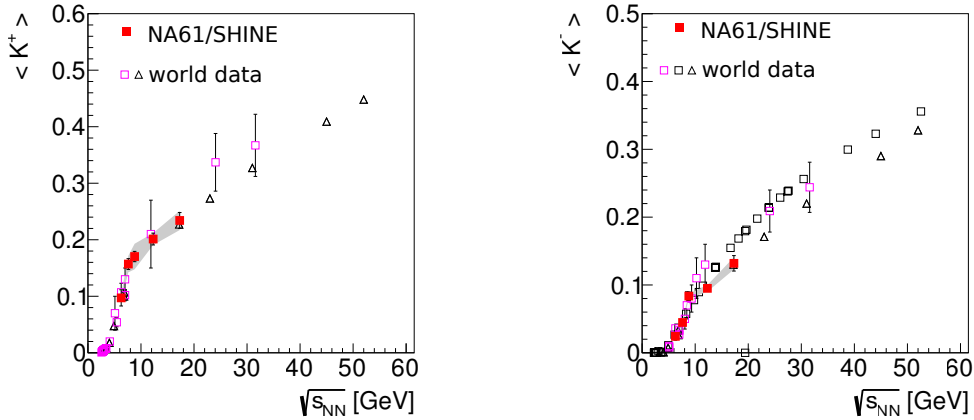
FIGURE 10.1: Mean kaons multiplicity produced in $p + p$ interactions as function of collision energy. Statistical uncertainties and systematical uncertainties of NA61/SHINE measurements are presented by lines and shadow band, respectively. Black empty triangles represent the compilation of world data, fully corrected for different effects [36]. Magenta empty squares came from Gazdzicki et al. [40]. Empty black squares are based on the parametrisation of the old bubble chamber data with statistical error of $20 - 70\%$ [42–47].
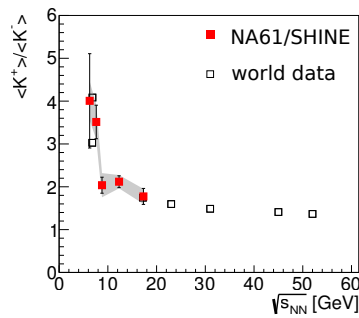
FIGURE 10.2: Ratio of mean charged kaons multiplicities as function of collision energy.

The NA61/SHINE measurements allow to study pions production properties. Dependence of the mean negatively and positively charged pions produced per an inelastic event is shown in Fig. 10.3. It can be seen, that $\langle \pi^{-/+} \rangle$ increases smoothly with the collision energy.

Ratio of mean charged pions multiplicities is presented in Fig. 10.4. It can be observed that at SPS energies range, $\langle \pi^+ \rangle / \langle \pi^- \rangle$ ratio slowly decreases with the collision energy. The NA61/SHINE results are in the agreement with other experiments data.
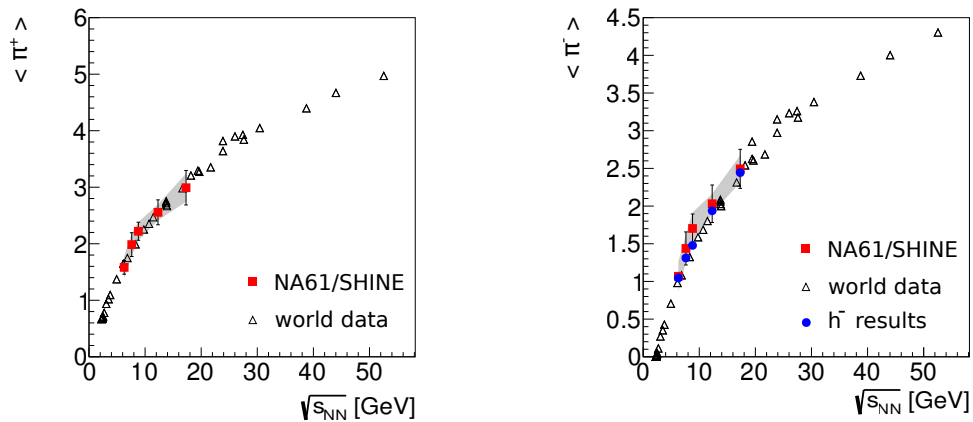
FIGURE 10.3: Mean pions multiplicity as the function of the collision energy. Black empty triangles represents the world data [48].
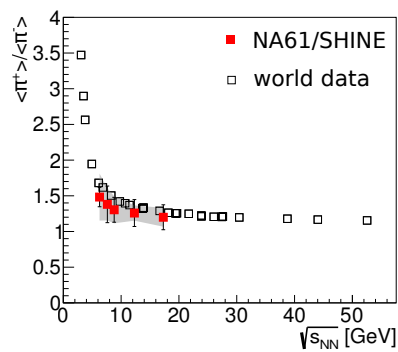
FIGURE 10.4: Ratio of $\langle \pi^+ \rangle / \langle \pi^- \rangle$ multiplicities in $p + p$ interactions as the function of the collision energy. World data is presented without uncertainties, thus the plot is more readable.

10.2 Transverse flow in $p + p$ and $Pb + Pb$ interactions at $158A\ GeV/c$

Spectra of transverse mass (m_T) of negatively and positively charged pions, kaons, protons and Λ hyperons [49] produced in inelastic $p + p$ interactions at $158\ GeV/c$ at mid-rapidity are presented in Fig. 10.5 (left panel). The corresponding data for central $Pb + Pb$ collisions measured by the NA49 experiment [50–52] are shown in the right panel of Fig. 10.5. These data were fitted using the simplified blast wave model

parameterization [53]:

$$\frac{dN_i}{m_T dm_T dy} = A_i m_T K_1\left(\frac{m_T cosh\rho}{T}\right) I_0\left(\frac{p_T sinh\rho}{T}\right). \tag{10.1}$$

The transverse flow velocity β_T was calculated from the equation:

$$\rho = \tanh^{-1}\beta_T. \tag{10.2}$$
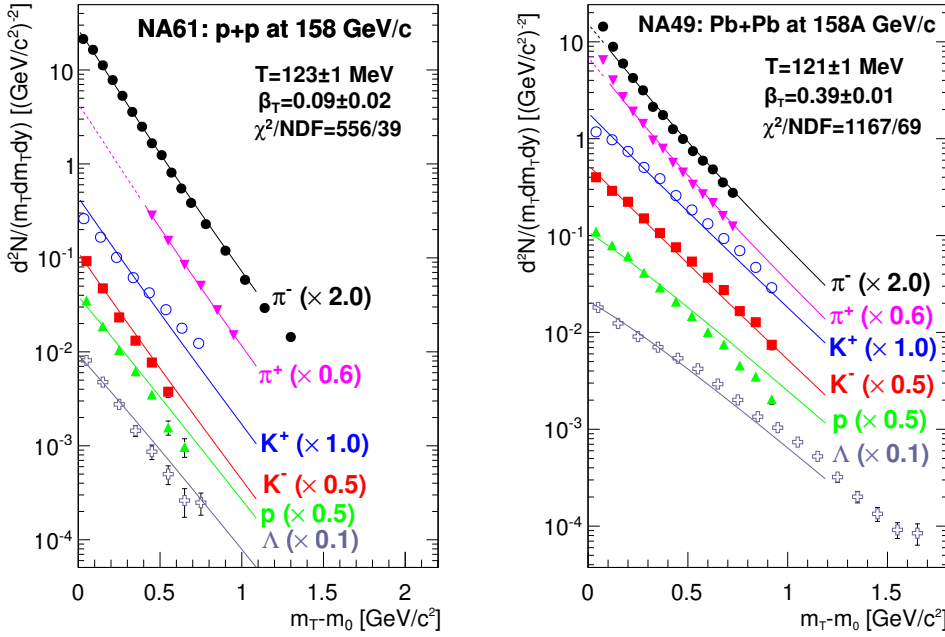
FIGURE 10.5: Scaled transverse mass spectra at mid-rapidity measured by the NA61/SHINE experiment in inelastic $p + p$ interactions (left panel) and corresponding results of NA49 [50–52] from central $Pb + Pb$ collisions at $158A$ GeV/c (right panel).

The shape of distribution is modified by the transverse flow and presented by the change of β_T value (see Table 10.1). The value of β_T is much higher in central $Pb + Pb$ collisions, than in $p + p$ reactions.

Parameter	$p + p$	$Pb + Pb$
T $[MeV]$	123 ± 1	121 ± 1
β_T	0.09 ± 0.02	0.39 ± 0.01

TABLE 10.1: Calculated blast wave fit parameters in $p + p$ and $Pb + Pb$ interaction at $158A$ GeV/c .

10.3 Study of the onset of deconfinement and theoretical models

10.3.1 Rapidity width of π^- spectra - dale

Rapidity distributions of π^- produced in inelastic $p+p$ collisions [39] and energy dependence of the width (σ) of the rapidity distribution divided by beam rapidity (σ/y_{beam}) or by the hydrodynamic model prediction (σ/σ_{LS}) [54, 55] are presented in Fig. 10.6. The shape of the rapidity distribution is approximately Gaussian, however the best fit was obtained by a sum of two Gaussian distributions. It can be seen that σ/y_{beam} decreases with the collision energy and the values of σ/σ_{LS} and σ/y_{beam} are smaller in $p+p$ than in $Pb+Pb$ interactions. There is not significant difference observed of the energy dependence for the width of the π^- rapidity distribution in $p+p$ and $Pb+Pb$ interactions.
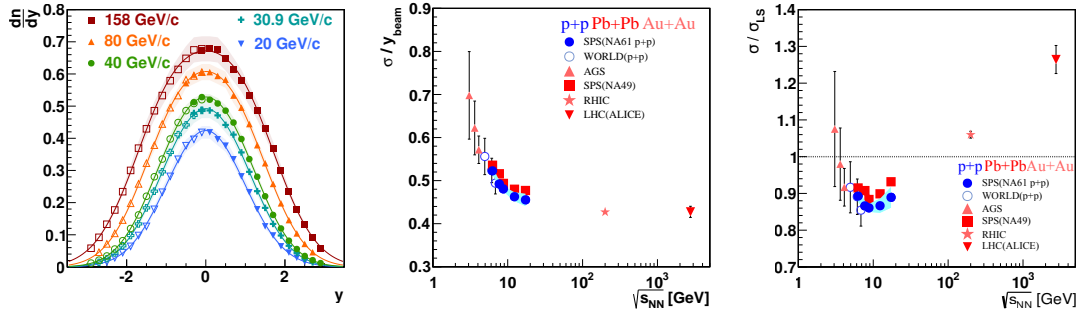
FIGURE 10.6: Rapidity distributions of π^- measured in inelastic $p+p$ collisions at 20, 30.9, 40, 80 and 158 GeV/c (left panel). Dependence of the scaled width of the rapidity distribution of collision energy (middle and right panels) compared with world data [56–58].

10.3.2 Mean pion multiplicity - kink

The presented results are an important step towards the study of the system size dependence of signals of the onset of deconfinement observed in central $Pb+Pb$ collisions (kink, horn and step) [51, 59]. The total π multiplicity at SPS energies shown in Fig. 10.7 increases faster in the central $Pb+Pb$ than in the inelastic $p+p$ collisions (kink structure). Moreover these two dependencies cross each other at about $40A\ GeV/c$.
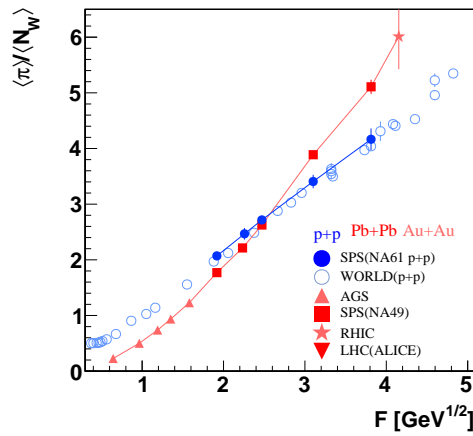
FIGURE 10.7: Comparison of the energy dependence of π multiplicity for $p + p$ and $Pb + Pb/Au + Au$ interactions.

10.3.3 Inverse slope parameter of kaons transverse mass spectra - step

The NA61/SHINE measurements allow to significantly improve the world data on the inverse slope parameter T of transverse mass spectra of kaons [60] as well as the ratio of K^+ and π^+ yields at the mid-rapidity region [40, 48].

Positively and negatively charged kaons spectra at mid-rapidity ($0.0 < y < 0.2$) are shown in Fig. 10.8. The p_T spectra were parametrized by the exponential function [61, 62]:

$$\frac{d^2n}{dp_T dy} = \frac{S \ p_T}{T^2 + m_K T} \exp\left(-\frac{\sqrt{p_T^2 + m_K^2} - m_K}{T}\right), \tag{10.3}$$

where: S and T are the yield integral and the inverse slope parameter, respectively. For better separation, spectra were scaled by the appropriate factors. Shadow bands correspond to systematic uncertainty of the measurements.

Figure 10.9 presents the energy dependence of the inverse slope parameter T of kaons (step structure). Surprisingly the NA61/SHINE results from inelastic $p + p$ collisions exhibit rapid changes like observed in central $Pb + Pb$ interactions.
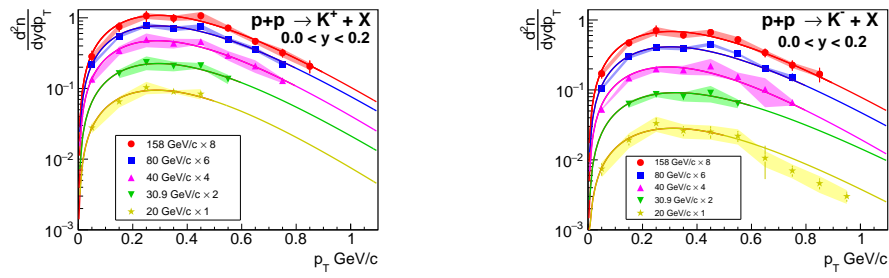
FIGURE 10.8: Transverse momentum spectra of K^+ and K^- mesons produced at $y \approx 0$ in inelastic $p + p$ interactions measured by the NA61/SHINE experiment. Color lines represent fitted function (Eq. 10.3).
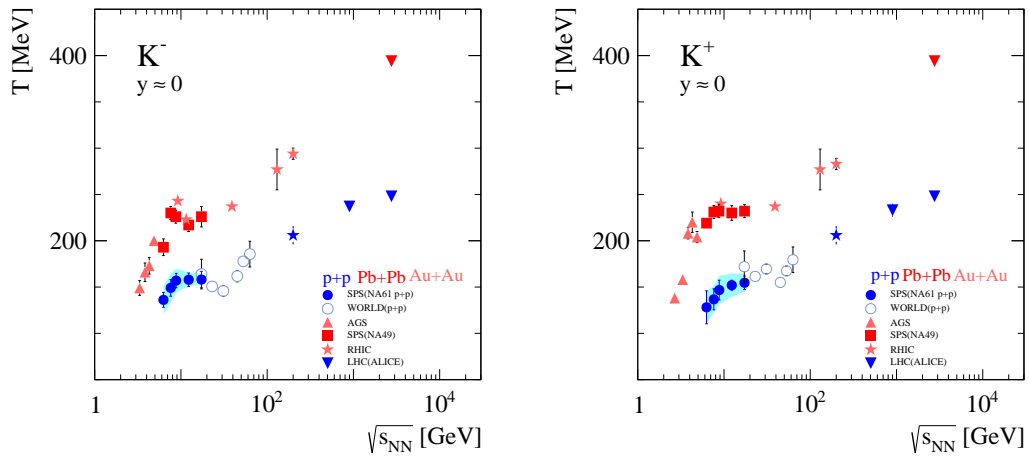
FIGURE 10.9: Energy dependence of the inverse slope parameter T of transverse mass spectra of kaons for inelastic $p+p$ interactions and central $Pb+Pb/Au+Au$ collisions [60, 63–65].

10.3.4 Kaons to pions ratio - horn

The acceptance of the identification methods used by NA61/SHINE does not allow to measure spectra of positive pions close to mid-rapidity region. Negatively charged pion spectra were obtained by NA61/SHINE in positive hemisphere using the h^- method. However this method cannot be used for positively charged pions due to the huge contribution of protons and positive kaons.

Therefore, in order to determine the mid-rapidity yield of positively charged pions, the following procedure was used:

- the $\langle \pi + \rangle / \langle \pi^- \rangle$ yields were calculated (within the acceptance of the $tof - dE/dx$

and dE/dx methods) and compared with EPOS model [66] predictions as a function of collision energy (see Fig. 10.10) with the agreement better than 0.1%,

- the mid-rapidity ratio of the π^+ and π^- yields was calculated from the EPOS model,

- the π^+ mid-rapidity yield was calculated as the product of the measured π^- yield (from h^- method) at $y = 0$, the measured $\frac{\pi+}{\pi-}$ ratio in the $tof - dE/dx$ acceptance and applying the EPOS correction factor:

$$\pi^+ (y = 0) = \pi^- (y = 0) \frac{\pi^+}{\pi^-} (tof - dE/dx) \, C_{MC}, \qquad (10.4)$$

where:

$$C_{MC} = \left[\frac{\frac{\pi^+}{\pi^-}(y = 0)}{\frac{\pi^+}{\pi^-}(tof)} \right]_{MC} \approx 5\%. \qquad (10.5)$$

The obtained values of the correction factor are presented in Fig. 10.10.
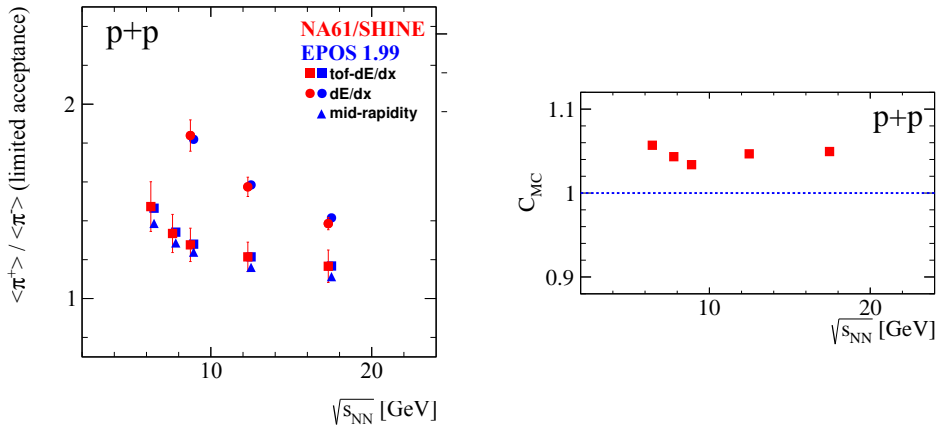
FIGURE 10.10: The $\langle \pi+ \rangle / \langle \pi^- \rangle$ in inelastic $p + p$ interactions calculated in the acceptance of the $tof - dE/dx$ and dE/dx identification methods. The NA61/SHINE results are compared to predictions of the EPOS model (left panel). The correction factor used to obtain π^+ yields from the measured π^- yields is presented in right panel.

Further study of the phase transition between hadron gas and quark-gluon plasma requires investigation of the strangeness to entropy ratio. This can be realized by study the ratio of koans to pions. The energy dependence of the K^+/π^+ and K^-/π^- ratios at mid-rapidity for inelastic $p + p$ interactions and central $Pb + Pb/Au + Au$ collisions are presented in Fig. 10.11. The NA61/SHINE data suggest that even in inelastic $p + p$ interactions the energy dependence of the K^+/π^+ ratio exhibits rapid changes in the SPS energy range. However, the horn structure is significantly reduced/modified in comparison to that observed in central $Pb + Pb$ collisions. In the Fig. 10.11 also the world

data [40, 48, 65, 67, 68] is plotted to present the global trend outside the SPS energy range.

The NA61/SHINE results were compared with theoretical models predictions [69], namely with EPOS [66], UrQMD [23, 24], Pythia 8 [70] and HSD [71]. It can be concluded that these models models do not describe well the NA61/SHINE results on $p + p$ interactions (see Fig. 10.12). However, high precision of NA61/SHINE data should result in significant improvement of models.
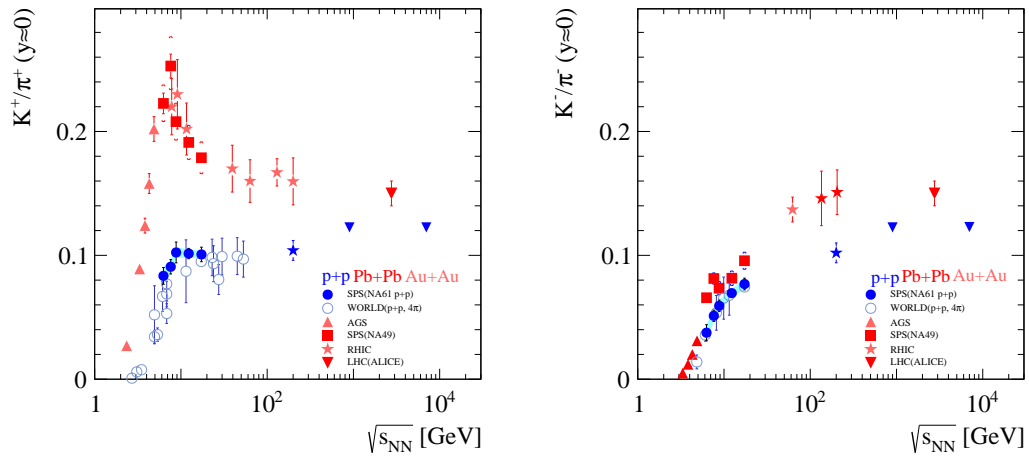
FIGURE 10.11: The K^+/π^+ and K^-/π^- ratios in inelastic $p + p$ and central $Pb + Pb/Au + Au$ reactions for different experimental data.
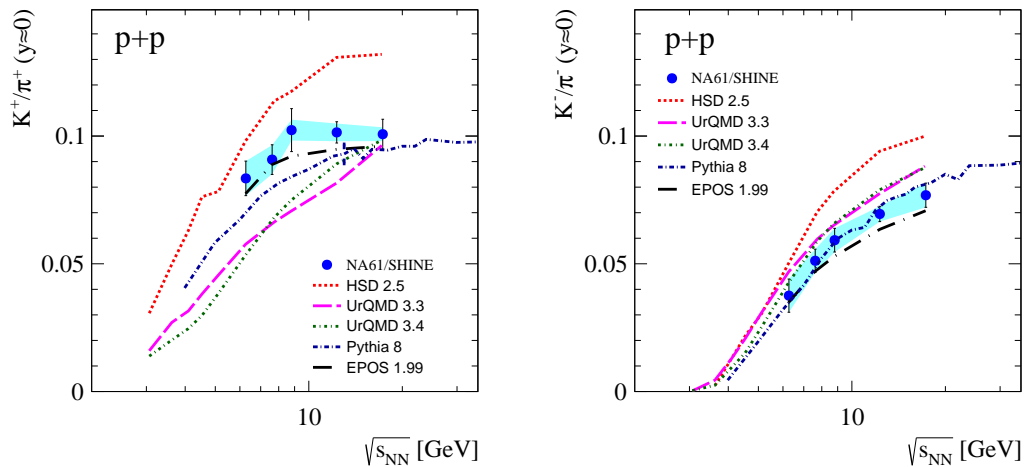
FIGURE 10.12: Comparison of $K^{+/-}/\pi^{+/-}$ ratios in inelastic $p + p$ collisions at SPS energies with theoretical models.

10.4   Mean transverse mass of protons

Proton transverse momentum spectra and mean proton transverse mass $\langle m_T \rangle$, around mid-rapidity, in inelastic $p + p$ interactions at SPS energies were also study. The results are presented, and compared with theoretical models, in Fig. 10.13. Mean m_T of protons was calculated from the data parametrization according to

$$\frac{d^2n}{dp_T dy} = \frac{S\ p_T}{T^2 + m_p T} \exp\left(-\frac{\sqrt{p_T^2 + m_p^2} - m_p}{T}\right). \tag{10.6}$$

It exhibits a slow increase with the collision energy in contradiction to the UrQMD or HSD models predictions [69].
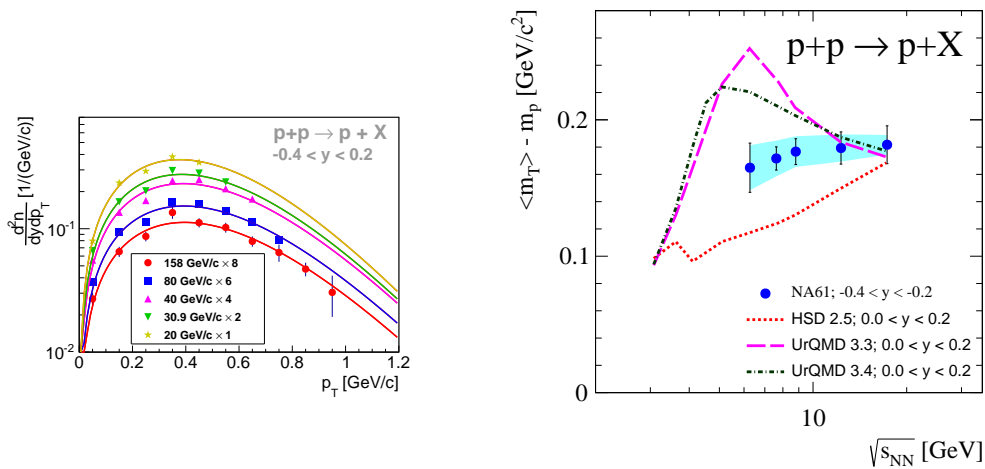
FIGURE 10.13: Proton transverse momentum spectra (left panel) and mean transverse mass m_T (right panel), around mid-rapidity, in inelastic $p + p$ interactions at SPS energies compared with theoretical models.

Presented in this chapter results show that $p + p$ collisions are unexpectedly interesting. Their suggest that even in inelastic $p + p$ interactions the energy dependence of the K^+/π^+ ratio and the inverse slope parameter of kaon transverse mass spectra (T) exhibits rapid changes in the SPS energy range. However, the structures, e.g. the step and horn, are significantly reduced/modified in comparison to those observed in central $Pb + Pb$ collisions. Understanding and explanation of this behavior is a new puzzle in heavy ion physics. The current level of knowledge and theoretical calculations based on the statistical models, with exact strangeness conservation, suggest that even in $p + p$ collisions we deal with the phase transition [72]. An alternative theory explain observed behavior as associated with the threshold and isospin effects [73]. Finally it can be concluded that new high precision NA61/SHINE results present challenges for models and should allow for their improvement.

Summary

The presented results were obtained from data collected by the NA61/SHINE collaboration at CERN SPS and they are the first step to study the onset of deconfinement.

The main goal of presented thesis was to calculate multiplicities of π^+, π^-, K^+, K^-, p and $\bar{p}$ produced in the inelastic $p + p$ collisions at following SPS momentum: 20, 30.9, 40, 80, 158 GeV/c. New analysis techniques based on the energy loss dE/dx and combined time of flight and energy loss $tof - dE/dx$ measurements were developed and described. These methods not only identify the particles but also allow to determine the particle yields independently of the detector effects, and correct them for particles originating from the weak decays. Additionally, statistical and systematic uncertainties were analyzed and presented.

The precise measurement of charged hadrons multiplicities presented in the thesis, is unique because for the first time results are presented in the two-dimensional distributions of rapidity and transverse momentum for five energies. Moreover, presented work completed the first level of the system size and collision energy scan of NA61/SHINE experiment.

Existing world data, mainly due to poor quality suggested that there is a smooth behavior of the quantities consider as the signatures of the onset of deconfinement. Due to good quality of the data analysed in this thesis shows that even in inelastic $p + p$ interactions, one can observer a signatures of the phase transition. Presented results show that even in inelastic $p + p$ interactions, the energy dependence of the K^+/π^+ ratio (horn structure) and the inverse slope parameter of kaon transverse mass spectra (step structure) exhibits rapid changes in the SPS energy range. However, the structures are significantly modified in comparison to those observed in the central $Pb + Pb$ collisions.

Understanding and explanation of presented high precision results is a new puzzle for heavy ion physics and present challenges for theoretical models. Additionally, in future NA61/SHINE collaboration plans to extended $p + p$ energy scan by the measurement of $p + p$ interactions at 350 GeV/c beam momentum to better understand presented structures.

Acknowledgements

List of Figures

List of Tables

Abbreviations

ADC   **A**nalog to **D**igital **C**onverter

BPD   **B**eam **P**osition **D**etector

CP   **C**ritical **P**oint

GTPC   **G**ap **T**ime **P**rojection **C**hamber

HG   **H**adron **G**as

LHT   **L**iquid **H**ydrogen **T**arget

MC   **M**onte-**C**arlo Simulation

MTPC   **M**ain **T**ime **P**rojection **C**hamber

MWPC   **M**ulti-**W**ire **P**roportional **C**hamber

PMT   **P**hoto**m**ultiplier **T**ube

PSD   **P**article **S**pectator **D**etector

QDC   **Charge** to **D**igital **C**onverter

QGP   **Q**uark-**G**luon **P**lasma

SMES   **S**tatistical **M**odel of the **E**arly **S**tage

SPS   **S**uper **P**roton **S**ynchrotron

TDC   **T**ime to **D**igital **C**onverter

THC   **T**hres**h**old **C**ounter

ToF   **T**ime **of** **F**light detector

tof   **t**ime **of** **f**light measurement

ToF-F   **F**orward **T**ime **of** **F**light detector

ToF-L   **L**eft **T**ime **of** **F**light detector

ToF-R   **R**ight **T**ime **of** **F**light detector

TPC   **T**ime **P**rojection **C**hamber

VTPC   **V**ertex **T**ime **P**rojection **C**hamber

WFA   **W**ave **F**orm **A**nalyzer

Appendix A

Kinematic Variables

This appendix introduces the main observables used in the heavy ion collisions.

A.1 Collision energy

A.1.1 Lorentz factor

The Lorentz factor, γ:

$$\gamma = \frac{1}{\sqrt{1 - \beta^2}} \ ,\tag{A.1}$$

where E and m are energy and mass of an object, respectively, and $\beta = v/c$ is the velocity expressed as a fraction of the speed of light.

A.1.2 Centre of Mass Energy

Two types of heavy ion experiments: fixed target and collider are performed. In the fixed target experiment, the energy is characterised by the incident beam energy or beam momentum. In collider experiments, the center of mass energy is used. The energy in the centre of mass frame per nucleon pair is given as:

$$\sqrt{s_{NN}} = \sqrt{(E_{beam} + E_{taget})^2 - |\mathbf{p}_{beam} + \mathbf{p}_{target}|^2} \ ,\tag{A.2}$$

where E and $\mathbf{p}$ denote energy and momentum vector of beam and target, respectively. In a fixed target experiment, the centre of mass energy is equal to

$$\sqrt{s_{NN}} = (E_{beam} + m_{target})^2 - p_{beam}^2 = 2E_{beam}m_{target} + m_{beam}^2 + m_{target}^2 \ , \qquad \text{(A.3)}$$

where m_{beam} and m_{target} are masses of beam and target nucleus or nuclei, respectively. In a collider experiment, the centre of mass energy per nucleon pair is merely the sum of energies of the incoming nucleons:

$$\sqrt{s_{NN}} = E_{beam} + E_{target} \ . \qquad \text{(A.4)}$$

A.2 Kinematic Variables

A.2.1 Total, transverse momentum and azimuthal angle

The total momentum is defined by the sum of all components of the momentum vector

$$p_{tot} = \sqrt{p_x^2 + p_y^2 + p_z^2} \ . \qquad \text{(A.5)}$$

Usually, the z coordinate is defined along the beam axis thus, the transverse momentum, p_T, which is perpendicular to the beam axis, reads

$$p_T = \sqrt{p_x^2 + p_y^2} \ . \qquad \text{(A.6)}$$

Also, commonly used is the so-called transverse mass, which is defined as:

$$m_T = \sqrt{p_T^2 + m^2} \ , \qquad \text{(A.7)}$$

where m is the rest mass of a particle.

The azimuthal angle is defined as:

$$\phi = arctan\left(\frac{p_y}{p_x}\right) \ . \qquad \text{(A.8)}$$

A.2.2 Rapidity

The rapidity, y is defined as follows:

$$y = \frac{1}{2}ln\left(\frac{E + p_z}{E - p_z}\right) = arctanh\left(\frac{p_z}{E}\right) = arctanh\left(\beta\right) \ . \tag{A.9}$$

The shape of rapidity distribution is invariant under the Lorentz transformation along the z (beam) axis, thus, transformation from the laboratory to centre-of-mass system frame is a linear shift in the y scale.

Appendix B

Numerical results

B.1 π^-, π^+ spectra

y	p_T [GeV/c]				
	0.1	0.2	0.2	0.4	0.5
-1.1	—	—	—	—	—
-0.9	—	—	—	—	—
-0.7	—	—	—	—	—
-0.5	—	—	—	—	—
-0.3	—	—	—	—	—
-0.1	—	—	—	—	—
0.1	—	—	—	—	—
0.3	—	—	—	0.8931±0.0301±0.0998	0.6138±0.0274±0.0976
0.5	0.3162±0.0204±0.0350	0.7209±0.0295±0.0806	1.0134±0.0441±0.1847	0.6273±0.0265±0.1060	0.4384±0.0166±0.0687
0.7	0.3351±0.0133±0.0375	0.7480±0.0285±0.1411	0.8594±0.0281±0.1464	0.6397±0.0225±0.0701	0.4157±0.0156±0.0545
0.9	0.3425±0.0148±0.0661	0.7664±0.0263±0.1331	0.8632±0.0290±0.1118	0.5975±0.0226±0.0554	0.3586±0.0146±0.0303
1.1	0.3795±0.0158±0.0644	0.8308±0.0329±0.1411	—	0.2901±0.0636±0.0233	0.1763±0.0237±0.0127
1.3	—	—	0.4801±0.1166±0.0288	0.3250±0.0253±0.0229	0.2272±0.0207±0.0189
1.5	—	—	0.3553±0.0306±0.0221	0.2493±0.0188±0.0214	0.1282±0.0737±0.0094
1.7	—	0.2571±0.0415±0.0207	0.3076±0.0190±0.0199	0.1414±0.0146±0.0105	—
1.9	0.1265±0.0884±0.0078	0.2874±0.0197±0.0198	0.2372±0.0136±0.0199	0.0822±0.0221±0.0068	—
2.1	0.1647±0.0141±0.0099	0.1441±0.0149±0.0110	0.0918±0.0164±0.0079	—	—
2.3	0.0749±0.0103±0.0054	0.1102±0.0132±0.0069	0.0491±0.0088±0.0030	—	—
2.5	0.0568±0.0083±0.0042	0.0489±0.0187±0.0038	—	—	—
2.7	0.0276±0.0086±0.0022	0.0324±0.0040±0.0026	—	—	—
2.9	—	—	—	—	—

y	p_T [GeV/c]				
	0.6	0.7	0.8	0.9	1.0
-1.1	—	—	—	—	—
-0.9	—	—	—	—	—
-0.7	—	—	—	—	—
-0.5	—	—	—	—	—
-0.3	—	—	—	—	—
-0.1	—	—	—	—	—
0.1	—	—	—	—	—
0.3	0.3643±0.0191±0.1176	0.2043±0.0143±0.0216	0.1217±0.0135±0.0145	0.0674±0.0124±0.0110	0.0363±0.0129±0.0040
0.5	0.2460±0.0161±0.0669	0.1395±0.0147±0.0216	0.0726±0.0072±0.0177	0.0395±0.0074±0.0065	0.0146±0.0017±0.0009
0.7	0.2349±0.0129±0.0217	0.1194±0.0124±0.0211	0.0614±0.0038±0.0049	0.0329±0.0033±0.0035	0.0160±0.0023±0.0014
0.9	0.2845±0.0207±0.0202	0.0915±0.0159±0.0055	0.0434±0.0159±0.0034	—	—
1.1	0.1552±0.0177±0.0136	0.0517±0.0311±0.0039	—	—	—
1.3	0.0899±0.0612±0.0056	—	—	—	—
1.5	—	—	—	—	—
1.7	—	—	—	—	—
1.9	—	—	—	—	—
2.1	—	—	—	—	—
2.3	—	—	—	—	—
2.5	—	—	—	—	—
2.7	—	—	—	—	—
2.9	—	—	—	—	—

TABLE B.1: Numerical results: $\frac{d^2n}{dydp_T}$ spectra of π^- produced in inelastic $p+p$ collisions at 20 GeV/c. Rapidity (y) and transverse momentum (p_T) values correspond to center of bins.

y	$p_T\ [GeV/c]$				
	0.1	0.2	0.3	0.4	0.5
-1.1	—	—	—	—	—
-0.9	—	—	—	—	—
-0.7	—	—	—	—	—
-0.5	—	—	—	—	—
-0.3	—	—	—	—	—
-0.1	—	—	—	—	—
0.1	—	—	—	—	0.7526±0.1822±0.0795
0.3	—	—	1.2426±0.2455±0.1640	—	0.7488±0.0390±0.1031
0.5	0.3880±0.0413±0.0000	1.0765±0.0632±0.1280	1.2156±0.0558±0.1841	0.9811±0.0643±0.1626	0.6815±0.0390±0.0983
0.7	0.3698±0.0149±0.0760	1.0380±0.0554±0.1498	1.1230±0.0627±0.1794	0.8967±0.0487±0.1388	0.6019±0.1602±0.0636
0.9	0.3601±0.0229±0.0693	0.9278±0.0568±0.1387	1.0019±0.0420±0.1320	0.8074±0.0988±0.0903	0.4115±0.0087±0.0339
1.1	0.3504±0.0152±0.0490	0.8894±0.0493±0.1047	—	0.5349±0.0104±0.0427	0.3745±0.0084±0.0298
1.3	—	—	0.6263±0.0116±0.0424	0.4312±0.0082±0.0317	0.2876±0.0068±0.0226
1.5	—	—	0.4756±0.0078±0.0410	0.3100±0.0064±0.0265	0.1940±0.0052±0.0149
1.7	—	0.4336±0.0076±0.0267	0.3685±0.0066±0.0293	0.2319±0.0053±0.0155	0.1364±0.0041±0.0084
1.9	0.1821±0.0053±0.0121	0.3471±0.0064±0.0248	0.2658±0.0056±0.0178	0.1572±0.0043±0.0123	0.0802±0.0031±0.0053
2.1	0.1396±0.0039±0.0112	0.2624±0.0056±0.0206	0.1827±0.0046±0.0158	0.0922±0.0033±0.0057	0.0446±0.0027±0.0038
2.3	0.1086±0.0035±0.0092	0.1840±0.0046±0.0150	0.1128±0.0037±0.0095	0.0487±0.0027±0.0030	—
2.5	0.0774±0.0031±0.0058	0.1111±0.0036±0.0094	0.0628±0.0029±0.0041	—	—
2.7	0.0693±0.0032±0.0045	0.0722±0.0030±0.0045	—	—	—
2.9	—	—	—	—	—

y	$p_T\ [GeV/c]$				
	0.6	0.7	0.8	0.9	1.0
-1.1	—	—	—	—	—
-0.9	—	—	—	—	—
-0.7	—	—	—	—	—
-0.5	—	—	—	—	—
-0.3	—	—	—	—	—
-0.1	—	—	—	—	—
0.1	0.4825±0.0391±0.0969	—	—	—	—
0.3	0.4480±0.0197±0.0840	—	—	0.0901±0.0042±0.0063	—
0.5	0.4182±0.0567±0.0593	0.2334±0.0068±0.0160	0.1448±0.0052±0.0124	0.0822±0.0039±0.0065	—
0.7	0.3396±0.0078±0.0275	0.2016±0.0060±0.0167	0.1237±0.0047±0.0089	0.0667±0.0035±0.0049	—
0.9	0.2734±0.0071±0.0180	0.1651±0.0055±0.0121	0.1042±0.0045±0.0093	—	—
1.1	0.2210±0.0066±0.0148	0.1422±0.0053±0.0095	0.0857±0.0044±0.0058	—	—
1.3	0.1607±0.0052±0.0127	0.0966±0.0040±0.0067	—	—	—
1.5	0.1096±0.0039±0.0082	0.0856±0.0040±0.0076	—	—	—
1.7	0.1161±0.0049±0.0093	—	—	—	—
1.9	—	—	—	—	—
2.1	—	—	—	—	—
2.3	—	—	—	—	—
2.5	—	—	—	—	—
2.7	—	—	—	—	—
2.9	—	—	—	—	—

TABLE B.2: Numerical results: $\frac{d^2n}{dydp_T}$ spectra of π^- produced in inelastic $p+p$ collisions at 30.9 GeV/c. Rapidity (y) and transverse momentum (p_T) values correspond to center of bins.

y	p_T [GeV/c]				
	0.1	0.2	0.2	0.4	0.5
-1.1	—	—	—	—	—
-0.9	—	—	—	—	—
-0.7	—	—	—	—	—
-0.5	—	—	—	—	—
-0.3	—	—	—	—	—
-0.1	—	—	—	—	—
0.1	—	—	—	—	0.6401±0.3121±0.0676
0.3	—	—	1.0590±0.2515±0.1397	0.9112±0.0448±0.1281	0.6397±0.0312±0.0881
0.5	—	0.9261±0.2540±0.1101	1.0355±0.0521±0.1568	0.8437±0.0488±0.1399	0.5919±0.0273±0.0854
0.7	0.3102±0.0208±0.0637	0.8852±0.0498±0.1278	0.9675±0.0518±0.1545	0.7769±0.0453±0.1202	0.5298±0.0205±0.0560
0.9	0.3004±0.0159±0.0578	0.7973±0.0441±0.1192	0.8720±0.0411±0.1149	0.7053±0.1188±0.0789	0.5054±0.0071±0.0000
1.1	0.2967±0.0160±0.0415	0.7659±0.0373±0.0902	0.7380±0.2043±0.0694	0.6517±0.0076±0.0000	0.4551±0.0065±0.0144
1.3	0.2580±0.0159±0.0343	0.7768±0.0199±0.0000	0.7434±0.0074±0.0000	0.5368±0.0064±0.0170	0.3585±0.0053±0.0135
1.5	—	0.6678±0.0078±0.0000	0.5940±0.0062±0.0168	0.4039±0.0052±0.0074	0.2624±0.0042±0.0053
1.7	0.2517±0.0062±0.0000	0.5350±0.0058±0.0293	0.4628±0.0054±0.0148	0.3047±0.0044±0.0052	0.1823±0.0034±0.0060
1.9	0.2096±0.0036±0.0000	0.4215±0.0052±0.0152	0.3468±0.0047±0.0046	0.2107±0.0037±0.0022	0.1180±0.0028±0.0000
2.1	0.1579±0.0031±0.0097	0.3183±0.0045±0.0081	0.2363±0.0039±0.0034	0.1346±0.0030±0.0023	0.0693±0.0022±0.0000
2.3	0.1329±0.0029±0.0094	0.2331±0.0039±0.0070	0.1502±0.0031±0.0019	0.0836±0.0024±0.0000	0.1121±0.0054±0.0000
2.5	0.0940±0.0025±0.0065	0.1591±0.0032±0.0034	0.0940±0.0025±0.0000	0.0973±0.0040±0.0000	—
2.7	0.0703±0.0022±0.0045	0.1148±0.0029±0.0036	0.0757±0.0027±0.0000	—	—
2.9	—	—	—	—	—

y	p_T [GeV/c]				
	0.6	0.7	0.8	0.9	1.0
-1.1	—	—	—	—	—
-0.9	—	—	—	—	—
-0.7	—	—	—	—	—
-0.5	—	—	—	—	—
-0.3	—	—	—	—	—
-0.1	—	—	—	—	—
0.1	0.4186±0.0536±0.0841	—	0.1549±0.0760±0.0339	0.1093±0.0036±0.0000	—
0.3	0.3856±0.0175±0.0723	0.2323±0.0268±0.0504	0.1448±0.0064±0.0250	0.1123±0.0034±0.0000	—
0.5	0.3663±0.0199±0.0519	0.2201±0.0117±0.0366	0.1208±0.0065±0.0249	0.0953±0.0030±0.0000	—
0.7	0.3112±0.0204±0.0307	0.1808±0.0270±0.0108	0.1389±0.0037±0.0029	0.0848±0.0029±0.0000	—
0.9	0.3428±0.0060±0.0135	0.2001±0.0045±0.0102	0.1207±0.0036±0.0062	0.1112±0.0043±0.0000	—
1.1	0.2836±0.0053±0.0131	0.1674±0.0041±0.0080	0.1002±0.0032±0.0077	—	—
1.3	0.2208±0.0041±0.0061	0.1290±0.0032±0.0000	0.1564±0.0057±0.0000	—	—
1.5	0.1605±0.0033±0.0049	0.0849±0.0024±0.0000	—	—	—
1.7	0.1035±0.0026±0.0000	0.1692±0.0065±0.0000	—	—	—
1.9	0.0616±0.0020±0.0000	—	—	—	—
2.1	0.0952±0.0048±0.0000	—	—	—	—
2.3	—	—	—	—	—
2.5	—	—	—	—	—
2.7	—	—	—	—	—
2.9	—	—	—	—	—

TABLE B.3: Numerical results: $\frac{d^2n}{dydp_T}$ spectra of π^- produced in inelastic $p+p$ collisions at 40 GeV/c. Rapidity (y) and transverse momentum (p_T) values correspond to center of bins.

y	p_T [GeV/c]				
	0.1	0.2	0.2	0.4	0.5
-1.1	—	—	—	—	—
-0.9	—	—	—	—	—
-0.7	—	—	—	—	—
-0.5	—	—	—	—	—
-0.3	—	—	—	—	—
-0.1	—	—	—	—	—
0.1	—	—	—	—	—
0.3	—	—	—	1.2707±0.3961±0.1184	0.8989±0.0690±0.1206
0.5	—	—	1.4788±0.9625±0.1430	1.2022±0.0639±0.1732	0.8428±0.0562±0.0494
0.7	—	1.2796±0.3172±0.0710	1.4044±0.1189±0.1352	1.1336±0.0804±0.0619	0.7847±0.0555±0.0500
0.9	0.4195±0.0366±0.0482	1.1455±0.0512±0.1240	1.3011±0.0880±0.0728	1.0637±0.0832±0.0477	0.6792±0.2481±0.0212
1.1	0.4072±0.0200±0.0202	1.1068±0.0726±0.0662	1.1366±0.1140±0.0577	0.7783±0.0071±0.0552	0.5340±0.0058±0.0551
1.3	0.3614±0.0208±0.0235	1.0005±0.0778±0.0482	0.8702±0.0075±0.0689	0.6515±0.0065±0.0715	0.4413±0.0053±0.0436
1.5	0.3242±0.0216±0.0187	0.8368±0.4804±0.0291	0.7318±0.0068±0.0752	0.5576±0.0060±0.0480	0.3732±0.0049±0.0355
1.7	0.2702±0.0042±0.0165	0.6182±0.0063±0.0409	0.5887±0.0061±0.0629	0.4289±0.0052±0.0424	0.2883±0.0043±0.0202
1.9	0.2232±0.0038±0.0161	0.5085±0.0057±0.0394	0.4611±0.0054±0.0385	0.3221±0.0045±0.0328	0.2027±0.0036±0.0191
2.1	0.1905±0.0035±0.0116	0.3865±0.0050±0.0321	0.3535±0.0048±0.0317	0.2311±0.0038±0.0247	0.1335±0.0029±0.0090
2.3	0.1583±0.0032±0.0135	0.3003±0.0044±0.0246	0.2467±0.0040±0.0207	0.1503±0.0031±0.0165	—
2.5	0.1201±0.0028±0.0130	0.2246±0.0038±0.0141	0.1673±0.0033±0.0180	0.0857±0.0023±0.0083	—
2.7	0.0905±0.0024±0.0099	0.1546±0.0031±0.0122	0.1023±0.0026±0.0066	—	—
2.9	—	—	—	—	—

y	p_T [GeV/c]				
	0.6	0.7	0.8	0.9	1.0
-1.1	—	—	—	—	—
-0.9	—	—	—	—	—
-0.7	—	—	—	—	—
-0.5	—	—	—	—	—
-0.3	—	—	—	—	—
-0.1	—	—	—	—	—
0.1	—	0.3475±0.0237±0.0221	0.2052±0.0036±0.0139	—	—
0.3	0.5496±0.0355±0.0531	0.3343±0.0201±0.0171	0.2150±0.0137±0.0106	0.1311±0.0029±0.0106	—
0.5	0.5349±0.0358±0.0348	0.3333±0.0266±0.0193	0.1894±0.0826±0.0170	—	—
0.7	0.4756±0.0438±0.0138	0.2840±0.0043±0.0283	0.1759±0.0034±0.0127	—	—
0.9	0.3768±0.0049±0.0263	0.2529±0.0040±0.0173	0.1473±0.0031±0.0146	—	—
1.1	0.3513±0.0047±0.0316	0.2141±0.0037±0.0181	0.1288±0.0029±0.0135	—	—
1.3	0.2775±0.0042±0.0173	0.1741±0.0033±0.0178	0.1063±0.0026±0.0085	0.0606±0.0020±0.0037	0.0296±0.0014±0.0019
1.5	0.2381±0.0039±0.0183	0.1346±0.0029±0.0143	0.0910±0.0024±0.0066	—	0.0246±0.0013±0.0017
1.7	0.1824±0.0034±0.0163	0.1137±0.0027±0.0117	—	—	—
1.9	0.1245±0.0028±0.0088	—	—	—	—
2.1	0.0719±0.0021±0.0077	—	—	—	—
2.3	—	—	—	—	—
2.5	—	—	—	—	—
2.7	—	—	—	—	—
2.9	—	—	—	—	—

TABLE B.4: Numerical results: $\frac{d^2n}{dydp_T}$ spectra of π^- produced in inelastic $p+p$ collisions at 80 GeV/c. Rapidity (y) and transverse momentum (p_T) values correspond to center of bins.

y	p_T [GeV/c]				
	0.1	0.2	0.2	0.4	0.5
-1.1	—	—	—	—	—
-0.9	—	—	—	—	—
-0.7	—	—	—	—	—
-0.5	—	—	—	—	—
-0.3	—	—	—	—	—
-0.1	—	—	—	—	—
0.1	—	—	—	—	—
0.3	—	—	—	—	0.9394±0.3899±0.1816
0.5	—	—	—	1.2534±0.4307±0.1523	0.9219±0.0802±0.0851
0.7	—	—	1.4880±0.6731±0.3909	1.2733±0.1232±0.1450	0.8745±0.0769±0.0794
0.9	—	—	1.4927±0.1315±0.1954	1.2036±0.1123±0.1126	0.7884±0.0779±0.0753
1.1	—	1.2051±0.1009±0.1501	1.3470±0.1105±0.1252	1.1111±0.1359±0.1143	0.6579±0.0064±0.0430
1.3	0.4874±0.0584±0.0609	1.0761±0.0800±0.0983	1.2165±0.1302±0.1151	0.8725±0.0073±0.0554	0.6013±0.0061±0.0410
1.5	0.4529±0.0431±0.0432	0.9853±0.0775±0.0924	0.9855±0.0078±0.0652	0.7660±0.0069±0.0534	0.5299±0.0057±0.0420
1.7	0.4045±0.0352±0.0408	0.8889±0.3170±0.0875	0.8469±0.0072±0.0579	0.6503±0.0063±0.0479	0.4491±0.0053±0.0362
1.9	0.3609±0.0660±0.0372	0.7056±0.0066±0.0499	0.7073±0.0066±0.0453	0.5258±0.0057±0.0430	0.3516±0.0047±0.0276
2.1	0.2566±0.0040±0.0160	0.5762±0.0060±0.0425	0.5637±0.0059±0.0434	0.4031±0.0050±0.0320	0.2640±0.0040±0.0243
2.3	0.2121±0.0036±0.0141	0.4672±0.0054±0.0305	0.4290±0.0051±0.0370	0.2902±0.0042±0.0214	0.1800±0.0033±0.0141
2.5	0.1833±0.0034±0.0085	0.3819±0.0049±0.0250	0.3198±0.0044±0.0259	0.2063±0.0036±0.0109	0.1180±0.0027±0.0113
2.7	0.1536±0.0031±0.0068	0.2896±0.0042±0.0203	0.2250±0.0037±0.0186	0.1403±0.0029±0.0418	—
2.9	—	—	—	—	—

y	p_T [GeV/c]				
	0.6	0.7	0.8	0.9	1.0
-1.1	—	—	—	—	—
-0.9	—	—	—	—	—
-0.7	—	—	—	—	—
-0.5	—	—	—	—	—
-0.3	—	—	—	0.1486±0.0030±0.0094	—
-0.1	—	0.3630±0.0047±0.0272	0.2261±0.0037±0.0249	0.1468±0.0030±0.0099	0.0936±0.0024±0.0065
0.1	0.5681±0.0059±0.0351	0.3711±0.0383±0.0379	0.2392±0.0663±0.0196	0.1533±0.0143±0.0135	0.0950±0.0024±0.0059
0.3	0.5992±0.0496±0.0573	0.3742±0.0297±0.0331	0.2418±0.0222±0.0221	0.1510±0.0198±0.0134	0.1045±0.0025±0.0079
0.5	0.5738±0.0466±0.0515	0.3580±0.0294±0.0331	0.2199±0.0479±0.0185	0.1355±0.0573±0.0110	0.0823±0.0023±0.0061
0.7	0.5395±0.0479±0.0483	0.3290±0.0509±0.0303	0.2088±0.0036±0.0124	0.1305±0.0028±0.0081	0.0870±0.0023±0.0077
0.9	0.4866±0.2389±0.0475	0.2910±0.0042±0.0201	0.1842±0.0034±0.0137	0.1120±0.0026±0.0069	0.0730±0.0021±0.0134
1.1	0.4401±0.0052±0.0368	0.2778±0.0041±0.0153	0.1746±0.0033±0.0094	0.1052±0.0025±0.0075	0.0613±0.0019±0.0065
1.3	0.3994±0.0050±0.0259	0.2420±0.0039±0.0194	0.1559±0.0031±0.0101	0.0956±0.0024±0.0072	—
1.5	0.3429±0.0046±0.0286	0.2108±0.0036±0.0137	0.1376±0.0029±0.0100	0.0786±0.0022±0.0138	0.0433±0.0016±0.0063
1.7	0.2879±0.0042±0.0217	0.1752±0.0033±0.0135	0.1068±0.0026±0.0110	0.0628±0.0020±0.0065	0.0330±0.0014±0.0035
1.9	0.2322±0.0038±0.0168	0.1310±0.0028±0.0095	0.0820±0.0022±0.0094	—	0.0246±0.0012±0.0024
2.1	0.1630±0.0032±0.0117	0.0971±0.0024±0.0121	—	—	—
2.3	0.1091±0.0026±0.0132	0.0565±0.0019±0.0042	—	—	—
2.5	—	—	—	—	—
2.7	—	—	—	—	—
2.9	—	—	—	—	—

TABLE B.5: Numerical results: $\frac{d^2n}{dydp_T}$ spectra of π^- produced in inelastic $p+p$ collisions at 158 GeV/c. Rapidity (y) and transverse momentum (p_T) values correspond to center of bins.

y	p_T [GeV/c]				
	0.1	0.2	0.2	0.4	0.5
-1.1	—	—	—	—	—
-0.9	—	—	—	—	—
-0.7	—	—	—	—	—
-0.5	—	—	—	—	—
-0.3	—	—	—	—	—
-0.1	—	—	—	—	—
0.1	—	—	—	—	—
0.3	—	—	—	1.2559±0.0709±0.1404	0.8091±0.0379±0.1235
0.5	0.4676±0.0236±0.0522	1.1203±0.0431±0.1253	1.3512±0.0623±0.2295	0.8914±0.0466±0.1183	0.6042±0.0330±0.0651
0.7	0.5094±0.0203±0.0570	1.2455±0.0484±0.2026	1.3604±0.0509±0.2144	0.9206±0.0332±0.0894	0.5773±0.0254±0.0371
0.9	0.5123±0.0187±0.0868	1.1493±0.0406±0.1981	1.5461±0.0509±0.1848	0.9782±0.0367±0.0667	0.5790±0.0859±0.0955
1.1	0.5037±0.0199±0.0849	1.0926±0.0594±0.1222	—	0.5377±0.0843±0.0356	0.3004±0.0290±0.0211
1.3	—	—	0.8925±0.1380±0.0458	0.6806±0.0340±0.0549	0.4358±0.0258±0.0298
1.5	—	—	0.7100±0.0417±0.0491	0.5665±0.0267±0.0442	0.2816±0.0195±0.0231
1.7	—	0.4620±0.0569±0.0411	0.6840±0.0274±0.0577	0.3567±0.0215±0.0195	0.2369±0.0153±0.0168
1.9	0.2138±0.1545±0.0163	0.5743±0.0295±0.0326	0.5888±0.0220±0.0310	0.2270±0.0149±0.0189	0.0897±0.0099±0.0071
2.1	0.3018±0.0214±0.0214	0.3168±0.0239±0.0254	0.2578±0.0183±0.0157	0.1617±0.0130±0.0093	0.0259±0.0069±0.0022
2.3	0.1527±0.0169±0.0118	0.2759±0.0205±0.0197	0.1546±0.0137±0.0091	0.0480±0.0086±0.0041	0.0092±0.0037±0.0007
2.5	0.1327±0.0156±0.0100	0.1434±0.0159±0.0112	0.0705±0.0101±0.0054	0.0229±0.0053±0.0019	0.0014±0.0027±0.0001
2.7	0.0718±0.0121±0.0040	0.1048±0.0120±0.0056	0.0341±0.0068±0.0026	0.0018±0.0038±0.0001	—
2.9	—	—	—	—	—

y	p_T [GeV/c]				
	0.6	0.7	0.8	0.9	1.0
-1.1	—	—	—	—	—
-0.9	—	—	—	—	—
-0.7	—	—	—	—	—
-0.5	—	—	—	—	—
-0.3	—	—	—	—	—
-0.1	—	—	—	—	—
0.1	—	—	—	0.0975±0.0097±0.0109	—
0.3	0.4883±0.0319±0.0412	0.2821±0.0222±0.0190	0.1525±0.0126±0.0142	0.0920±0.0115±0.0202	—
0.5	0.3415±0.0270±0.0322	0.1947±0.0215±0.0229	0.1066±0.0118±0.0135	0.0568±0.0119±0.0091	0.0205±0.0174±0.0011
0.7	0.3543±0.0262±0.0412	0.1968±0.0127±0.0151	0.0941±0.0118±0.0131	0.0509±0.0035±0.0044	0.0261±0.0087±0.0019
0.9	0.4562±0.0259±0.0323	0.1529±0.0203±0.0083	0.0789±0.0155±0.0069	0.0518±0.0107±0.0028	0.0137±0.0073±0.0010
1.1	0.2727±0.0228±0.0155	0.1006±0.0176±0.0056	0.0542±0.0127±0.0034	0.0297±0.0095±0.0019	0.0161±0.0069±0.0010
1.3	0.1836±0.0192±0.0157	0.0730±0.0154±0.0056	0.0387±0.0105±0.0031	0.0149±0.0182±0.0012	0.0054±0.8855±0.0004
1.5	0.1439±0.0141±0.0107	0.0490±0.0108±0.0032	0.0308±0.0075±0.0019	—	—
1.7	0.0827±0.0103±0.0053	0.0243±0.0073±0.0014	0.0089±0.0035±0.0006	—	—
1.9	0.0427±0.0066±0.0037	0.0070±0.0032±0.0006	0.0024±0.0007±0.0002	—	—
2.1	0.0109±0.0029±0.0009	0.0014±0.0012±0.0001	0.0000±0.0008±0.0000	—	—
2.3	0.0009±0.0010±0.0001	0.0000±0.0001±0.0000	—	—	—
2.5	—	—	—	—	—
2.7	—	—	—	—	—
2.9	—	—	—	—	—

TABLE B.6: Numerical results: $\frac{d^2n}{dydp_T}$ spectra of π^+ produced in inelastic $p + p$ collisions at 20 GeV/c. Rapidity (y) and transverse momentum (p_T) values correspond to center of bins.

y	$p_T \ [GeV/c]$				
	0.1	0.2	0.2	0.4	0.5
-1.1	—	—	—	—	—
-0.9	—	—	—	—	—
-0.7	—	—	—	—	—
-0.5	—	—	—	—	—
-0.3	—	—	—	—	—
-0.1	—	—	—	—	—
0.1	—	—	—	—	0.9099±0.4183±0.1381
0.3	—	—	1.5939±0.2952±0.1222	—	0.8987±0.0377±0.1342
0.5	0.5479±0.1089±0.0000	1.5265±0.0829±0.2102	1.6661±0.0835±0.2520	1.2655±0.0854±0.2293	0.8184±0.0440±0.1598
0.7	0.5121±0.0190±0.0764	1.4091±0.0711±0.1942	1.6236±0.1014±0.2974	1.1744±0.0532±0.2091	0.7699±0.0927±0.1363
0.9	0.5083±0.0378±0.0886	1.3374±0.0695±0.2534	1.4998±0.0587±0.2454	1.1420±0.1852±0.2009	0.6101±0.0105±0.0439
1.1	0.4735±0.0170±0.0912	1.2298±0.0767±0.2027	—	0.7931±0.0124±0.0514	0.5400±0.0099±0.0270
1.3	—	—	0.9642±0.0141±0.0616	0.6515±0.0099±0.0527	0.4361±0.0083±0.0229
1.5	—	—	0.8634±0.0106±0.0453	0.5714±0.0088±0.0355	0.3529±0.0070±0.0289
1.7	—	0.7613±0.0102±0.0383	0.7214±0.0093±0.0488	0.4440±0.0074±0.0324	0.2445±0.0055±0.0182
1.9	0.2718±0.0068±0.0171	0.6593±0.0089±0.0566	0.5734±0.0083±0.0376	0.3279±0.0063±0.0236	0.1707±0.0046±0.0099
2.1	0.2461±0.0055±0.0195	0.5731±0.0083±0.0428	0.4107±0.0070±0.0353	0.2115±0.0051±0.0185	0.0941±0.0034±0.0047
2.3	0.2197±0.0052±0.0181	0.4642±0.0074±0.0340	0.2475±0.0054±0.0157	0.1317±0.0040±0.0103	0.0416±0.0023±0.0033
2.5	0.2068±0.0051±0.0143	0.3282±0.0063±0.0256	0.1583±0.0044±0.0096	0.0631±0.0029±0.0035	0.0131±0.0014±0.0011
2.7	0.1882±0.0049±0.0134	0.2107±0.0051±0.0175	0.0825±0.0033±0.0051	0.0210±0.0018±0.0014	0.0022±0.0007±0.0002
2.9	—	—	—	—	—

y	$p_T \ [GeV/c]$				
	0.6	0.7	0.8	0.9	1.0
-1.1	—	—	—	—	—
-0.9	—	—	—	—	—
-0.7	—	—	—	—	—
-0.5	—	—	—	—	—
-0.3	—	—	—	—	—
-0.1	—	—	—	—	—
0.1	0.5613±0.0515±0.0765	—	0.2016±0.0941±0.0550	—	0.0805±0.0043±0.0062
0.3	0.5669±0.0226±0.1083	0.3357±0.0471±0.0684	0.2016±0.0085±0.0388	0.1155±0.0047±0.0068	0.0715±0.0037±0.0061
0.5	0.4978±0.0197±0.0896	0.2970±0.0114±0.0431	0.1725±0.0067±0.0238	0.1156±0.0046±0.0096	0.0709±0.0036±0.0040
0.7	0.4530±0.0177±0.0775	0.2807±0.0305±0.0610	0.1533±0.0172±0.0000	0.0999±0.0042±0.0078	0.0574±0.0032±0.0044
0.9	0.4103±0.0086±0.0226	0.2481±0.0067±0.0133	0.1525±0.0052±0.0116	0.0776±0.0037±0.0040	0.0534±0.0031±0.0029
1.1	0.3437±0.0080±0.0253	0.2166±0.0064±0.0167	0.1262±0.0049±0.0083	0.0672±0.0035±0.0058	0.0422±0.0028±0.0029
1.3	0.2848±0.0069±0.0151	0.1701±0.0054±0.0144	0.1003±0.0041±0.0068	0.0513±0.0030±0.0040	0.0227±0.0019±0.0013
1.5	0.2026±0.0054±0.0162	0.1194±0.0041±0.0060	0.0574±0.0029±0.0041	0.0313±0.0022±0.0027	0.0101±0.0012±0.0007
1.7	0.1431±0.0042±0.0112	0.0714±0.0030±0.0063	0.0306±0.0020±0.0018	0.0112±0.0012±0.0009	0.0043±0.0008±0.0002
1.9	0.0816±0.0032±0.0064	0.0327±0.0020±0.0024	0.0094±0.0011±0.0005	0.0036±0.0007±0.0003	0.0005±0.0003±0.0000
2.1	0.0342±0.0021±0.0023	0.0110±0.0012±0.0006	0.0013±0.0004±0.0001	0.0003±0.0002±0.0000	—
2.3	0.0093±0.0011±0.0006	0.0026±0.0006±0.0002	—	—	—
2.5	0.0027±0.0008±0.0002	—	—	—	—
2.7	—	—	—	—	—
2.9	—	—	—	—	—

TABLE B.7: Numerical results: $\frac{d^2n}{dy dp_T}$ spectra of π^+ produced in inelastic $p + p$ collisions at 30.9 GeV/c. Rapidity (y) and transverse momentum (p_T) values correspond to center of bins.

y	p_T [GeV/c]				
	0.1	0.2	0.2	0.4	0.5
-1.1	—	—	—	—	—
-0.9	—	—	—	—	—
-0.7	—	—	—	—	—
-0.5	—	—	—	—	—
-0.3	—	—	—	—	—
-0.1	—	—	—	—	—
0.1	—	—	—	—	—
0.3	—	—	1.6386±0.4767±0.1256	1.4088±0.0707±0.3302	0.9365±0.0390±0.1399
0.5	—	1.5579±0.4623±0.2146	1.6952±0.1021±0.2564	1.3133±0.0652±0.2380	0.8543±0.0392±0.1669
0.7	0.5249±0.0314±0.0783	1.4632±0.0758±0.2017	1.6555±0.0849±0.3033	1.2131±0.0555±0.2159	0.8145±0.0302±0.1441
0.9	0.5204±0.0281±0.0907	1.3932±0.0733±0.2640	1.5546±0.0612±0.2544	1.1867±0.1640±0.2087	0.6922±0.0081±0.0214
1.1	0.4808±0.0223±0.0926	1.2925±0.0450±0.2131	1.2409±0.0149±0.0000	0.9031±0.0089±0.0000	0.6402±0.0076±0.0189
1.3	0.4340±0.0236±0.0744	1.0903±0.0232±0.0000	1.1495±0.0093±0.0000	0.8356±0.0080±0.0278	0.5513±0.0065±0.0154
1.5	—	0.9847±0.0095±0.0000	1.0019±0.0081±0.0168	0.6928±0.0069±0.0181	0.4465±0.0055±0.0161
1.7	0.3309±0.0073±0.0000	0.8563±0.0075±0.0218	0.8591±0.0075±0.0086	0.5691±0.0061±0.0144	0.3433±0.0048±0.0083
1.9	0.2875±0.0044±0.0000	0.7106±0.0068±0.0139	0.6971±0.0067±0.0067	0.4317±0.0053±0.0113	0.2367±0.0040±0.0072
2.1	0.2602±0.0042±0.0194	0.6280±0.0064±0.0173	0.5088±0.0057±0.0083	0.2842±0.0043±0.0084	0.1494±0.0032±0.0072
2.3	0.2329±0.0039±0.0242	0.5320±0.0059±0.0152	0.3608±0.0048±0.0079	0.1848±0.0035±0.0111	0.0812±0.0024±0.0047
2.5	0.2150±0.0038±0.0251	0.4274±0.0053±0.0212	0.2315±0.0039±0.0124	0.1056±0.0027±0.0066	0.0287±0.0015±0.0022
2.7	0.2058±0.0038±0.0177	0.2916±0.0045±0.0212	0.1336±0.0031±0.0134	0.0417±0.0018±0.0045	0.0074±0.0008±0.0032
2.9	—	—	—	—	—

y	p_T [GeV/c]				
	0.6	0.7	0.8	0.9	1.0
-1.1	—	—	—	—	—
-0.9	—	—	—	—	—
-0.7	—	—	—	—	—
-0.5	—	—	—	—	—
-0.3	—	—	—	—	—
-0.1	—	—	—	—	0.0897±0.0044±0.0000
0.1	0.5850±0.0413±0.0797	0.3660±0.0149±0.0438	0.2129±0.0886±0.0580	0.1321±0.0057±0.0211	0.0879±0.0031±0.0000
0.3	0.5977±0.0273±0.1141	0.3581±0.0145±0.0730	0.2181±0.0093±0.0420	0.1239±0.0052±0.0250	0.0841±0.0029±0.0041
0.5	0.5359±0.0197±0.0964	0.3212±0.0111±0.0467	0.1907±0.0068±0.0263	0.1120±0.0061±0.0161	0.0787±0.0027±0.0051
0.7	0.4930±0.0342±0.0843	0.3120±0.0844±0.0678	0.1943±0.0043±0.0061	0.1087±0.0032±0.0038	0.0739±0.0026±0.0071
0.9	0.4613±0.0067±0.0117	0.2953±0.0054±0.0174	0.1739±0.0042±0.0059	0.0986±0.0032±0.0053	0.0606±0.0025±0.0019
1.1	0.4241±0.0063±0.0153	0.2693±0.0051±0.0072	0.1574±0.0039±0.0060	0.0877±0.0030±0.0036	0.0483±0.0022±0.0036
1.3	0.3589±0.0053±0.0133	0.2205±0.0042±0.0063	0.1264±0.0032±0.0043	0.0709±0.0024±0.0060	0.0328±0.0017±0.0045
1.5	0.2811±0.0044±0.0104	0.1730±0.0035±0.0058	0.0917±0.0025±0.0040	0.0461±0.0018±0.0032	0.0213±0.0012±0.0012
1.7	0.2025±0.0037±0.0067	0.1151±0.0028±0.0056	0.0591±0.0020±0.0026	0.0243±0.0013±0.0027	0.0088±0.0008±0.0025
1.9	0.1217±0.0029±0.0043	0.0606±0.0020±0.0067	0.0244±0.0013±0.0017	0.0083±0.0008±0.0003	0.0020±0.0004±0.0007
2.1	0.0625±0.0021±0.0065	0.0231±0.0013±0.0020	0.0074±0.0007±0.0017	0.0018±0.0004±0.0007	—
2.3	0.0220±0.0013±0.0025	0.0076±0.0008±0.0028	0.0017±0.0004±0.0013	0.0004±0.0002±0.0000	—
2.5	0.0053±0.0007±0.0010	0.0015±0.0004±0.0000	0.0031±0.0022±0.0000	—	—
2.7	0.0021±0.0005±0.0000	—	—	—	—
2.9	—	—	—	—	—

TABLE B.8: Numerical results: $\frac{d^2n}{dydp_T}$ spectra of π^+ produced in inelastic $p+p$ collisions at 40 GeV/c. Rapidity (y) and transverse momentum (p_T) values correspond to center of bins.

y	p_T [GeV/c]				
	0.1	0.2	0.2	0.4	0.5
-1.1	—	—	—	—	—
-0.9	—	—	—	—	—
-0.7	—	—	—	—	—
-0.5	—	—	—	—	—
-0.3	—	—	—	—	—
-0.1	—	—	—	—	—
0.1	—	—	—	—	1.0018±0.7452±0.0700
0.3	—	—	—	1.4925±0.4781±0.1018	1.0038±0.0693±0.0725
0.5	—	—	1.7853±0.5378±0.1243	1.3953±0.0781±0.1016	0.9378±0.0555±0.0612
0.7	—	1.5216±0.4102±0.1112	1.7352±0.1086±0.1269	1.3149±0.0802±0.0801	0.9138±0.0536±0.0394
0.9	0.5565±0.0636±0.0470	1.5019±0.0828±0.1102	1.6192±0.1004±0.0955	1.2903±0.0798±0.0536	0.8739±0.5971±0.0409
1.1	0.5095±0.0233±0.0363	1.4217±0.0859±0.0888	1.5727±0.1308±0.0561	1.0051±0.0080±0.0000	0.7205±0.0068±0.0000
1.3	0.4597±0.0263±0.0294	1.2677±0.0895±0.0530	1.1809±0.0087±0.0000	0.9002±0.0076±0.0000	0.6289±0.0063±0.0000
1.5	0.4535±0.0308±0.0153	1.0086±0.0080±0.0000	1.0803±0.0083±0.0000	0.8350±0.0073±0.0000	0.5657±0.0060±0.0000
1.7	0.3328±0.0046±0.0000	0.8876±0.0075±0.0000	0.9577±0.0078±0.0000	0.6840±0.0066±0.0000	0.4727±0.0055±0.0000
1.9	0.2935±0.0043±0.0000	0.7525±0.0069±0.0000	0.7804±0.0071±0.0000	0.5665±0.0060±0.0000	0.3621±0.0048±0.0000
2.1	0.2484±0.0040±0.0000	0.6330±0.0064±0.0000	0.6495±0.0064±0.0000	0.4508±0.0054±0.0000	0.2697±0.0042±0.0000
2.3	0.2249±0.0038±0.0000	0.5485±0.0059±0.0000	0.5064±0.0057±0.0000	0.3278±0.0046±0.0000	0.1808±0.0034±0.0000
2.5	0.2043±0.0036±0.0000	0.4828±0.0056±0.0000	0.3853±0.0050±0.0000	0.2198±0.0038±0.0000	0.1130±0.0027±0.0000
2.7	0.1722±0.0033±0.0000	0.3867±0.0050±0.0000	0.2608±0.0041±0.0000	0.1350±0.0029±0.0000	0.0553±0.0019±0.0000
2.9	—	—	—	—	—

y	p_T [GeV/c]				
	0.6	0.7	0.8	0.9	1.0
-1.1	—	—	—	—	—
-0.9	—	—	—	—	—
-0.7	—	—	—	—	—
-0.5	—	—	—	—	—
-0.3	—	—	—	—	—
-0.1	—	—	0.2468±0.0269±0.0158	—	—
0.1	0.6350±0.0475±0.0503	0.3991±0.0267±0.0200	0.2408±0.0130±0.0106	0.1519±0.0418±0.0139	0.1018±0.0026±0.0000
0.3	0.6504±0.0426±0.0356	0.3984±0.0236±0.0254	0.2512±0.0137±0.0104	0.1472±0.0448±0.0070	0.1011±0.0025±0.0000
0.5	0.5875±0.0335±0.0299	0.3648±0.0211±0.0136	0.2239±0.0615±0.0076	0.1500±0.0031±0.0000	0.0965±0.0025±0.0000
0.7	0.5616±0.0554±0.0506	0.3512±0.0047±0.0000	0.2195±0.0037±0.0000	0.1376±0.0030±0.0000	0.0848±0.0023±0.0000
0.9	0.5125±0.0057±0.0000	0.3186±0.0045±0.0000	0.1940±0.0035±0.0000	0.1221±0.0028±0.0000	0.0710±0.0021±0.0000
1.1	0.4703±0.0055±0.0000	0.2997±0.0044±0.0000	0.1829±0.0034±0.0000	0.1084±0.0026±0.0000	0.0626±0.0020±0.0000
1.3	0.4290±0.0052±0.0000	0.2618±0.0041±0.0000	0.1588±0.0032±0.0000	0.0937±0.0024±0.0000	0.0544±0.0019±0.0000
1.5	0.3737±0.0049±0.0000	0.2349±0.0039±0.0000	0.1350±0.0029±0.0000	0.0758±0.0022±0.0000	0.0406±0.0016±0.0000
1.7	0.3039±0.0044±0.0000	0.1904±0.0035±0.0000	0.1062±0.0026±0.0000	0.0591±0.0019±0.0000	0.0293±0.0014±0.0000
1.9	0.2293±0.0038±0.0000	0.1406±0.0030±0.0000	0.0760±0.0022±0.0000	0.0386±0.0016±0.0000	0.0168±0.0010±0.0000
2.1	0.1562±0.0032±0.0000	0.0917±0.0024±0.0000	0.0440±0.0017±0.0000	0.0183±0.0011±0.0000	0.0073±0.0007±0.0000
2.3	0.0889±0.0024±0.0000	0.0506±0.0018±0.0000	0.0200±0.0011±0.0000	0.0080±0.0007±0.0000	0.0025±0.0004±0.0000
2.5	0.0528±0.0018±0.0000	0.0183±0.0011±0.0000	0.0059±0.0006±0.0000	0.0020±0.0004±0.0000	0.0005±0.0002±0.0000
2.7	0.0180±0.0011±0.0000	—	—	0.0003±0.0001±0.0000	—
2.9	—	—	—	—	—

TABLE B.9: Numerical results: $\frac{d^2n}{dydp_T}$ spectra of π^+ produced in inelastic $p + p$ collisions at 80 GeV/c. Rapidity (y) and transverse momentum (p_T) values correspond to center of bins.

y	p_T [GeV/c]				
	0.1	0.2	0.2	0.4	0.5
-1.1	—	—	—	—	—
-0.9	—	—	—	—	—
-0.7	—	—	—	—	—
-0.5	—	—	—	—	—
-0.3	—	—	—	—	—
-0.1	—	—	—	—	—
0.1	—	—	—	—	—
0.3	—	—	—	—	1.0306±0.5150±0.1198
0.5	—	—	—	1.4244±0.4784±0.1613	1.0165±0.0802±0.0915
0.7	—	—	1.7179±0.8077±0.1893	1.3839±0.1178±0.1800	0.9682±0.0799±0.0819
0.9	—	—	1.6989±0.1410±0.1464	1.3675±0.1164±0.1158	0.9577±0.1036±0.0891
1.1	—	1.4363±0.1171±0.1548	1.5694±0.1189±0.1295	1.2425±0.1275±0.1150	0.8206±0.0071±0.0616
1.3	0.6231±0.0844±0.0687	1.4911±0.1254±0.1249	1.5062±0.1623±0.1341	1.1150±0.0083±0.0819	0.7828±0.0069±0.0581
1.5	0.5451±0.0487±0.0486	1.2956±0.1068±0.1179	1.2847±0.0089±0.0931	1.0173±0.0079±0.0785	0.7244±0.0067±0.0565
1.7	0.5221±0.0498±0.0495	1.1784±0.3914±0.1219	1.1788±0.0085±0.0856	0.9120±0.0075±0.0716	0.6606±0.0064±0.0500
1.9	0.4665±0.1439±0.0448	0.9408±0.0076±0.0566	1.0318±0.0080±0.0610	0.7999±0.0070±0.0639	0.5531±0.0058±0.0484
2.1	0.3167±0.0044±0.0219	0.8105±0.0071±0.0586	0.8937±0.0074±0.0436	0.6671±0.0064±0.0495	0.4654±0.0054±0.0393
2.3	0.2813±0.0042±0.0166	0.7158±0.0066±0.0356	0.7538±0.0068±0.0393	0.5506±0.0058±0.0378	0.3643±0.0047±0.0267
2.5	0.2420±0.0039±0.0129	0.6185±0.0062±0.0412	0.6008±0.0061±0.0231	0.4272±0.0051±0.0284	0.2528±0.0039±0.0257
2.7	0.2234±0.0037±0.0132	0.5314±0.0057±0.0318	0.4769±0.0054±0.0196	0.3071±0.0044±0.0321	0.1700±0.0032±0.0165
2.9	—	—	—	—	—

y	p_T [GeV/c]				
	0.6	0.7	0.8	0.9	1.0
-1.1	—	—	—	—	—
-0.9	—	—	—	—	—
-0.7	—	—	—	—	—
-0.5	—	—	—	—	—
-0.3	—	—	—	0.1700±0.0032±0.0064	—
-0.1	—	0.4042±0.0050±0.0232	0.2608±0.0040±0.0152	0.1762±0.0033±0.0150	0.1018±0.0284±0.0092
0.1	0.6236±0.0062±0.0462	0.4090±0.0805±0.0423	0.2521±0.0761±0.0264	0.1643±0.0148±0.0141	0.0974±0.0196±0.0087
0.3	0.6766±0.0584±0.0728	0.4178±0.0322±0.0355	0.2548±0.0203±0.0240	0.1658±0.0205±0.0133	0.0956±0.0307±0.0075
0.5	0.6305±0.0480±0.0521	0.4062±0.0335±0.0356	0.2485±0.0399±0.0278	0.1529±0.0578±0.0172	0.0956±0.2023±0.0078
0.7	0.6266±0.0492±0.0566	0.3973±0.0678±0.0367	0.2387±0.0038±0.0175	0.1515±0.0031±0.0121	0.0982±0.0025±0.0066
0.9	0.5763±0.4018±0.0533	0.3596±0.0047±0.0267	0.2374±0.0038±0.0202	0.1407±0.0029±0.0131	0.0974±0.0024±0.0110
1.1	0.5376±0.0058±0.0420	0.3496±0.0046±0.0191	0.2208±0.0037±0.0188	0.1319±0.0029±0.0071	0.0904±0.0024±0.0092
1.3	0.5167±0.0056±0.0381	0.3336±0.0045±0.0223	0.2112±0.0036±0.0125	0.1234±0.0028±0.0075	—
1.5	0.4888±0.0055±0.0367	0.3102±0.0044±0.0264	0.1881±0.0034±0.0115	0.1074±0.0026±0.0074	—
1.7	0.4371±0.0052±0.0431	0.2725±0.0041±0.0180	0.1704±0.0032±0.0117	0.0849±0.0023±0.0111	—
1.9	0.3814±0.0048±0.0270	0.2432±0.0039±0.0174	0.1441±0.0030±0.0157	0.0795±0.0022±0.0072	—
2.1	0.3081±0.0044±0.0291	0.1945±0.0035±0.0223	0.1141±0.0027±0.0162	0.0640±0.0020±0.0064	—
2.3	0.2272±0.0037±0.0199	0.1402±0.0029±0.0126	0.0808±0.0022±0.0106	—	—
2.5	0.1511±0.0031±0.0180	0.0830±0.0023±0.0120	—	—	—
2.7	—	—	—	—	—
2.9	—	—	—	—	—

TABLE B.10: Numerical results: $\frac{d^2n}{dydp_T}$ spectra of π^+ produced in inelastic $p + p$ collisions at 158 GeV/c. Rapidity (y) and transverse momentum (p_T) values correspond to center of bins.

B.2 K^-, K^+ spectra

y	p_T [GeV/c]				
	0.1	0.2	0.2	0.4	0.5
-1.1	—	—	—	—	—
-0.9	—	—	—	—	—
-0.7	0.0042±0.0008±0.0012	—	—	—	—
-0.5	0.0050±0.0009±0.0013	0.0162±0.0035±0.0039	—	—	—
-0.3	0.0066±0.0013±0.0018	0.0190±0.0035±0.0052	0.0256±0.0054±0.0066	—	—
-0.1	0.0066±0.0013±0.0018	0.0210±0.0042±0.0057	0.0274±0.0053±0.0063	0.0298±0.0048±0.0080	0.0254±0.0046±0.0069
0.1	0.0075±0.0015±0.0018	0.0193±0.0032±0.0047	0.0333±0.0067±0.0082	0.0261±0.0043±0.0060	0.0252±0.0051±0.0057
0.3	—	0.0180±0.0033±0.0050	0.0274±0.0058±0.0076	0.0266±0.0052±0.0071	0.0247±0.0050±0.0066
0.5	—	—	—	0.0202±0.0044±0.0046	0.0197±0.0040±0.0046
0.7	—	—	0.0223±0.0043±0.0033	0.0181±0.0095±0.0029	0.0126±0.0060±0.0017
0.9	0.0051±0.0006±0.0007	0.0097±0.0056±0.0015	0.0113±0.0048±0.0017	0.0118±0.0063±0.0019	0.0095±0.0052±0.0010
1.1	0.0020±0.0003±0.0002	0.0053±0.0038±0.0006	0.0108±0.0043±0.0012	0.0049±0.0009±0.0006	0.0037±0.0007±0.0004
1.3	0.0014±0.0002±0.0002	0.0038±0.0028±0.0004	0.0051±0.0024±0.0007	0.0041±0.0028±0.0005	—
1.5	0.0009±0.0002±0.0001	0.0032±0.0005±0.0004	0.0025±0.0004±0.0003	0.0021±0.0004±0.0002	—
1.7	—	—	—	—	—
1.9	—	—	—	—	—
2.1	—	—	—	—	—
2.3	—	—	—	—	—
2.5	—	—	—	—	—
2.7	—	—	—	—	—
2.9	—	—	—	—	—

y	p_T [GeV/c]				
	0.6	0.7	0.8	0.9	1.0
-1.1	—	—	—	—	—
-0.9	—	—	—	—	—
-0.7	—	—	—	—	—
-0.5	—	—	—	—	—
-0.3	—	—	—	—	—
-0.1	0.0206±0.0045±0.0054	—	—	—	—
0.1	0.0219±0.0040±0.0054	0.0106±0.0021±0.0028	0.0070±0.0013±0.0016	0.0046±0.0008±0.0012	0.0030±0.0005±0.0007
0.3	0.0176±0.0036±0.0045	0.0111±0.0020±0.0028	0.0065±0.0013±0.0017	0.0050±0.0009±0.0011	0.0020±0.0003±0.0005
0.5	0.0173±0.0029±0.0041	0.0086±0.0015±0.0021	0.0062±0.0012±0.0014	0.0030±0.0006±0.0007	—
0.7	0.0085±0.0044±0.0011	0.0025±0.0005±0.0003	0.0019±0.0004±0.0003	—	—
0.9	0.0089±0.0054±0.0011	0.0030±0.0005±0.0004	0.0015±0.0003±0.0002	—	—
1.1	0.0036±0.0006±0.0004	—	—	—	—
1.3	—	—	—	—	—
1.5	—	—	—	—	—
1.7	—	—	—	—	—
1.9	—	—	—	—	—
2.1	—	—	—	—	—
2.3	—	—	—	—	—
2.5	—	—	—	—	—
2.7	—	—	—	—	—
2.9	—	—	—	—	—

TABLE B.11: Numerical results: $\frac{d^2n}{dydp_T}$ spectra of K^- produced in inelastic $p + p$ collisions at 20 GeV/c. Rapidity (y) and transverse momentum (p_T) values correspond to center of bins.

y	p_T [GeV/c]				
	0.1	0.2	0.2	0.4	0.5
-1.1	—	—	—	—	—
-0.9	—	—	—	—	—
-0.7	—	—	—	—	—
-0.5	0.0095±0.0016±0.0030	—	—	—	—
-0.3	0.0105±0.0006±0.0028	0.0296±0.0017±0.0099	0.0412±0.0038±0.0143	—	—
-0.1	0.0116±0.0015±0.0005	0.0299±0.0017±0.0053	0.0445±0.0023±0.0094	—	0.0475±0.0040±0.0114
0.1	0.0116±0.0015±0.0014	0.0313±0.0030±0.0035	0.0431±0.0033±0.0037	0.0401±0.0043±0.0060	0.0450±0.0025±0.0120
0.3	0.0105±0.0006±0.0015	0.0296±0.0017±0.0036	0.0434±0.0087±0.0039	0.0399±0.0058±0.0039	0.0392±0.0078±0.0032
0.5	0.0095±0.0016±0.0013	—	—	—	0.0257±0.0033±0.0035
0.7	0.0090±0.0015±0.0012	0.0225±0.0020±0.0037	0.0349±0.0024±0.0032	0.0335±0.0025±0.0050	0.0214±0.0021±0.0035
0.9	0.0065±0.0009±0.0010	0.0188±0.0016±0.0018	0.0219±0.0018±0.0026	0.0324±0.0023±0.0033	0.0228±0.0021±0.0037
1.1	0.0044±0.0008±0.0007	0.0132±0.0013±0.0018	0.0167±0.0015±0.0028	0.0157±0.0015±0.0021	0.0161±0.0016±0.0019
1.3	0.0030±0.0006±0.0004	0.0112±0.0012±0.0012	0.0106±0.0012±0.0017	0.0099±0.0011±0.0012	0.0084±0.0011±0.0013
1.5	0.0025±0.0006±0.0003	0.0052±0.0008±0.0005	0.0075±0.0010±0.0010	0.0072±0.0010±0.0007	0.0048±0.0008±0.0005
1.7	—	0.0042±0.0007±0.0007	0.0038±0.0007±0.0004	0.0037±0.0007±0.0004	0.0014±0.0004±0.0002
1.9	—	0.0021±0.0005±0.0003	0.0020±0.0006±0.0003	—	—
2.1	—	—	—	—	—
2.3	—	—	—	—	—
2.5	—	—	—	—	—
2.7	—	—	—	—	—
2.9	—	—	—	—	—

y	p_T [GeV/c]				
	0.6	0.7	0.8	0.9	1.0
-1.1	—	—	—	—	—
-0.9	—	—	—	—	—
-0.7	—	—	—	—	—
-0.5	—	—	—	—	—
-0.3	—	—	—	—	—
-0.1	0.0318±0.0022±0.0044	—	—	—	—
0.1	0.0320±0.0019±0.0046	—	—	0.0081±0.0014±0.0013	—
0.3	—	0.0150±0.0018±0.0020	0.0081±0.0013±0.0011	0.0093±0.0014±0.0011	—
0.5	0.0201±0.0026±0.0034	0.0158±0.0025±0.0018	0.0094±0.0015±0.0014	0.0083±0.0013±0.0011	—
0.7	0.0159±0.0018±0.0024	0.0120±0.0015±0.0013	0.0064±0.0011±0.0007	—	—
0.9	0.0139±0.0017±0.0019	0.0088±0.0014±0.0015	0.0074±0.0013±0.0011	—	—
1.1	0.0131±0.0015±0.0018	0.0054±0.0010±0.0008	—	—	—
1.3	0.0057±0.0009±0.0005	0.0039±0.0009±0.0005	—	—	—
1.5	—	—	—	—	—
1.7	—	—	—	—	—
1.9	—	—	—	—	—
2.1	—	—	—	—	—
2.3	—	—	—	—	—
2.5	—	—	—	—	—
2.7	—	—	—	—	—
2.9	—	—	—	—	—

TABLE B.12: Numerical results: $\frac{d^2n}{dydp_T}$ spectra of K^- produced in inelastic $p+p$ collisions at 30.9 GeV/c. Rapidity (y) and transverse momentum (p_T) values correspond to center of bins.

y	p_T [GeV/c]				
	0.1	0.2	0.2	0.4	0.5
-1.1	—	—	—	—	—
-0.9	—	—	—	—	—
-0.7	—	—	—	—	—
-0.5	0.0120±0.0008±0.0038	—	—	—	—
-0.3	0.0133±0.0007±0.0036	0.0352±0.0024±0.0117	0.0469±0.0070±0.0162	0.0471±0.0095±0.0113	—
-0.1	0.0132±0.0007±0.0005	0.0357±0.0017±0.0064	0.0535±0.0027±0.0112	0.0498±0.0047±0.0139	0.0561±0.0047±0.0135
0.1	0.0132±0.0013±0.0004	0.0370±0.0027±0.0041	0.0497±0.0021±0.0043	0.0482±0.0025±0.0073	0.0549±0.0047±0.0146
0.3	—	0.0356±0.0127±0.0036	0.0513±0.0024±0.0047	0.0478±0.0036±0.0046	0.0472±0.0034±0.0039
0.5	0.0078±0.0016±0.0000	0.0296±0.0024±0.0000	0.0468±0.0024±0.0000	0.0427±0.0022±0.0000	0.0466±0.0126±0.0025
0.7	0.0101±0.0009±0.0000	0.0251±0.0014±0.0000	0.0343±0.0017±0.0000	0.0385±0.0019±0.0042	0.0269±0.0017±0.0017
0.9	0.0079±0.0008±0.0007	0.0227±0.0013±0.0020	0.0273±0.0014±0.0016	0.0310±0.0016±0.0021	0.0244±0.0015±0.0023
1.1	0.0069±0.0007±0.0004	0.0166±0.0011±0.0011	0.0227±0.0013±0.0012	0.0216±0.0013±0.0013	0.0163±0.0011±0.0013
1.3	0.0049±0.0006±0.0007	0.0129±0.0010±0.0007	0.0165±0.0011±0.0010	0.0152±0.0010±0.0007	0.0111±0.0009±0.0006
1.5	0.0040±0.0005±0.0004	0.0089±0.0008±0.0005	0.0111±0.0009±0.0008	0.0104±0.0009±0.0004	0.0071±0.0007±0.0003
1.7	0.0044±0.0008±0.0005	0.0053±0.0006±0.0003	0.0064±0.0007±0.0006	0.0053±0.0006±0.0000	0.0036±0.0005±0.0000
1.9	—	0.0059±0.0009±0.0000	0.0038±0.0005±0.0000	0.0032±0.0005±0.0000	0.0025±0.0006±0.0000
2.1	—	—	0.0018±0.0006±0.0000	—	—
2.3	—	—	—	—	—
2.5	—	—	—	—	—
2.7	—	—	—	—	—
2.9	—	—	—	—	—

y	p_T [GeV/c]				
	0.6	0.7	0.8	0.9	1.0
-1.1	—	—	—	—	—
-0.9	—	—	—	—	—
-0.7	—	—	—	—	—
-0.5	—	—	—	—	—
-0.3	—	—	—	—	—
-0.1	0.0375±0.0025±0.0052	—	0.0114±0.0025±0.0000	0.0083±0.0013±0.0000	—
0.1	0.0387±0.0023±0.0056	0.0255±0.0017±0.0113	0.0165±0.0016±0.0016	0.0075±0.0009±0.0000	—
0.3	0.0381±0.0022±0.0051	0.0248±0.0016±0.0053	0.0164±0.0013±0.0025	0.0098±0.0010±0.0000	—
0.5	0.0256±0.0016±0.0020	0.0154±0.0013±0.0013	0.0114±0.0011±0.0006	0.0085±0.0010±0.0000	—
0.7	0.0194±0.0015±0.0004	0.0148±0.0013±0.0010	0.0080±0.0009±0.0000	0.0070±0.0009±0.0000	—
0.9	0.0185±0.0013±0.0007	0.0129±0.0012±0.0011	0.0081±0.0010±0.0004	—	—
1.1	0.0144±0.0011±0.0011	0.0097±0.0009±0.0000	0.0107±0.0013±0.0000	—	—
1.3	0.0069±0.0007±0.0007	0.0055±0.0006±0.0000	—	—	—
1.5	0.0038±0.0005±0.0000	0.0131±0.0021±0.0000	—	—	—
1.7	0.0027±0.0005±0.0000	—	—	—	—
1.9	—	—	—	—	—
2.1	—	—	—	—	—
2.3	—	—	—	—	—
2.5	—	—	—	—	—
2.7	—	—	—	—	—
2.9	—	—	—	—	—

TABLE B.13: Numerical results: $\frac{d^2n}{dydp_T}$ spectra of K^- produced in inelastic $p + p$ collisions at 40 GeV/c. Rapidity (y) and transverse momentum (p_T) values correspond to center of bins.

y	p_T [GeV/c]				
	0.1	0.2	0.2	0.4	0.5
-1.1	—	—	—	—	—
-0.9	—	—	—	—	—
-0.7	—	—	—	—	—
-0.5	—	—	—	—	—
-0.3	—	—	—	—	—
-0.1	0.0175±0.0011±0.0011	0.0466±0.0032±0.0046	0.0710±0.0127±0.0097	0.0652±0.0055±0.0073	0.0785±0.0127±0.0076
0.1	0.0175±0.0011±0.0010	0.0494±0.0032±0.0031	0.0668±0.0044±0.0037	0.0646±0.0041±0.0035	0.0751±0.0088±0.0041
0.3	0.0184±0.0013±0.0010	0.0473±0.0034±0.0021	0.0687±0.0053±0.0058	0.0721±0.0021±0.0073	0.0533±0.0018±0.0051
0.5	0.0152±0.0010±0.0004	0.0434±0.0017±0.0034	0.0627±0.0020±0.0071	0.0623±0.0020±0.0069	0.0546±0.0019±0.0053
0.7	0.0143±0.0010±0.0005	0.0428±0.0017±0.0034	0.0508±0.0018±0.0048	0.0529±0.0018±0.0051	0.0445±0.0017±0.0036
0.9	0.0147±0.0010±0.0005	0.0336±0.0015±0.0022	0.0452±0.0017±0.0038	0.0468±0.0017±0.0040	0.0446±0.0017±0.0037
1.1	0.0106±0.0008±0.0002	0.0285±0.0014±0.0016	0.0342±0.0015±0.0022	0.0365±0.0015±0.0025	0.0262±0.0013±0.0013
1.3	0.0086±0.0007±0.0002	0.0219±0.0012±0.0009	0.0268±0.0013±0.0013	0.0309±0.0014±0.0018	0.0226±0.0012±0.0009
1.5	0.0060±0.0006±0.0001	0.0174±0.0011±0.0006	0.0199±0.0011±0.0007	0.0202±0.0011±0.0008	0.0157±0.0010±0.0005
1.7	0.0066±0.0006±0.0001	0.0114±0.0009±0.0003	0.0146±0.0010±0.0004	0.0111±0.0008±0.0002	0.0126±0.0009±0.0003
1.9	0.0031±0.0004±0.0000	0.0068±0.0007±0.0001	0.0073±0.0007±0.0001	0.0060±0.0006±0.0001	—
2.1	0.0006±0.0002±0.0000	0.0051±0.0006±0.0000	0.0029±0.0004±0.0000	—	—
2.3	—	—	—	—	—
2.5	—	—	—	—	—
2.7	—	—	—	—	—
2.9	—	—	—	—	—

y	p_T [GeV/c]				
	0.6	0.7	0.8	0.9	1.0
-1.1	—	—	—	—	—
-0.9	—	—	—	—	—
-0.7	—	—	—	—	—
-0.5	—	—	—	—	—
-0.3	—	—	—	—	—
-0.1	0.0504±0.0111±0.0055	0.0363±0.0035±0.0020	—	—	—
0.1	0.0392±0.0016±0.0021	0.0273±0.0013±0.0013	0.0208±0.0012±0.0008	0.0132±0.0009±0.0000	—
0.3	0.0422±0.0016±0.0032	0.0282±0.0013±0.0015	0.0213±0.0012±0.0008	—	—
0.5	0.0413±0.0016±0.0030	0.0268±0.0013±0.0014	0.0238±0.0012±0.0010	—	—
0.7	0.0369±0.0015±0.0025	0.0241±0.0012±0.0011	0.0217±0.0012±0.0009	—	—
0.9	0.0292±0.0014±0.0016	0.0166±0.0010±0.0005	0.0116±0.0009±0.0003	—	—
1.1	0.0238±0.0012±0.0011	0.0150±0.0010±0.0004	0.0096±0.0008±0.0002	0.0040±0.0005±0.0000	—
1.3	0.0164±0.0010±0.0005	0.0089±0.0008±0.0001	0.0063±0.0006±0.0001	—	0.0021±0.0004±0.0000
1.5	0.0114±0.0009±0.0002	0.0081±0.0007±0.0001	—	—	—
1.7	0.0057±0.0006±0.0001	—	—	—	—
1.9	—	—	—	—	—
2.1	—	—	—	—	—
2.3	—	—	—	—	—
2.5	—	—	—	—	—
2.7	—	—	—	—	—
2.9	—	—	—	—	—

TABLE B.14: Numerical results: $\frac{d^2n}{dydp_T}$ spectra of K^- produced in inelastic $p + p$ collisions at 80 GeV/c. Rapidity (y) and transverse momentum (p_T) values correspond to center of bins.

y	p_T [GeV/c]				
	0.1	0.2	0.2	0.4	0.5
-1.1	—	—	—	—	—
-0.9	—	—	—	—	—
-0.7	—	—	—	—	—
-0.5	—	—	—	—	—
-0.3	—	—	—	—	—
-0.1	—	—	—	—	0.0667±0.0020±0.0123
0.1	0.0214±0.0033±0.0020	0.0587±0.0061±0.0050	0.0880±0.0160±0.0113	0.0760±0.0075±0.0075	0.0830±0.0087±0.0080
0.3	0.0224±0.0023±0.0018	0.0588±0.0049±0.0053	0.0835±0.0077±0.0075	0.0843±0.0076±0.0072	0.0807±0.0093±0.0075
0.5	0.0205±0.0021±0.0016	0.0532±0.0045±0.0046	0.0808±0.0073±0.0070	0.0772±0.0067±0.0069	0.0784±0.0110±0.0078
0.7	0.0202±0.0024±0.0019	0.0518±0.0063±0.0046	0.0780±0.0118±0.0074	0.0746±0.0192±0.0075	0.0612±0.0019±0.0039
0.9	0.0163±0.0010±0.0019	0.0443±0.0017±0.0041	0.0630±0.0020±0.0063	0.0630±0.0020±0.0062	0.0530±0.0018±0.0041
1.1	0.0159±0.0010±0.0016	0.0403±0.0016±0.0040	0.0538±0.0018±0.0044	0.0550±0.0018±0.0046	0.0490±0.0017±0.0032
1.3	0.0118±0.0009±0.0015	0.0320±0.0014±0.0025	0.0455±0.0017±0.0044	0.0416±0.0016±0.0036	0.0353±0.0015±0.0048
1.5	0.0100±0.0008±0.0014	0.0238±0.0012±0.0027	0.0367±0.0015±0.0023	0.0347±0.0015±0.0042	0.0294±0.0013±0.0026
1.7	0.0061±0.0006±0.0010	0.0197±0.0011±0.0025	0.0246±0.0012±0.0019	0.0264±0.0013±0.0032	0.0228±0.0012±0.0025
1.9	0.0053±0.0006±0.0004	0.0155±0.0010±0.0013	0.0173±0.0010±0.0016	0.0161±0.0010±0.0011	0.0119±0.0009±0.0011
2.1	0.0035±0.0005±0.0002	0.0102±0.0008±0.0009	0.0105±0.0008±0.0011	0.0099±0.0008±0.0000	0.0079±0.0007±0.0005
2.3	0.0028±0.0004±0.0002	0.0047±0.0005±0.0005	0.0054±0.0006±0.0017	0.0058±0.0006±0.0000	0.0047±0.0005±0.0000
2.5	0.0002±0.0001±0.0000	0.0010±0.0003±0.0004	—	—	—
2.7	—	—	—	—	—
2.9	—	—	—	—	—

y	p_T [GeV/c]				
	0.6	0.7	0.8	0.9	1.0
-1.1	—	—	—	—	—
-0.9	—	—	—	—	—
-0.7	—	—	—	—	—
-0.5	—	—	—	—	—
-0.3	—	0.0399±0.0016±0.0130	0.0264±0.0013±0.0055	0.0200±0.0011±0.0028	0.0099±0.0008±0.0010
-0.1	0.0617±0.0307±0.0063	0.0413±0.0079±0.0034	0.0314±0.0133±0.0028	0.0205±0.0036±0.0020	0.0119±0.0009±0.0020
0.1	0.0653±0.0073±0.0061	0.0426±0.0060±0.0037	0.0283±0.0047±0.0025	0.0210±0.0049±0.0022	0.0139±0.0009±0.0018
0.3	0.0613±0.0066±0.0057	0.0440±0.0056±0.0039	0.0306±0.0075±0.0035	0.0207±0.0091±0.0024	—
0.5	0.0606±0.0090±0.0058	0.0387±0.0079±0.0036	0.0269±0.0013±0.0014	0.0158±0.0010±0.0020	0.0110±0.0008±0.0013
0.7	0.0506±0.0018±0.0049	0.0381±0.0015±0.0040	0.0268±0.0013±0.0039	0.0187±0.0011±0.0015	—
0.9	0.0416±0.0016±0.0026	0.0336±0.0014±0.0029	0.0202±0.0011±0.0020	0.0156±0.0010±0.0016	0.0096±0.0008±0.0022
1.1	0.0378±0.0015±0.0047	0.0246±0.0012±0.0027	0.0188±0.0011±0.0010	0.0115±0.0008±0.0023	0.0073±0.0007±0.0012
1.3	0.0311±0.0014±0.0028	0.0187±0.0011±0.0028	0.0122±0.0009±0.0009	0.0074±0.0007±0.0007	—
1.5	0.0216±0.0012±0.0024	0.0165±0.0010±0.0032	0.0091±0.0007±0.0008	0.0044±0.0005±0.0000	0.0030±0.0004±0.0003
1.7	0.0142±0.0009±0.0009	0.0108±0.0008±0.0013	0.0032±0.0004±0.0003	—	0.0005±0.0002±0.0001
1.9	0.0086±0.0007±0.0009	0.0044±0.0005±0.0008	—	0.0015±0.0003±0.0002	—
2.1	0.0024±0.0004±0.0002	—	—	—	—
2.3	—	—	—	—	—
2.5	—	—	—	—	—
2.7	—	—	—	—	—
2.9	—	—	—	—	—

TABLE B.15: Numerical results: $\frac{d^2n}{dydp_T}$ spectra of K^- produced in inelastic $p + p$ collisions at 158 GeV/c. Rapidity (y) and transverse momentum (p_T) values correspond to center of bins.

y	p_T [GeV/c]				
	0.1	0.2	0.2	0.4	0.5
-1.1	—	—	—	—	—
-0.9	—	—	—	—	—
-0.7	0.0132±0.0033±0.0023	—	—	—	—
-0.5	0.0222±0.0007±0.0026	0.0614±0.0016±0.0098	—	—	—
-0.3	0.0279±0.0012±0.0029	0.0652±0.0019±0.0070	0.0897±0.0042±0.0113	—	—
-0.1	0.0279±0.0004±0.0048	0.0651±0.0020±0.0085	0.1035±0.0060±0.0149	0.0129±0.0007±0.0015	0.0838±0.0035±0.0132
0.1	0.0266±0.0010±0.0030	0.0703±0.0024±0.0116	0.0971±0.0052±0.0119	0.0758±0.0054±0.0120	0.0836±0.0053±0.0125
0.3	—	0.0673±0.0020±0.0070	0.1010±0.0052±0.0155	0.0778±0.0041±0.0099	0.0790±0.0039±0.0130
0.5	—	—	—	0.0692±0.0130±0.0096	0.0485±0.0045±0.0076
0.7	—	—	0.0903±0.0139±0.0117	0.0689±0.0058±0.0110	0.0402±0.0042±0.0051
0.9	0.0231±0.0023±0.0037	0.0444±0.0033±0.0051	0.0547±0.0035±0.0074	0.0531±0.0046±0.0095	0.0372±0.0055±0.0057
1.1	0.0104±0.0019±0.0016	0.0282±0.0031±0.0035	0.0622±0.0043±0.0106	0.0285±0.0051±0.0048	0.0167±0.0054±0.0024
1.3	0.0092±0.0027±0.0014	0.0261±0.0040±0.0031	0.0393±0.0050±0.0051	0.0315±0.0056±0.0037	0.0203±0.0048±0.0030
1.5	0.0086±0.0031±0.0015	0.0301±0.0042±0.0032	0.0264±0.0048±0.0045	0.0203±0.0036±0.0033	0.0100±0.0041±0.0016
1.7	0.0075±0.0037±0.0012	0.0119±0.0037±0.0013	0.0182±0.0047±0.0020	0.0078±0.0038±0.0008	0.0067±0.0039±0.0008
1.9	0.0028±0.0034±0.0003	0.0077±0.0046±0.0013	0.0088±0.0051±0.0012	0.0043±0.0049±0.0005	0.0025±0.0037±0.0003
2.1	0.0026±0.0052±0.0003	0.0031±0.0062±0.0004	0.0027±0.0058±0.0004	0.0018±0.0042±0.0002	0.0003±0.0007±0.0000
2.3	0.0005±0.0372±0.0001	0.0009±0.0045±0.0002	0.0005±0.0010±0.0001	0.0000±0.0014±0.0000	—
2.5	—	—	—	—	—
2.7	—	—	—	—	—
2.9	—	—	—	—	—

y	p_T [GeV/c]				
	0.6	0.7	0.8	0.9	1.0
-1.1	—	—	—	—	—
-0.9	—	—	—	—	—
-0.7	—	—	—	—	—
-0.5	—	—	—	—	—
-0.3	—	—	—	—	—
-0.1	0.0009±0.0001±0.0001	—	—	—	—
0.1	0.0472±0.0059±0.0081	—	—	—	—
0.3	0.0566±0.0036±0.0083	—	—	—	0.0045±0.0128±0.0007
0.5	—	—	—	0.0040±0.0061±0.0007	0.0022±0.0036±0.0003
0.7	0.0258±0.0041±0.0032	0.0074±0.0049±0.0013	0.0058±0.0050±0.0009	0.0067±0.0050±0.0010	0.0026±0.0046±0.0004
0.9	0.0282±0.0061±0.0043	0.0100±0.0054±0.0012	0.0058±0.0055±0.0007	0.0045±0.0052±0.0005	0.0012±0.0036±0.0002
1.1	0.0140±0.0071±0.0020	0.0057±0.0064±0.0010	0.0035±0.0048±0.0004	0.0026±0.0072±0.0004	0.0016±0.0142±0.0002
1.3	0.0082±0.0061±0.0010	0.0039±0.0055±0.0006	0.0023±0.0043±0.0003	—	—
1.5	0.0058±0.0055±0.0010	0.0028±0.0056±0.0003	0.0022±0.0031±0.0003	—	—
1.7	0.0035±0.0045±0.0004	0.0015±0.0035±0.0002	0.0006±0.0029±0.0001	—	—
1.9	0.0016±0.0045±0.0002	0.0002±0.0035±0.0000	0.0000±0.0028±0.0000	—	—
2.1	0.0001±0.0112±0.0000	—	—	—	—
2.3	—	—	—	—	—
2.5	—	—	—	—	—
2.7	—	—	—	—	—
2.9	—	—	—	—	—

TABLE B.16: Numerical results: $\frac{d^2n}{dydp_T}$ spectra of K^+ produced in inelastic $p + p$ collisions at 20 GeV/c. Rapidity (y) and transverse momentum (p_T) values correspond to center of bins.

y	p_T [GeV/c]				
	0.1	0.2	0.2	0.4	0.5
-1.1	—	—	—	—	—
-0.9	—	—	—	—	—
-0.7	—	—	—	—	—
-0.5	0.0280±0.0045±0.0032	—	—	—	—
-0.3	0.0304±0.0026±0.0033	0.0792±0.0167±0.0085	0.1082±0.0066±0.0183	—	—
-0.1	0.0327±0.0036±0.0034	0.0805±0.0081±0.0135	0.1152±0.0112±0.0157	0.1108±0.0261±0.0127	0.1088±0.0082±0.0122
0.1	0.0327±0.0036±0.0038	0.0812±0.0038±0.0128	0.1165±0.0056±0.0146	0.1036±0.0047±0.0134	0.1051±0.0067±0.0156
0.3	0.0304±0.0026±0.0053	0.0792±0.0167±0.0117	0.1063±0.0129±0.0181	0.1012±0.0057±0.0140	0.0960±0.0058±0.0131
0.5	0.0280±0.0045±0.0035	—	—	—	0.0848±0.0129±0.0124
0.7	0.0191±0.0022±0.0019	0.0578±0.0033±0.0085	0.0854±0.0037±0.0105	0.0790±0.0039±0.0135	0.0664±0.0036±0.0079
0.9	0.0176±0.0016±0.0028	0.0490±0.0026±0.0074	0.0685±0.0031±0.0104	0.0754±0.0035±0.0120	0.0636±0.0034±0.0084
1.1	0.0179±0.0016±0.0026	0.0480±0.0026±0.0080	0.0630±0.0029±0.0074	0.0646±0.0030±0.0101	0.0614±0.0031±0.0090
1.3	0.0163±0.0015±0.0021	0.0438±0.0024±0.0049	0.0482±0.0025±0.0063	0.0575±0.0028±0.0068	0.0494±0.0026±0.0077
1.5	0.0143±0.0014±0.0018	0.0374±0.0022±0.0056	0.0489±0.0026±0.0056	0.0452±0.0025±0.0056	0.0442±0.0024±0.0071
1.7	0.0126±0.0014±0.0022	0.0340±0.0022±0.0054	0.0427±0.0024±0.0052	0.0357±0.0022±0.0040	0.0366±0.0022±0.0047
1.9	0.0116±0.0013±0.0017	0.0269±0.0019±0.0041	0.0349±0.0022±0.0061	0.0278±0.0019±0.0030	0.0261±0.0019±0.0033
2.1	0.0106±0.0013±0.0014	0.0201±0.0017±0.0020	0.0271±0.0021±0.0033	0.0223±0.0018±0.0028	0.0194±0.0018±0.0027
2.3	—	0.0246±0.0024±0.0026	0.0279±0.0023±0.0043	0.0195±0.0020±0.0026	0.0118±0.0016±0.0014
2.5	—	—	—	0.0074±0.0018±0.0011	—
2.7	—	—	—	—	—
2.9	—	—	—	—	—

y	p_T [GeV/c]				
	0.6	0.7	0.8	0.9	1.0
-1.1	—	—	—	—	—
-0.9	—	—	—	—	—
-0.7	—	—	—	—	—
-0.5	—	—	—	—	—
-0.3	—	—	—	—	—
-0.1	0.0724±0.0048±0.0080	—	—	—	—
0.1	0.0678±0.0045±0.0086	—	—	0.0217±0.0022±0.0023	0.0161±0.0018±0.0018
0.3	0.0706±0.0033±0.0105	0.0532±0.0032±0.0089	0.0379±0.0027±0.0066	0.0215±0.0020±0.0032	0.0161±0.0018±0.0024
0.5	0.0680±0.0088±0.0111	0.0463±0.0057±0.0079	0.0335±0.0049±0.0038	0.0226±0.0034±0.0030	0.0154±0.0016±0.0017
0.7	0.0531±0.0032±0.0060	0.0413±0.0029±0.0068	0.0340±0.0026±0.0036	0.0207±0.0019±0.0023	0.0154±0.0017±0.0020
0.9	0.0498±0.0032±0.0089	0.0395±0.0028±0.0055	0.0286±0.0024±0.0034	0.0174±0.0019±0.0021	0.0125±0.0016±0.0021
1.1	0.0512±0.0029±0.0089	0.0377±0.0026±0.0066	0.0251±0.0023±0.0041	0.0149±0.0018±0.0016	0.0070±0.0012±0.0011
1.3	0.0466±0.0026±0.0081	0.0306±0.0021±0.0032	0.0192±0.0017±0.0030	0.0135±0.0015±0.0019	0.0056±0.0009±0.0008
1.5	0.0322±0.0021±0.0033	0.0227±0.0018±0.0030	0.0146±0.0014±0.0020	0.0084±0.0011±0.0010	0.0055±0.0009±0.0010
1.7	0.0239±0.0018±0.0036	0.0170±0.0015±0.0024	0.0079±0.0010±0.0012	0.0047±0.0008±0.0006	0.0025±0.0007±0.0003
1.9	0.0197±0.0017±0.0023	0.0077±0.0011±0.0009	0.0046±0.0008±0.0006	0.0019±0.0005±0.0002	—
2.1	0.0093±0.0012±0.0013	0.0045±0.0009±0.0007	0.0011±0.0004±0.0001	—	—
2.3	0.0039±0.0011±0.0005	—	—	—	—
2.5	—	—	—	—	—
2.7	—	—	—	—	—
2.9	—	—	—	—	—

TABLE B.17: Numerical results: $\frac{d^2n}{dydp_T}$ spectra of K^+ produced in inelastic $p+p$ collisions at 30.9 GeV/c. Rapidity (y) and transverse momentum (p_T) values correspond to center of bins.

y	p_T [GeV/c]				
	0.1	0.2	0.2	0.4	0.5
-1.1	—	—	—	—	—
-0.9	—	—	—	—	—
-0.7	—	—	—	—	—
-0.5	0.0303±0.0098±0.0034	—	—	—	—
-0.3	0.0317±0.0017±0.0031	0.0840±0.0068±0.0134	0.1152±0.0131±0.0334	0.1087±0.0196±0.0123	—
-0.1	0.0336±0.0025±0.0042	0.0859±0.0050±0.0134	0.1220±0.0076±0.0188	0.1172±0.0050±0.0230	0.1181±0.0092±0.0247
0.1	0.0338±0.0032±0.0048	0.0860±0.0052±0.0122	0.1229±0.0104±0.0272	0.1091±0.0062±0.0172	0.1150±0.0101±0.0103
0.3	—	0.0847±0.0139±0.0242	0.1119±0.0057±0.0245	0.1105±0.0085±0.0195	0.1034±0.0064±0.0186
0.5	0.0181±0.0026±0.0000	0.0559±0.0033±0.0000	0.0839±0.0031±0.0000	0.0797±0.0028±0.0000	0.0946±0.0391±0.0209
0.7	0.0216±0.0013±0.0000	0.0534±0.0020±0.0000	0.0753±0.0025±0.0156	0.0838±0.0028±0.0158	0.0612±0.0025±0.0149
0.9	0.0187±0.0012±0.0050	0.0484±0.0019±0.0112	0.0674±0.0022±0.0146	0.0729±0.0024±0.0155	0.0673±0.0024±0.0143
1.1	0.0149±0.0011±0.0056	0.0439±0.0018±0.0109	0.0593±0.0021±0.0155	0.0618±0.0021±0.0154	0.0630±0.0022±0.0179
1.3	0.0142±0.0010±0.0040	0.0354±0.0016±0.0079	0.0508±0.0019±0.0128	0.0526±0.0019±0.0139	0.0547±0.0020±0.0133
1.5	0.0124±0.0010±0.0047	0.0337±0.0016±0.0093	0.0463±0.0018±0.0129	0.0469±0.0018±0.0133	0.0464±0.0018±0.0118
1.7	0.0114±0.0009±0.0000	0.0296±0.0015±0.0126	0.0354±0.0016±0.0130	0.0383±0.0017±0.0130	0.0439±0.0018±0.0139
1.9	0.0095±0.0009±0.0000	0.0262±0.0014±0.0000	0.0327±0.0016±0.0139	0.0350±0.0016±0.0123	0.0365±0.0016±0.0127
2.1	0.0095±0.0009±0.0000	0.0228±0.0013±0.0000	0.0269±0.0014±0.0105	0.0225±0.0013±0.0059	0.0325±0.0016±0.0143
2.3	0.0053±0.0008±0.0000	0.0165±0.0012±0.0000	0.0155±0.0011±0.0054	0.0122±0.0010±0.0000	0.0208±0.0015±0.0000
2.5	—	0.0086±0.0016±0.0000	0.0152±0.0017±0.0000	0.0099±0.0011±0.0000	0.0059±0.0009±0.0000
2.7	—	—	—	0.0005±0.0002±0.0000	—
2.9	—	—	—	—	—

y	p_T [GeV/c]				
	0.6	0.7	0.8	0.9	1.0
-1.1	—	—	—	—	—
-0.9	—	—	—	—	—
-0.7	—	—	—	—	—
-0.5	—	—	—	—	—
-0.3	—	—	—	—	—
-0.1	0.0797±0.0046±0.0141	—	—	0.0163±0.0017±0.0000	0.0128±0.0013±0.0000
0.1	0.0733±0.0039±0.0112	0.0520±0.0029±0.0106	0.0323±0.0021±0.0026	0.0173±0.0014±0.0000	0.0143±0.0013±0.0000
0.3	0.0759±0.0041±0.0115	0.0530±0.0031±0.0026	0.0321±0.0028±0.0027	0.0216±0.0015±0.0091	0.0128±0.0011±0.0000
0.5	0.0639±0.0191±0.0057	0.0429±0.0191±0.0023	0.0295±0.0092±0.0066	0.0188±0.0014±0.0060	0.0134±0.0012±0.0051
0.7	0.0508±0.0023±0.0113	0.0426±0.0021±0.0133	0.0290±0.0018±0.0085	0.0162±0.0013±0.0024	0.0130±0.0012±0.0031
0.9	0.0581±0.0024±0.0131	0.0436±0.0021±0.0100	0.0338±0.0019±0.0088	0.0198±0.0015±0.0038	0.0128±0.0012±0.0000
1.1	0.0538±0.0021±0.0148	0.0426±0.0019±0.0141	0.0277±0.0016±0.0079	0.0204±0.0014±0.0067	0.0138±0.0012±0.0000
1.3	0.0451±0.0018±0.0131	0.0308±0.0015±0.0095	0.0232±0.0013±0.0086	0.0169±0.0011±0.0000	0.0111±0.0009±0.0000
1.5	0.0370±0.0016±0.0113	0.0256±0.0013±0.0064	0.0214±0.0013±0.0076	0.0115±0.0009±0.0000	0.0058±0.0007±0.0000
1.7	0.0359±0.0016±0.0080	0.0220±0.0013±0.0096	0.0134±0.0010±0.0065	0.0080±0.0008±0.0024	0.0052±0.0006±0.0016
1.9	0.0257±0.0014±0.0000	0.0176±0.0012±0.0000	0.0083±0.0008±0.0022	0.0068±0.0007±0.0029	0.0068±0.0014±0.0000
2.1	0.0174±0.0012±0.0073	0.0106±0.0009±0.0052	0.0034±0.0005±0.0012	0.0026±0.0006±0.0000	—
2.3	0.0098±0.0011±0.0000	0.0032±0.0007±0.0000	0.0003±0.0002±0.0000	—	—
2.5	0.0007±0.0002±0.0000	—	—	—	—
2.7	—	—	—	—	—
2.9	—	—	—	—	—

TABLE B.18: Numerical results: $\frac{d^2n}{dydp_T}$ spectra of K^+ produced in inelastic $p + p$ collisions at 40 GeV/c. Rapidity (y) and transverse momentum (p_T) values correspond to center of bins.

y	p_T [GeV/c]				
	0.1	0.2	0.2	0.4	0.5
-1.1	—	—	—	—	—
-0.9	—	—	—	—	—
-0.7	—	—	—	—	—
-0.5	—	—	—	—	—
-0.3	—	—	—	—	—
-0.1	0.0375±0.0026±0.0015	0.0903±0.0049±0.0116	0.1291±0.0129±0.0151	0.1245±0.0121±0.0141	0.1293±0.0147±0.0154
0.1	0.0361±0.0028±0.0024	0.0905±0.0066±0.0040	0.1314±0.0126±0.0093	0.1167±0.0082±0.0088	0.1252±0.0108±0.0100
0.3	0.0347±0.0029±0.0012	0.0908±0.0074±0.0045	0.1197±0.0095±0.0046	0.1204±0.0080±0.0052	0.1151±0.0093±0.0050
0.5	0.0343±0.0099±0.0038	0.0867±0.0207±0.0023	0.1268±0.0418±0.0040	0.1200±0.0241±0.0057	0.1116±0.0131±0.0077
0.7	0.0267±0.0013±0.0025	0.0705±0.0021±0.0084	0.0936±0.0024±0.0104	0.1060±0.0026±0.0087	0.1027±0.0026±0.0117
0.9	0.0276±0.0013±0.0030	0.0626±0.0020±0.0058	0.0867±0.0024±0.0102	0.0952±0.0025±0.0085	0.0902±0.0024±0.0078
1.1	0.0222±0.0012±0.0023	0.0571±0.0019±0.0065	0.0806±0.0023±0.0072	0.0870±0.0024±0.0082	0.0754±0.0022±0.0075
1.3	0.0207±0.0012±0.0018	0.0492±0.0018±0.0058	0.0673±0.0021±0.0067	0.0729±0.0022±0.0071	0.0718±0.0021±0.0071
1.5	0.0152±0.0010±0.0013	0.0455±0.0017±0.0047	0.0605±0.0020±0.0054	0.0669±0.0021±0.0057	0.0561±0.0019±0.0062
1.7	0.0147±0.0010±0.0016	0.0385±0.0016±0.0036	0.0489±0.0018±0.0051	0.0520±0.0018±0.0049	0.0479±0.0018±0.0043
1.9	0.0125±0.0009±0.0011	0.0287±0.0014±0.0031	0.0409±0.0016±0.0046	0.0389±0.0016±0.0037	0.0445±0.0017±0.0045
2.1	0.0047±0.0005±0.0004	0.0147±0.0010±0.0012	0.0298±0.0014±0.0031	0.0401±0.0016±0.0032	0.0254±0.0013±0.0026
2.3	0.0010±0.0002±0.0001	0.0122±0.0009±0.0010	0.0165±0.0010±0.0017	0.0323±0.0014±0.0031	0.0053±0.0006±0.0005
2.5	—	0.0049±0.0006±0.0005	0.0038±0.0005±0.0003	—	—
2.7	—	—	—	—	—
2.9	—	—	—	—	—

y	p_T [GeV/c]				
	0.6	0.7	0.8	0.9	1.0
-1.1	—	—	—	—	—
-0.9	—	—	—	—	—
-0.7	—	—	—	—	—
-0.5	—	—	—	—	—
-0.3	—	—	—	—	—
-0.1	0.0883±0.0063±0.0088	0.0591±0.0055±0.0034	0.0391±0.0040±0.0020	0.0356±0.0015±0.0031	—
0.1	0.0826±0.0056±0.0053	0.0599±0.0049±0.0040	0.0369±0.0041±0.0020	0.0349±0.0015±0.0034	—
0.3	0.0863±0.0061±0.0033	0.0616±0.0047±0.0026	0.0387±0.0040±0.0031	0.0312±0.0014±0.0028	0.0249±0.0013±0.0022
0.5	0.0772±0.0372±0.0046	0.0614±0.0020±0.0068	0.0386±0.0016±0.0034	0.0303±0.0014±0.0035	0.0242±0.0012±0.0025
0.7	0.0780±0.0022±0.0075	0.0664±0.0021±0.0054	0.0447±0.0017±0.0037	0.0311±0.0014±0.0035	0.0229±0.0012±0.0023
0.9	0.0762±0.0022±0.0062	0.0532±0.0018±0.0045	0.0382±0.0016±0.0045	0.0219±0.0012±0.0024	—
1.1	0.0600±0.0020±0.0068	0.0467±0.0017±0.0050	0.0317±0.0014±0.0028	0.0233±0.0012±0.0019	0.0135±0.0009±0.0013
1.3	0.0554±0.0019±0.0066	0.0426±0.0017±0.0050	0.0285±0.0013±0.0023	0.0160±0.0010±0.0019	0.0125±0.0009±0.0014
1.5	0.0408±0.0016±0.0036	0.0335±0.0015±0.0037	0.0206±0.0011±0.0024	0.0134±0.0009±0.0016	0.0092±0.0008±0.0009
1.7	0.0359±0.0015±0.0031	0.0272±0.0013±0.0029	0.0164±0.0010±0.0013	0.0129±0.0009±0.0015	0.0075±0.0007±0.0007
1.9	0.0289±0.0014±0.0034	0.0139±0.0009±0.0016	0.0083±0.0007±0.0009	—	—
2.1	0.0152±0.0010±0.0014	0.0022±0.0004±0.0002	0.0000±0.0000±0.0000	—	0.0001±0.0001±0.0000
2.3	0.0009±0.0002±0.0001	—	0.0017±0.0003±0.0002	0.0002±0.0001±0.0000	—
2.5	—	—	—	—	—
2.7	—	—	—	—	—
2.9	—	—	—	—	—

TABLE B.19: Numerical results: $\frac{d^2n}{dydp_T}$ spectra of K^+ produced in inelastic $p + p$ collisions at 80 GeV/c. Rapidity (y) and transverse momentum (p_T) values correspond to center of bins.

y	p_T [GeV/c]				
	0.1	0.2	0.2	0.4	0.5
-1.1	—	—	—	—	—
-0.9	—	—	—	—	—
-0.7	—	—	—	—	—
-0.5	—	—	—	—	—
-0.3	—	—	—	—	—
-0.1	—	—	—	—	0.0667±0.0020±0.0123
0.1	0.0214±0.0033±0.0020	0.0587±0.0061±0.0050	0.0880±0.0160±0.0113	0.0760±0.0075±0.0075	0.0830±0.0087±0.0080
0.3	0.0224±0.0023±0.0018	0.0588±0.0049±0.0053	0.0835±0.0077±0.0075	0.0843±0.0076±0.0072	0.0807±0.0093±0.0075
0.5	0.0205±0.0021±0.0016	0.0532±0.0045±0.0046	0.0808±0.0073±0.0070	0.0772±0.0067±0.0069	0.0784±0.0110±0.0078
0.7	0.0202±0.0024±0.0019	0.0518±0.0063±0.0046	0.0780±0.0118±0.0074	0.0746±0.0192±0.0075	0.0612±0.0019±0.0039
0.9	0.0163±0.0010±0.0019	0.0443±0.0017±0.0041	0.0630±0.0020±0.0063	0.0630±0.0020±0.0062	0.0530±0.0018±0.0041
1.1	0.0159±0.0010±0.0016	0.0403±0.0016±0.0040	0.0538±0.0018±0.0044	0.0550±0.0018±0.0046	0.0490±0.0017±0.0032
1.3	0.0118±0.0009±0.0015	0.0320±0.0014±0.0025	0.0455±0.0017±0.0044	0.0416±0.0016±0.0036	0.0353±0.0015±0.0048
1.5	0.0100±0.0008±0.0014	0.0238±0.0012±0.0027	0.0367±0.0015±0.0023	0.0347±0.0015±0.0042	0.0294±0.0013±0.0026
1.7	0.0061±0.0006±0.0010	0.0197±0.0011±0.0025	0.0246±0.0012±0.0019	0.0264±0.0013±0.0032	0.0228±0.0012±0.0025
1.9	0.0053±0.0006±0.0004	0.0155±0.0010±0.0013	0.0173±0.0010±0.0016	0.0161±0.0010±0.0011	0.0119±0.0009±0.0011
2.1	0.0035±0.0005±0.0002	0.0102±0.0008±0.0009	0.0105±0.0008±0.0011	0.0099±0.0008±0.0000	0.0079±0.0007±0.0005
2.3	0.0028±0.0004±0.0002	0.0047±0.0005±0.0005	0.0054±0.0006±0.0017	0.0058±0.0006±0.0000	0.0047±0.0005±0.0000
2.5	0.0002±0.0001±0.0000	0.0010±0.0003±0.0004	—	—	—
2.7	—	—	—	—	—
2.9	—	—	—	—	—

y	p_T [GeV/c]				
	0.6	0.7	0.8	0.9	1.0
-1.1	—	—	—	—	—
-0.9	—	—	—	—	—
-0.7	—	—	—	—	—
-0.5	—	—	—	—	—
-0.3	—	0.0399±0.0016±0.0130	0.0264±0.0013±0.0055	0.0200±0.0011±0.0028	0.0099±0.0008±0.0010
-0.1	0.0617±0.0307±0.0063	0.0413±0.0079±0.0034	0.0314±0.0133±0.0028	0.0205±0.0036±0.0020	0.0119±0.0009±0.0020
0.1	0.0653±0.0073±0.0061	0.0426±0.0060±0.0037	0.0283±0.0047±0.0025	0.0210±0.0049±0.0022	0.0139±0.0009±0.0018
0.3	0.0613±0.0066±0.0057	0.0440±0.0056±0.0039	0.0306±0.0075±0.0035	0.0207±0.0091±0.0024	—
0.5	0.0606±0.0090±0.0058	0.0387±0.0079±0.0036	0.0269±0.0013±0.0014	0.0158±0.0010±0.0020	0.0110±0.0008±0.0013
0.7	0.0506±0.0018±0.0049	0.0381±0.0015±0.0040	0.0268±0.0013±0.0039	0.0187±0.0011±0.0015	—
0.9	0.0416±0.0016±0.0026	0.0336±0.0014±0.0029	0.0202±0.0011±0.0020	0.0156±0.0010±0.0016	0.0096±0.0008±0.0022
1.1	0.0378±0.0015±0.0047	0.0246±0.0012±0.0027	0.0188±0.0011±0.0010	0.0115±0.0008±0.0023	0.0073±0.0007±0.0012
1.3	0.0311±0.0014±0.0028	0.0187±0.0011±0.0028	0.0122±0.0009±0.0009	0.0074±0.0007±0.0007	—
1.5	0.0216±0.0012±0.0024	0.0165±0.0010±0.0032	0.0091±0.0007±0.0008	0.0044±0.0005±0.0000	0.0030±0.0004±0.0003
1.7	0.0142±0.0009±0.0009	0.0108±0.0008±0.0013	0.0032±0.0004±0.0003	—	0.0005±0.0002±0.0001
1.9	0.0086±0.0007±0.0009	0.0044±0.0005±0.0008	—	0.0015±0.0003±0.0002	—
2.1	0.0024±0.0004±0.0002	—	—	—	—
2.3	—	—	—	—	—
2.5	—	—	—	—	—
2.7	—	—	—	—	—
2.9	—	—	—	—	—

TABLE B.20: Numerical results: $\frac{d^2n}{dydp_T}$ spectra of K^- produced in inelastic $p + p$ collisions at 158 GeV/c. Rapidity (y) and transverse momentum (p_T) values correspond to center of bins.

B.3 $\bar{p}$, p spectra

y	p_T [GeV/c]				
	0.1	0.2	0.2	0.4	0.5
-1.1	—	—	—	—	—
-0.9	—	—	—	—	—
-0.7	—	—	—	—	—
-0.5	—	—	—	—	—
-0.3	—	—	—	—	—
-0.1	—	—	—	—	—
0.1	0.0012±0.0004±0.0002	0.0037±0.0007±0.0005	0.0065±0.0009±0.0008	0.0058±0.0009±0.0009	0.0047±0.0008±0.0006
0.3	0.0012±0.0003±0.0002	0.0040±0.0006±0.0007	0.0059±0.0008±0.0009	0.0070±0.0010±0.0009	0.0038±0.0008±0.0006
0.5	0.0006±0.0002±0.0001	0.0023±0.0005±0.0004	0.0035±0.0006±0.0005	0.0053±0.0008±0.0009	0.0034±0.0007±0.0005
0.7	0.0006±0.0002±0.0001	0.0016±0.0004±0.0003	0.0022±0.0005±0.0003	0.0034±0.0006±0.0005	0.0015±0.0004±0.0002
0.9	0.0005±0.0002±0.0001	0.0010±0.0003±0.0002	0.0017±0.0004±0.0003	0.0019±0.0004±0.0002	0.0017±0.0004±0.0002
1.1	—	0.0006±0.0002±0.0001	0.0007±0.0003±0.0001	0.0009±0.0003±0.0001	0.0009±0.0003±0.0001
1.3	—	0.0000±0.0000±0.0000	0.0003±0.0002±0.0000	0.0001±0.0001±0.0000	0.0004±0.0003±0.0000
1.5	—	—	—	—	—
1.7	—	—	—	—	—
1.9	—	—	—	—	—
2.1	—	—	—	—	—
2.3	—	—	—	—	—
2.5	—	—	—	—	—
2.7	—	—	—	—	—
2.9	—	—	—	—	—

y	p_T [GeV/c]				
	0.6	0.7	0.8	0.9	1.0
-1.1	—	—	—	—	—
-0.9	—	—	—	—	—
-0.7	—	—	—	—	—
-0.5	—	—	—	—	—
-0.3	—	—	—	—	—
-0.1	—	0.0036±0.0010±0.0005	0.0014±0.0005±0.0002	0.0011±0.0004±0.0002	—
0.1	0.0033±0.0007±0.0005	0.0026±0.0006±0.0004	0.0027±0.0007±0.0004	0.0025±0.0007±0.0004	—
0.3	0.0042±0.0008±0.0006	0.0035±0.0007±0.0004	0.0017±0.0005±0.0002	0.0026±0.0007±0.0004	—
0.5	0.0022±0.0006±0.0003	0.0017±0.0005±0.0002	0.0015±0.0005±0.0002	—	—
0.7	0.0019±0.0005±0.0003	0.0019±0.0005±0.0003	—	—	—
0.9	0.0006±0.0003±0.0001	0.0003±0.0002±0.0000	—	—	—
1.1	0.0016±0.0006±0.0002	—	—	—	—
1.3	—	—	—	—	—
1.5	—	—	—	—	—
1.7	—	—	—	—	—
1.9	—	—	—	—	—
2.1	—	—	—	—	—
2.3	—	—	—	—	—
2.5	—	—	—	—	—
2.7	—	—	—	—	—
2.9	—	—	—	—	—

TABLE B.21: Numerical results: $\frac{d^2n}{dydp_T}$ spectra of $\bar{p}$ produced in inelastic $p + p$ collisions at 30.9 GeV/c. Rapidity (y) and transverse momentum (p_T) values correspond to center of bins.

y	p_T [GeV/c]				
	0.1	0.2	0.2	0.4	0.5
-1.1	—	—	—	—	—
-0.9	—	—	—	—	—
-0.7	—	—	—	—	—
-0.5	—	—	—	—	—
-0.3	—	—	—	—	—
-0.1	—	—	—	—	—
0.1	—	—	—	—	0.0063±0.0006±0.0008
0.3	0.0015±0.0003±0.0002	0.0033±0.0004±0.0005	0.0055±0.0006±0.0007	0.0068±0.0006±0.0011	0.0055±0.0006±0.0008
0.5	0.0013±0.0003±0.0002	0.0031±0.0004±0.0004	0.0056±0.0006±0.0009	0.0051±0.0006±0.0007	0.0051±0.0006±0.0006
0.7	0.0003±0.0001±0.0000	0.0020±0.0004±0.0003	0.0026±0.0004±0.0004	0.0032±0.0004±0.0005	0.0030±0.0004±0.0004
0.9	0.0004±0.0002±0.0001	0.0009±0.0002±0.0001	0.0019±0.0003±0.0002	0.0022±0.0004±0.0003	0.0019±0.0003±0.0003
1.1	—	—	—	—	—
1.3	—	—	—	—	—
1.5	—	—	—	—	—
1.7	—	—	—	—	—
1.9	—	—	—	—	—
2.1	—	—	—	—	—
2.3	—	—	—	—	—
2.5	—	—	—	—	—
2.7	—	—	—	—	—
2.9	—	—	—	—	—

y	p_T [GeV/c]				
	0.6	0.7	0.8	0.9	1.0
-1.1	—	—	—	—	—
-0.9	—	—	—	—	—
-0.7	—	—	—	—	—
-0.5	—	—	—	—	—
-0.3	—	—	—	—	—
-0.1	—	—	—	—	—
0.1	0.0050±0.0006±0.0007	0.0027±0.0004±0.0004	0.0029±0.0004±0.0004	0.0015±0.0003±0.0002	—
0.3	0.0043±0.0005±0.0006	0.0039±0.0005±0.0006	0.0034±0.0005±0.0005	—	0.0009±0.0002±0.0002
0.5	0.0031±0.0004±0.0004	0.0029±0.0004±0.0005	—	—	—
0.7	0.0030±0.0004±0.0004	0.0020±0.0003±0.0002	0.0010±0.0002±0.0001	—	—
0.9	0.0011±0.0003±0.0002	0.0007±0.0002±0.0001	0.0004±0.0002±0.0001	—	—
1.1	—	—	—	—	—
1.3	—	—	—	—	—
1.5	—	—	—	—	—
1.7	—	—	—	—	—
1.9	—	—	—	—	—
2.1	—	—	—	—	—
2.3	—	—	—	—	—
2.5	—	—	—	—	—
2.7	—	—	—	—	—
2.9	—	—	—	—	—

TABLE B.22: Numerical results: $\frac{d^2n}{dydp_T}$ spectra of $\bar{p}$ produced in inelastic $p + p$ collisions at 40 GeV/c. Rapidity (y) and transverse momentum (p_T) values correspond to center of bins.

y	$p_T \, [GeV/c]$				
	0.1	0.2	0.2	0.4	0.5
-1.1	—	—	—	—	—
-0.9	—	—	—	—	—
-0.7	—	—	—	—	—
-0.5	0.0050±0.0028±0.0008	0.0166±0.0032±0.0022	0.0208±0.0028±0.0034	0.0140±0.0022±0.0021	0.0126±0.0016±0.0018
-0.3	0.0044±0.0006±0.0006	0.0111±0.0011±0.0014	0.0198±0.0013±0.0024	0.0167±0.0013±0.0027	0.0173±0.0014±0.0025
-0.1	0.0058±0.0007±0.0007	0.0130±0.0010±0.0022	0.0157±0.0011±0.0025	0.0170±0.0013±0.0022	0.0171±0.0013±0.0026
0.1	0.0035±0.0005±0.0005	0.0115±0.0009±0.0014	0.0138±0.0012±0.0020	0.0151±0.0012±0.0023	0.0138±0.0012±0.0023
0.3	0.0035±0.0005±0.0006	0.0083±0.0009±0.0010	0.0135±0.0011±0.0023	0.0187±0.0012±0.0029	0.0148±0.0012±0.0025
0.5	0.0031±0.0005±0.0005	0.0075±0.0007±0.0010	0.0114±0.0009±0.0018	0.0124±0.0010±0.0021	0.0116±0.0010±0.0020
0.7	0.0023±0.0004±0.0004	0.0064±0.0007±0.0009	0.0106±0.0008±0.0014	0.0098±0.0009±0.0013	0.0083±0.0009±0.0013
0.9	0.0015±0.0004±0.0002	0.0055±0.0007±0.0009	0.0086±0.0008±0.0014	0.0072±0.0008±0.0010	0.0069±0.0008±0.0010
1.1	0.0008±0.0003±0.0001	0.0033±0.0005±0.0004	0.0042±0.0006±0.0006	0.0037±0.0007±0.0004	0.0045±0.0006±0.0007
1.3	0.0006±0.0002±0.0001	0.0017±0.0004±0.0003	0.0028±0.0004±0.0004	0.0032±0.0005±0.0004	0.0019±0.0004±0.0003
1.5	0.0003±0.0001±0.0000	0.0021±0.0005±0.0003	0.0015±0.0003±0.0002	0.0011±0.0003±0.0002	0.0010±0.0003±0.0001
1.7	0.0000±0.0001±0.0000	0.0010±0.0003±0.0002	0.0014±0.0004±0.0002	0.0012±0.0003±0.0002	0.0012±0.0004±0.0002
1.9	—	0.0000±0.0001±0.0000	0.0013±0.0008±0.0002	0.0000±0.0000±0.0000	—
2.1	—	—	—	—	—
2.3	—	—	—	—	—
2.5	—	—	—	—	—
2.7	—	—	—	—	—
2.9	—	—	—	—	—

y	$p_T \, [GeV/c]$				
	0.6	0.7	0.8	0.9	1.0
-1.1	—	—	—	—	—
-0.9	—	—	—	—	0.0000±0.0001±0.0000
-0.7	—	0.0071±0.0027±0.0010	0.0038±0.0015±0.0006	0.0018±0.0009±0.0002	0.0023±0.0007±0.0003
-0.5	0.0090±0.0013±0.0015	0.0056±0.0010±0.0008	0.0057±0.0009±0.0010	0.0036±0.0008±0.0006	0.0027±0.0006±0.0003
-0.3	0.0172±0.0013±0.0027	0.0080±0.0011±0.0011	0.0078±0.0010±0.0013	0.0036±0.0007±0.0005	0.0030±0.0007±0.0004
-0.1	0.0126±0.0015±0.0020	0.0108±0.0012±0.0014	0.0083±0.0011±0.0011	0.0056±0.0010±0.0008	0.0034±0.0008±0.0005
0.1	0.0113±0.0011±0.0014	0.0112±0.0011±0.0019	0.0042±0.0009±0.0006	0.0057±0.0007±0.0008	0.0028±0.0007±0.0004
0.3	0.0153±0.0012±0.0021	0.0088±0.0009±0.0011	0.0073±0.0009±0.0009	0.0040±0.0006±0.0006	0.0019±0.0006±0.0002
0.5	0.0136±0.0011±0.0019	0.0069±0.0008±0.0011	0.0050±0.0008±0.0008	0.0027±0.0005±0.0004	0.0019±0.0005±0.0003
0.7	0.0086±0.0009±0.0011	0.0070±0.0008±0.0011	0.0050±0.0006±0.0007	0.0026±0.0006±0.0003	0.0018±0.0005±0.0003
0.9	0.0053±0.0008±0.0009	0.0037±0.0005±0.0006	0.0035±0.0006±0.0005	0.0019±0.0003±0.0003	0.0009±0.0004±0.0001
1.1	0.0039±0.0006±0.0005	0.0023±0.0005±0.0003	0.0019±0.0004±0.0003	0.0009±0.0003±0.0001	0.0008±0.0007±0.0001
1.3	0.0014±0.0004±0.0002	0.0021±0.0004±0.0003	0.0010±0.0003±0.0001	0.0006±0.0002±0.0001	—
1.5	0.0011±0.0003±0.0002	0.0006±0.0002±0.0001	0.0009±0.0004±0.0001	—	—
1.7	0.0006±0.0002±0.0001	0.0000±0.0000±0.0000	0.0003±0.0004±0.0001	—	—
1.9	—	—	—	—	—
2.1	—	—	—	—	—
2.3	—	—	—	—	—
2.5	—	—	—	—	—
2.7	—	—	—	—	—
2.9	—	—	—	—	—

TABLE B.23: Numerical results: $\frac{d^2n}{dydp_T}$ spectra of $\bar{p}$ produced in inelastic $p + p$ collisions at 80 GeV/c. Rapidity (y) and transverse momentum (p_T) values correspond to center of bins.

y	p_T [GeV/c]				
	0.1	0.2	0.2	0.4	0.5
-1.1	—	—	—	—	—
-0.9	—	—	—	—	—
-0.7	—	—	—	—	—
-0.5	0.0066±0.0006±0.0011	0.0164±0.0010±0.0027	0.0228±0.0012±0.0020	0.0221±0.0012±0.0006	0.0240±0.0012±0.0071
-0.3	0.0055±0.0006±0.0009	0.0166±0.0010±0.0021	0.0269±0.0013±0.0024	0.0259±0.0013±0.0019	0.0273±0.0013±0.0023
-0.1	0.0055±0.0006±0.0009	0.0180±0.0011±0.0022	0.0236±0.0012±0.0015	0.0291±0.0013±0.0022	0.0285±0.0013±0.0027
0.1	0.0056±0.0006±0.0008	0.0150±0.0010±0.0011	0.0222±0.0012±0.0031	0.0253±0.0012±0.0014	0.0289±0.0013±0.0022
0.3	0.0053±0.0006±0.0006	0.0141±0.0009±0.0015	0.0224±0.0012±0.0027	0.0256±0.0013±0.0020	0.0230±0.0012±0.0019
0.5	0.0052±0.0006±0.0005	0.0138±0.0009±0.0017	0.0202±0.0011±0.0018	0.0202±0.0011±0.0020	0.0221±0.0012±0.0018
0.7	0.0051±0.0006±0.0006	0.0129±0.0009±0.0006	0.0169±0.0010±0.0022	0.0194±0.0011±0.0014	0.0205±0.0011±0.0015
0.9	0.0044±0.0005±0.0009	0.0103±0.0008±0.0015	0.0145±0.0009±0.0013	0.0144±0.0009±0.0014	0.0144±0.0009±0.0024
1.1	0.0030±0.0004±0.0006	0.0068±0.0006±0.0007	0.0121±0.0009±0.0009	0.0125±0.0009±0.0019	0.0112±0.0008±0.0011
1.3	0.0025±0.0004±0.0004	0.0039±0.0005±0.0004	0.0086±0.0007±0.0013	0.0096±0.0008±0.0008	0.0081±0.0007±0.0007
1.5	0.0011±0.0003±0.0002	0.0026±0.0004±0.0002	0.0048±0.0005±0.0006	0.0054±0.0006±0.0008	0.0044±0.0005±0.0014
1.7	0.0007±0.0002±0.0001	0.0019±0.0003±0.0002	0.0032±0.0004±0.0012	0.0024±0.0004±0.0000	0.0034±0.0005±0.0005
1.9	0.0003±0.0001±0.0000	0.0014±0.0003±0.0003	0.0015±0.0003±0.0000	0.0012±0.0003±0.0000	0.0009±0.0002±0.0000
2.1	—	—	—	—	—
2.3	—	—	—	—	—
2.5	—	—	—	—	—
2.7	—	—	—	—	—
2.9	—	—	—	—	—

y	p_T [GeV/c]				
	0.6	0.7	0.8	0.9	1.0
-1.1	—	—	—	—	—
-0.9	—	—	—	—	—
-0.7	—	0.0111±0.0008±0.0000	0.0095±0.0008±0.0023	0.0057±0.0006±0.0000	—
-0.5	0.0196±0.0011±0.0059	0.0136±0.0009±0.0048	0.0107±0.0008±0.0041	0.0074±0.0007±0.0011	0.0038±0.0005±0.0010
-0.3	0.0252±0.0012±0.0037	0.0188±0.0011±0.0022	0.0120±0.0009±0.0039	0.0103±0.0008±0.0020	0.0064±0.0006±0.0005
-0.1	0.0216±0.0012±0.0009	0.0195±0.0011±0.0012	0.0129±0.0009±0.0035	0.0117±0.0008±0.0026	0.0089±0.0007±0.0024
0.1	0.0197±0.0011±0.0045	0.0170±0.0010±0.0017	0.0127±0.0009±0.0012	0.0103±0.0008±0.0010	—
0.3	0.0238±0.0012±0.0017	0.0172±0.0010±0.0014	0.0119±0.0009±0.0021	0.0095±0.0008±0.0011	0.0076±0.0007±0.0029
0.5	0.0209±0.0011±0.0024	0.0164±0.0010±0.0016	0.0116±0.0008±0.0022	0.0091±0.0007±0.0017	0.0061±0.0006±0.0008
0.7	0.0156±0.0010±0.0015	0.0146±0.0009±0.0010	0.0107±0.0008±0.0016	0.0085±0.0007±0.0020	0.0064±0.0006±0.0020
0.9	0.0136±0.0009±0.0015	0.0121±0.0009±0.0016	0.0102±0.0008±0.0025	0.0052±0.0006±0.0004	—
1.1	0.0099±0.0008±0.0011	0.0086±0.0007±0.0014	0.0054±0.0006±0.0006	—	—
1.3	0.0087±0.0007±0.0005	0.0056±0.0006±0.0012	0.0047±0.0005±0.0018	0.0030±0.0004±0.0000	0.0022±0.0004±0.0002
1.5	0.0061±0.0006±0.0016	0.0041±0.0005±0.0005	—	—	0.0009±0.0002±0.0000
1.7	0.0030±0.0004±0.0006	—	—	—	—
1.9	—	—	0.0007±0.0002±0.0000	—	—
2.1	—	—	—	—	—
2.3	—	—	—	—	—
2.5	—	—	—	—	—
2.7	—	—	—	—	—
2.9	—	—	—	—	—

TABLE B.24: Numerical results: $\frac{d^2n}{dydp_T}$ spectra of $\bar{p}$ produced in inelastic $p+p$ collisions at 158 GeV/c. Rapidity (y) and transverse momentum (p_T) values correspond to center of bins.

y	p_T [GeV/c]				
	0.1	0.2	0.2	0.4	0.5
-1.1	—	—	—	—	—
-0.9	—	0.3138±0.0124±0.0541	—	—	—
-0.7	0.0999±0.0040±0.0127	0.2687±0.0114±0.0352	0.3300±0.0145±0.0490	—	—
-0.5	0.0796±0.0046±0.0000	0.2357±0.0103±0.0323	0.2930±0.0114±0.0397	0.3838±0.0158±0.0630	0.3447±0.0178±0.0000
-0.3	—	—	0.2399±0.0090±0.0290	0.3700±0.0150±0.0338	0.3145±0.0145±0.0282
-0.1	—	—	—	0.3071±0.0120±0.0278	0.2540±0.0107±0.0239
0.1	—	—	—	0.3911±0.2622±0.0340	0.2728±0.0533±0.0277
0.3	0.1079±0.0114±0.0097	0.2804±0.0180±0.0297	0.4915±0.0204±0.0419	0.3987±0.0225±0.0438	0.3222±0.0223±0.0326
0.5	0.1661±0.0096±0.0163	0.3285±0.0158±0.0274	0.3267±0.0200±0.0350	0.4462±0.0233±0.0355	0.3650±0.0252±0.0277
0.7	0.1813±0.0107±0.0145	0.2903±0.0173±0.0244	0.6012±0.0211±0.0534	0.5604±0.0244±0.0580	0.4487±0.0260±0.0437
0.9	0.2234±0.0115±0.0201	0.4322±0.0198±0.0379	0.5514±0.0236±0.0491	0.6249±0.0252±0.0685	0.5982±0.0264±0.0648
1.1	0.1704±0.0132±0.0125	0.4378±0.0215±0.0405	0.9346±0.0261±0.0734	0.4952±0.0262±0.0375	0.4152±0.0261±0.0420
1.3	0.2500±0.0171±0.0275	0.6465±0.0258±0.0572	0.9118±0.0304±0.0965	0.8361±0.0302±0.0864	0.7935±0.0277±0.0637
1.5	0.2971±0.0296±0.0253	0.9770±0.0332±0.0785	0.8835±0.0367±0.0684	0.8458±0.0347±0.0803	0.5839±0.0307±0.0418
1.7	0.3932±0.0906±0.0420	0.5652±0.0605±0.0446	0.9211±0.0517±0.0742	0.5515±0.0586±0.0541	0.4259±0.0463±0.0441
1.9	—	0.3314±0.1332±0.0352	0.2306±0.1312±0.0230	0.0035±0.0237±0.0004	—
2.1	—	—	—	—	—
2.3	—	—	—	—	—
2.5	—	—	—	—	—
2.7	—	—	—	—	—
2.9	—	—	—	—	—

y	p_T [GeV/c]				
	0.6	0.7	0.8	0.9	1.0
-1.1	—	—	—	—	—
-0.9	—	—	—	—	—
-0.7	—	—	—	—	—
-0.5	—	—	—	—	—
-0.3	0.2743±0.0172±0.1145	0.1959±0.0107±0.0288	—	—	—
-0.1	0.2645±0.0120±0.0245	0.2043±0.0122±0.0157	0.1420±0.0943±0.0108	0.0957±-nan±0.0157	0.0537±0.0188±0.0041
0.1	0.1989±0.0309±0.0159	0.1230±0.0237±0.0096	0.1136±0.0168±0.0087	0.0561±0.3867±0.0057	0.0554±0.0413±0.0044
0.3	0.1844±0.0213±0.0132	0.1718±0.0195±0.0179	0.0819±0.0171±0.0070	0.0569±0.0147±0.0040	0.0395±0.0123±0.0029
0.5	0.2364±0.0224±0.0168	0.2192±0.0204±0.0164	0.1216±0.0177±0.0131	0.0469±0.0154±0.0047	0.0323±0.0133±0.0025
0.7	0.3643±0.0248±0.0287	0.1243±0.0233±0.0088	0.1155±0.0197±0.0102	0.1315±0.0165±0.0123	0.0631±0.0145±0.0068
0.9	0.6194±0.0246±0.0447	0.2793±0.0244±0.0301	0.1883±0.0216±0.0187	0.1606±0.0429±0.0176	0.0512±0.0917±0.0044
1.1	0.5134±0.0256±0.0408	0.2569±0.0238±0.0260	0.1810±0.0199±0.0195	—	—
1.3	0.4524±0.0242±0.0453	0.2457±0.0214±0.0205	0.1691±0.0181±0.0160	—	—
1.5	0.3939±0.0255±0.0408	0.1753±0.0213±0.0138	0.1474±0.0181±0.0107	—	—
1.7	0.1635±0.0325±0.0140	0.0473±0.0244±0.0043	0.0051±0.0121±0.0005	—	—
1.9	—	—	—	—	—
2.1	—	—	—	—	—
2.3	—	—	—	—	—
2.5	—	—	—	—	—
2.7	—	—	—	—	—
2.9	—	—	—	—	—

TABLE B.25: Numerical results: $\frac{d^2n}{dydp_T}$ spectra of p produced in inelastic $p+p$ collisions at 20 GeV/c. Rapidity (y) and transverse momentum (p_T) values correspond to center of bins.

y	p_T [GeV/c]				
	0.1	0.2	0.2	0.4	0.5
-1.1	0.1032±0.0103±0.0136	—	—	—	—
-0.9	0.0909±0.0072±0.0163	0.2213±0.0125±0.0189	—	—	—
-0.7	0.0798±0.0075±0.0148	0.1842±0.0118±0.0327	0.2521±0.0124±0.0320	—	—
-0.5	0.0671±0.0041±0.0119	0.1673±0.0114±0.0296	0.2104±0.0137±0.0406	0.2997±0.0268±0.0521	0.2982±0.0190±0.0394
-0.3	—	—	0.1875±0.0060±0.0276	0.2771±0.0312±0.0514	0.2303±0.0230±0.0452
-0.1	—	—	—	—	—
0.1	0.0441±0.0025±0.0041	0.1175±0.0039±0.0092	0.1547±0.0046±0.0117	0.1770±0.0052±0.0179	0.1820±0.0053±0.0145
0.3	0.0482±0.0022±0.0039	0.1279±0.0036±0.0128	0.1822±0.0045±0.0152	0.2003±0.0052±0.0189	0.1967±0.0056±0.0167
0.5	0.0568±0.0024±0.0041	0.1552±0.0040±0.0166	0.2333±0.0050±0.0184	0.2419±0.0054±0.0195	0.2323±0.0058±0.0228
0.7	0.0660±0.0027±0.0067	0.2014±0.0046±0.0166	0.2812±0.0055±0.0214	0.3140±0.0059±0.0233	0.3075±0.0063±0.0285
0.9	0.0883±0.0031±0.0095	0.2388±0.0051±0.0176	0.3497±0.0062±0.0319	0.4063±0.0067±0.0354	0.3845±0.0066±0.0317
1.1	0.0965±0.0033±0.0082	0.2741±0.0055±0.0238	0.4163±0.0068±0.0415	0.4754±0.0073±0.0339	0.4803±0.0074±0.0484
1.3	0.1227±0.0038±0.0109	0.3455±0.0062±0.0339	0.5109±0.0075±0.0521	0.5673±0.0080±0.0535	0.5294±0.0078±0.0457
1.5	0.1667±0.0052±0.0131	0.4563±0.0077±0.0408	0.6692±0.0090±0.0645	0.6735±0.0091±0.0517	0.6063±0.0087±0.0441
1.7	—	0.5935±0.0114±0.0539	0.7638±0.0110±0.0764	0.7949±0.0109±0.0642	0.6690±0.0100±0.0519
1.9	—	—	—	—	—
2.1	—	—	—	—	—
2.3	—	—	—	—	—
2.5	—	—	—	—	—
2.7	—	—	—	—	—
2.9	—	—	—	—	—

y	p_T [GeV/c]				
	0.6	0.7	0.8	0.9	1.0
-1.1	—	—	—	—	—
-0.9	—	—	—	—	—
-0.7	—	—	—	—	—
-0.5	0.2501±0.0198±0.0325	—	—	—	—
-0.3	0.2237±0.0131±0.0425	—	—	—	—
-0.1	0.2064±0.0171±0.0364	0.1208±0.0054±0.0120	0.0847±0.0040±0.0093	0.0742±0.0037±0.0063	0.0598±0.0033±0.0044
0.1	0.1577±0.0049±0.0160	0.1331±0.0046±0.0143	0.0990±0.0040±0.0109	0.0841±0.0038±0.0074	0.0602±0.0032±0.0064
0.3	0.1763±0.0054±0.0142	0.1460±0.0049±0.0113	0.1237±0.0045±0.0117	0.0803±0.0036±0.0057	0.0575±0.0031±0.0059
0.5	0.2091±0.0059±0.0217	0.1746±0.0055±0.0150	0.1367±0.0048±0.0124	0.1007±0.0041±0.0107	0.0777±0.0036±0.0082
0.7	0.2658±0.0062±0.0186	0.2264±0.0061±0.0210	0.1744±0.0056±0.0139	0.1261±0.0047±0.0093	0.0799±0.0038±0.0073
0.9	0.3561±0.0068±0.0307	0.2942±0.0065±0.0265	0.2173±0.0058±0.0167	0.1483±0.0049±0.0113	0.0974±0.0041±0.0081
1.1	0.4215±0.0070±0.0372	0.3296±0.0063±0.0348	0.2506±0.0058±0.0242	0.1806±0.0051±0.0181	0.1267±0.0044±0.0131
1.3	0.4752±0.0074±0.0382	0.3612±0.0065±0.0393	0.2733±0.0058±0.0285	0.1817±0.0048±0.0136	0.1150±0.0039±0.0104
1.5	0.4811±0.0078±0.0497	0.3412±0.0066±0.0339	0.2378±0.0056±0.0253	0.1538±0.0045±0.0165	0.1066±0.0044±0.0109
1.7	0.4934±0.0085±0.0521	0.3131±0.0069±0.0317	0.2220±0.0064±0.0228	0.1105±0.0049±0.0100	—
1.9	—	—	—	—	—
2.1	—	—	—	—	—
2.3	—	—	—	—	—
2.5	—	—	—	—	—
2.7	—	—	—	—	—
2.9	—	—	—	—	—

TABLE B.26: Numerical results: $\frac{d^2n}{dydp_T}$ spectra of p produced in inelastic $p + p$ collisions at 30.9 GeV/c. Rapidity (y) and transverse momentum (p_T) values correspond to center of bins.

y	$p_T \ [GeV/c]$				
	0.1	0.2	0.2	0.4	0.5
-1.1	—	—	—	—	—
-0.9	0.0779±0.0043±0.0140	0.1894±0.0429±0.0161	—	—	—
-0.7	0.0672±0.0042±0.0125	0.1533±0.0079±0.0272	0.2128±0.0077±0.0270	0.2925±0.0261±0.0327	—
-0.5	0.0581±0.0064±0.0103	0.1420±0.0082±0.0251	0.1753±0.0082±0.0338	0.2535±0.0155±0.0441	0.2553±0.0114±0.0337
-0.3	—	0.1190±0.0104±0.0163	0.1609±0.0065±0.0236	0.2335±0.0180±0.0433	0.1949±0.0110±0.0383
-0.1	0.0379±0.0024±0.0000	0.1140±0.0038±0.0000	0.1699±0.0047±0.0000	0.1832±0.0046±0.0000	0.2005±0.0043±0.0000
0.1	0.0396±0.0015±0.0000	0.1146±0.0025±0.0000	0.1660±0.0032±0.0000	0.1879±0.0038±0.0000	0.1910±0.0040±0.0381
0.3	0.0452±0.0016±0.0112	0.1227±0.0026±0.0317	0.1759±0.0032±0.0423	0.1950±0.0036±0.0476	0.1894±0.0039±0.0386
0.5	0.0517±0.0017±0.0135	0.1435±0.0029±0.0350	0.2127±0.0035±0.0462	0.2287±0.0037±0.0491	0.2251±0.0040±0.0410
0.7	0.0641±0.0020±0.0164	0.1850±0.0033±0.0316	0.2595±0.0039±0.0441	0.2970±0.0042±0.0554	0.2775±0.0042±0.0456
0.9	0.0763±0.0021±0.0126	0.2169±0.0036±0.0260	0.3178±0.0043±0.0415	0.3734±0.0048±0.0529	0.3646±0.0047±0.0446
1.1	0.0915±0.0023±0.0140	0.2755±0.0041±0.0307	0.3957±0.0049±0.0433	0.4542±0.0053±0.0484	0.4431±0.0052±0.0383
1.3	0.1035±0.0026±0.0230	0.3119±0.0043±0.0401	0.4674±0.0054±0.0380	0.5290±0.0057±0.0306	0.5324±0.0058±0.0398
1.5	0.1382±0.0030±0.0278	0.3797±0.0049±0.0408	0.5599±0.0059±0.0410	0.6241±0.0063±0.0291	0.5785±0.0061±0.0128
1.7	0.1491±0.0047±0.0000	0.5080±0.0065±0.0335	0.6598±0.0070±0.0409	0.7000±0.0071±0.0291	0.6309±0.0068±0.0167
1.9	—	0.4832±0.0119±0.0000	0.7761±0.0096±0.0000	0.7464±0.0085±0.0705	0.6107±0.0074±0.0718
2.1	—	—	—	0.8448±0.0154±0.0000	0.5432±0.0110±0.0000
2.3	—	—	—	—	—
2.5	—	—	—	—	—
2.7	—	—	—	—	—
2.9	—	—	—	—	—

y	$p_T \ [GeV/c]$				
	0.6	0.7	0.8	0.9	1.0
-1.1	—	—	—	—	—
-0.9	—	—	—	—	—
-0.7	—	—	—	—	—
-0.5	0.2133±0.0084±0.0277	0.1749±0.0165±0.0302	—	—	0.0577±0.0065±0.0000
-0.3	0.1906±0.0108±0.0362	0.1377±0.0061±0.0000	0.0982±0.0040±0.0000	0.0858±0.0031±0.0000	0.0597±0.0025±0.0000
-0.1	0.1681±0.0037±0.0000	0.1369±0.0034±0.0000	0.1058±0.0031±0.0000	0.0870±0.0029±0.0000	0.0539±0.0023±0.0133
0.1	0.1663±0.0037±0.0320	0.1354±0.0034±0.0299	0.1055±0.0030±0.0253	0.0842±0.0027±0.0144	0.0598±0.0023±0.0074
0.3	0.1756±0.0039±0.0389	0.1400±0.0035±0.0155	0.1116±0.0031±0.0161	0.0930±0.0028±0.0084	0.0647±0.0024±0.0075
0.5	0.2007±0.0040±0.0326	0.1695±0.0039±0.0249	0.1279±0.0035±0.0114	0.0971±0.0030±0.0089	0.0661±0.0025±0.0085
0.7	0.2501±0.0042±0.0410	0.2053±0.0040±0.0303	0.1588±0.0037±0.0167	0.1148±0.0033±0.0114	0.0750±0.0027±0.0082
0.9	0.3095±0.0044±0.0408	0.2535±0.0042±0.0268	0.2020±0.0039±0.0205	0.1393±0.0033±0.0112	0.0925±0.0028±0.0082
1.1	0.3963±0.0050±0.0318	0.3277±0.0046±0.0239	0.2419±0.0040±0.0155	0.1737±0.0035±0.0177	0.1115±0.0028±0.0061
1.3	0.4670±0.0054±0.0145	0.3765±0.0049±0.0158	0.2886±0.0043±0.0154	0.1981±0.0036±0.0134	0.1299±0.0030±0.0055
1.5	0.4700±0.0056±0.0143	0.3682±0.0050±0.0161	0.2624±0.0042±0.0096	0.1776±0.0035±0.0054	0.1156±0.0029±0.0065
1.7	0.4877±0.0061±0.0094	0.3420±0.0051±0.0069	0.2152±0.0041±0.0057	0.1315±0.0032±0.0070	0.2964±0.0116±0.0562
1.9	0.4722±0.0065±0.0925	0.3370±0.0060±0.1226	0.1991±0.0052±0.0000	0.0804±0.0039±0.0000	—
2.1	0.3226±0.0098±0.0000	0.1456±0.0085±0.0000	—	—	—
2.3	—	—	—	—	—
2.5	—	—	—	—	—
2.7	—	—	—	—	—
2.9	—	—	—	—	—

TABLE B.27: Numerical results: $\frac{d^2n}{dydp_T}$ spectra of p produced in inelastic $p + p$ collisions at 40 GeV/c. Rapidity (y) and transverse momentum (p_T) values correspond to center of bins.

y	p_T $[GeV/c]$				
	0.1	0.2	0.2	0.4	0.5
-1.1	—	—	—	—	—
-0.9	—	—	—	—	—
-0.7	0.0434±0.0011±0.0026	0.1022±0.0021±0.0064	0.1390±0.0108±0.0052	0.1893±0.0381±0.0261	—
-0.5	0.0381±0.0012±0.0023	0.0976±0.0026±0.0072	0.1203±0.0025±0.0058	0.1683±0.0041±0.0070	0.1695±0.0047±0.0059
-0.3	0.0341±0.0055±0.0012	0.0823±0.0103±0.0045	0.1115±0.0125±0.0061	0.1634±0.0269±0.0130	0.1360±0.0148±0.0111
-0.1	0.0231±0.0012±0.0016	0.0631±0.0020±0.0060	0.0835±0.0023±0.0083	0.0985±0.0025±0.0114	0.1038±0.0026±0.0069
0.1	0.0234±0.0012±0.0024	0.0665±0.0021±0.0056	0.0954±0.0025±0.0069	0.1088±0.0026±0.0083	0.1140±0.0027±0.0111
0.3	0.0225±0.0012±0.0026	0.0643±0.0020±0.0039	0.1049±0.0026±0.0109	0.1136±0.0027±0.0132	0.1103±0.0027±0.0118
0.5	0.0282±0.0013±0.0023	0.0745±0.0022±0.0071	0.1161±0.0027±0.0126	0.1303±0.0029±0.0110	0.1332±0.0029±0.0099
0.7	0.0341±0.0015±0.0036	0.0889±0.0024±0.0094	0.1289±0.0029±0.0138	0.1518±0.0031±0.0139	0.1502±0.0031±0.0174
0.9	0.0396±0.0016±0.0043	0.1133±0.0027±0.0124	0.1565±0.0032±0.0102	0.1868±0.0035±0.0159	0.1939±0.0035±0.0177
1.1	0.0517±0.0018±0.0031	0.1447±0.0030±0.0119	0.2093±0.0037±0.0196	0.2517±0.0040±0.0252	0.2402±0.0039±0.0161
1.3	0.0635±0.0020±0.0039	0.1769±0.0034±0.0207	0.2700±0.0042±0.0250	0.3085±0.0044±0.0215	0.3124±0.0045±0.0364
1.5	0.0740±0.0022±0.0080	0.2256±0.0038±0.0201	0.3295±0.0046±0.0279	0.3645±0.0048±0.0333	0.3767±0.0049±0.0358
1.7	0.0998±0.0025±0.0109	0.2611±0.0041±0.0202	0.3866±0.0050±0.0403	0.4190±0.0052±0.0329	0.4397±0.0053±0.0363
1.9	0.1328±0.0029±0.0109	0.3556±0.0048±0.0295	0.4783±0.0055±0.0355	0.5064±0.0057±0.0312	0.4913±0.0056±0.0507
2.1	—	—	—	—	—
2.3	—	—	—	—	—
2.5	—	—	—	—	—
2.7	—	—	—	—	—
2.9	—	—	—	—	—

y	p_T $[GeV/c]$				
	0.6	0.7	0.8	0.9	1.0
-1.1	—	—	—	—	—
-0.9	—	—	—	—	—
-0.7	—	—	—	—	—
-0.5	0.1420±0.0038±0.0093	0.1170±0.0058±0.0048	0.0842±0.0033±0.0042	—	—
-0.3	0.1111±0.0027±0.0092	0.0815±0.0023±0.0072	0.0715±0.0021±0.0052	0.0475±0.0017±0.0057	0.0469±0.0017±0.0037
-0.1	0.1030±0.0026±0.0082	0.0905±0.0024±0.0067	0.0771±0.0022±0.0057	0.0574±0.0019±0.0047	0.0399±0.0016±0.0029
0.1	0.0977±0.0025±0.0073	0.0849±0.0023±0.0092	0.0726±0.0022±0.0066	0.0495±0.0018±0.0037	0.0398±0.0016±0.0037
0.3	0.1095±0.0026±0.0083	0.0928±0.0024±0.0066	0.0763±0.0022±0.0083	0.0597±0.0020±0.0037	0.0386±0.0016±0.0032
0.5	0.1163±0.0027±0.0128	0.1010±0.0025±0.0080	0.0833±0.0023±0.0090	0.0663±0.0021±0.0041	0.0387±0.0016±0.0031
0.7	0.1426±0.0030±0.0171	0.1204±0.0028±0.0096	0.0942±0.0025±0.0074	0.0723±0.0022±0.0076	0.0566±0.0019±0.0045
0.9	0.1649±0.0032±0.0178	0.1433±0.0030±0.0159	0.1181±0.0027±0.0090	0.0802±0.0023±0.0070	0.0585±0.0019±0.0048
1.1	0.2208±0.0038±0.0185	0.1877±0.0035±0.0150	0.1455±0.0031±0.0172	0.1061±0.0026±0.0100	0.0727±0.0022±0.0073
1.3	0.2902±0.0043±0.0178	0.2326±0.0039±0.0143	0.1759±0.0034±0.0176	0.1300±0.0029±0.0124	0.0902±0.0024±0.0086
1.5	0.3343±0.0046±0.0369	0.2868±0.0043±0.0339	0.2259±0.0038±0.0224	0.1500±0.0031±0.0119	0.1102±0.0027±0.0123
1.7	0.3982±0.0050±0.0293	0.3216±0.0045±0.0342	0.2458±0.0040±0.0284	0.1723±0.0033±0.0107	0.1138±0.0027±0.0121
1.9	0.4107±0.0051±0.0375	0.3277±0.0046±0.0292	0.2349±0.0039±0.0267	—	0.0846±0.0023±0.0052
2.1	—	—	—	—	—
2.3	—	—	—	—	—
2.5	—	—	—	—	—
2.7	—	—	—	—	—
2.9	—	—	—	—	—

TABLE B.28: Numerical results: $\frac{d^2n}{dydp_T}$ spectra of p produced in inelastic $p + p$ collisions at 80 GeV/c. Rapidity (y) and transverse momentum (p_T) values correspond to center of bins.

y	$p_T \ [GeV/c]$				
	0.1	0.2	0.2	0.4	0.5
-1.1	—	—	—	—	—
-0.9	—	—	—	—	—
-0.7	—	—	—	—	—
-0.5	0.0255±0.0013±0.0024	0.0753±0.0022±0.0102	0.0944±0.0024±0.0055	0.1125±0.0026±0.0128	0.1132±0.0026±0.0051
-0.3	0.0213±0.0011±0.0037	0.0575±0.0019±0.0055	0.0871±0.0023±0.0041	0.1088±0.0026±0.0088	0.1042±0.0025±0.0062
-0.1	0.0223±0.0012±0.0040	0.0596±0.0019±0.0044	0.0850±0.0023±0.0075	0.0983±0.0025±0.0061	0.0981±0.0025±0.0067
0.1	0.0182±0.0011±0.0022	0.0585±0.0019±0.0065	0.0841±0.0023±0.0069	0.0958±0.0024±0.0070	0.1015±0.0025±0.0083
0.3	0.0200±0.0011±0.0019	0.0566±0.0019±0.0046	0.0823±0.0023±0.0072	0.0962±0.0024±0.0071	0.1017±0.0025±0.0053
0.5	0.0219±0.0012±0.0021	0.0587±0.0019±0.0052	0.0870±0.0023±0.0059	0.0987±0.0025±0.0064	0.1048±0.0025±0.0058
0.7	0.0264±0.0013±0.0017	0.0716±0.0021±0.0046	0.0974±0.0024±0.0057	0.1237±0.0028±0.0088	0.1184±0.0027±0.0084
0.9	0.0305±0.0014±0.0026	0.0833±0.0023±0.0065	0.1236±0.0028±0.0074	0.1291±0.0028±0.0112	0.1423±0.0030±0.0093
1.1	0.0328±0.0014±0.0043	0.0987±0.0025±0.0096	0.1533±0.0031±0.0103	0.1710±0.0032±0.0127	0.1670±0.0032±0.0117
1.3	0.0441±0.0016±0.0077	0.1237±0.0028±0.0101	0.1824±0.0034±0.0123	0.2202±0.0037±0.0196	0.2193±0.0037±0.0143
1.5	0.0569±0.0019±0.0055	0.1594±0.0031±0.0145	0.2367±0.0038±0.0186	0.2858±0.0042±0.0224	0.2765±0.0041±0.0188
1.7	0.0800±0.0022±0.0214	0.1927±0.0034±0.0203	0.3038±0.0043±0.0321	0.3561±0.0047±0.0345	0.3517±0.0047±0.0309
1.9	—	0.2260±0.0037±0.0211	0.3392±0.0046±0.0359	0.3962±0.0049±0.0487	0.4091±0.0050±0.0428
2.1	—	0.2949±0.0043±0.0264	0.3346±0.0206±0.0380	0.4784±0.0139±0.0547	0.4416±0.0096±0.0491
2.3	—	0.3969±0.0076±0.0400	0.4763±0.0076±0.0458	0.5349±0.0079±0.0643	0.4680±0.0074±0.0508
2.5	—	—	0.4557±0.0604±0.0505	0.5969±0.0392±0.0676	0.5044±0.0283±0.0557
2.7	—	—	—	—	—
2.9	—	—	—	—	—

y	$p_T \ [GeV/c]$				
	0.6	0.7	0.8	0.9	1.0
-1.1	—	—	—	—	—
-0.9	—	—	—	—	—
-0.7	—	0.0926±0.0024±0.0041	0.0646±0.0020±0.0031	0.0525±0.0018±0.0050	—
-0.5	0.1001±0.0025±0.0100	0.0877±0.0023±0.0061	0.0714±0.0021±0.0067	0.0572±0.0019±0.0037	0.0429±0.0016±0.0065
-0.3	0.0993±0.0025±0.0042	0.0875±0.0023±0.0067	0.0688±0.0021±0.0064	0.0572±0.0019±0.0036	0.0396±0.0016±0.0086
-0.1	0.0926±0.0024±0.0040	0.0802±0.0022±0.0044	0.0676±0.0020±0.0039	0.0505±0.0018±0.0026	0.0425±0.0016±0.0075
0.1	0.0880±0.0023±0.0067	0.0784±0.0022±0.0066	0.0628±0.0020±0.0053	0.0532±0.0018±0.0044	0.0368±0.0015±0.0029
0.3	0.0986±0.0025±0.0055	0.0751±0.0022±0.0067	0.0631±0.0020±0.0052	0.0488±0.0017±0.0043	0.0395±0.0016±0.0044
0.5	0.0971±0.0024±0.0064	0.0866±0.0023±0.0055	0.0698±0.0021±0.0050	0.0537±0.0018±0.0057	0.0388±0.0015±0.0053
0.7	0.1134±0.0026±0.0086	0.1010±0.0025±0.0071	0.0808±0.0022±0.0057	0.0609±0.0019±0.0059	0.0407±0.0016±0.0054
0.9	0.1273±0.0028±0.0124	0.1099±0.0026±0.0080	0.0905±0.0024±0.0083	0.0725±0.0021±0.0063	0.0664±0.0020±0.0228
1.1	0.1463±0.0030±0.0122	0.1227±0.0027±0.0114	0.1064±0.0026±0.0092	0.0811±0.0022±0.0078	—
1.3	0.1954±0.0035±0.0179	0.1617±0.0032±0.0127	0.1311±0.0028±0.0091	0.0999±0.0025±0.0086	—
1.5	0.2620±0.0040±0.0170	0.2115±0.0036±0.0233	0.1656±0.0032±0.0157	0.1220±0.0027±0.0100	—
1.7	0.3293±0.0045±0.0313	0.2718±0.0041±0.0260	0.2072±0.0036±0.0228	—	—
1.9	0.3724±0.0048±0.0350	0.3177±0.0044±0.0354	0.2558±0.0040±0.0213	—	—
2.1	0.3806±0.0071±0.0381	0.3117±0.0055±0.0361	0.2475±0.0046±0.0264	—	—
2.3	0.3810±0.0068±0.0452	0.2686±0.0059±0.0299	0.2035±0.0052±0.0216	—	—
2.5	0.3284±0.0217±0.0371	0.2021±0.0170±0.0188	0.1356±0.0156±0.0152	—	—
2.7	—	—	—	—	—
2.9	—	—	—	—	—

TABLE B.29: Numerical results: $\frac{d^2n}{dydp_T}$ spectra of p produced in inelastic $p + p$ collisions at 158 GeV/c. Rapidity (y) and transverse momentum (p_T) values correspond to center of bins.

Bibliography

[1] N. Antoniou *et al.* (NA61/SHINE), (2006), CERN-SPSC-2006-034.

[2] N. Abgrall *et al.* (NA61/SHINE), JINST **9**, P06005 (2014), arXiv:1401.4699 [physics.ins-det] .

[3] K. Abe *et al.* (T2K), Nucl. Instrum. Meth. **A659**, 106 (2011).

[4] A. Aab *et al.* (Pierre Auger Collaboration), Phys.Rev.D (2014), arXiv:1408.1421 [astro-ph.HE] .

[5] S. Johnson *et al.*, CERN-SPSC-2014-032 (2014).

[6] K. Grebieszkow (NA49 Collaboration, NA61 Collaboration), Acta Phys.Polon. **B41**, 427 (2010), arXiv:0911.1902 [nucl-ex] .

[7] M. Gazdzicki and M. I. Gorenstein, Acta Phys.Polon. **B30**, 2705 (1999), arXiv:hep-ph/9803462 [hep-ph] .

[8] Z. Fodor and S. Katz, JHEP **0404**, 050 (2004), arXiv:hep-lat/0402006 [hep-lat] .

[9] M. A. Stephanov, K. Rajagopal, and E. V. Shuryak, Phys.Rev. **D60**, 114028 (1999), arXiv:hep-ph/9903292 [hep-ph] .

[10] S. Adler *et al.* (PHENIX Collaboration), Phys.Rev.Lett. **91**, 072303 (2003), arXiv:nucl-ex/0306021 [nucl-ex] .

[11] M. Szuba, Indian J.Phys. **85**, 1057 (2011), arXiv:0805.4637 [nucl-ex] .

[12] M. Szuba (NA49 Collaboration), Nucl.Phys. **A830**, 159C (2009), arXiv:0907.4403 [nucl-ex] .

[13] A. Aduszkiewicz, School on Cosmic Matter in Heavy-Ion Collision Laboratories, Ladek Zdroj (2012).

[14] ALICE, poster ALICE Time Projection Chamber (2002).

[15] H. Bethe, Annalen Phys. **5**, 325 (1930).

[16] F. Bloch, UCRL-TRANS-972 (1933).

[17] J. Hernandez *et al.* (Particle Data Group), Phys.Lett. **B239**, 1 (1990).

[18] D. Nygren and J. Marx, Phys.Today **31N10**, 46 (1978).

[19] C. Bovet, R. Maleyran, L. Piemontese, A. Placci, and M. Placidi, (1982).

[20] C. Strabel, ETH-19538, CERN-THESIS-2011-295 (2011).

[21] A. Ferrari, P. R. Sala, A. Fasso, and J. Ranft, (2005).

[22] T. Böhlen, F. Cerutti, M. Chin, A. Fassò, A. Ferrari, P. Ortega, A. Mairani, P. Sala, G. Smirnov, and V. Vlachoudis, Nuclear Data Sheets **120**, 211 (2014).

[23] S. Bass, M. Belkacem, M. Bleicher, M. Brandstetter, L. Bravina, *et al.*, Prog.Part.Nucl.Phys. **41**, 255 (1998), arXiv:nucl-th/9803035 [nucl-th] .

[24] M. Bleicher, E. Zabrodin, C. Spieles, S. Bass, C. Ernst, *et al.*, J.Phys. **G25**, 1859 (1999), arXiv:hep-ph/9909407 [hep-ph] .

[25] K. Werner, Phys.Rept. **232**, 87 (1993).

[26] K. Werner, Nucl.Phys.Proc.Suppl. **175-176**, 81 (2008).

[27] A. Mishev and P. Velinov, (2014), arXiv:1409.7522 [astro-ph.HE] .

[28] T. Pierog, R. Engel, D. Heck, S. Ostapchenko, and K. Werner, **4**, 625 (2007), arXiv:0802.1262 [astro-ph] .

[29] E.-J. Ahn, R. Engel, T. K. Gaisser, P. Lipari, and T. Stanev, Phys.Rev. **D80**, 094003 (2009), arXiv:0906.4113 [hep-ph] .

[30] M. Unger (NA61/SHINE Collaboration), EPJ Web Conf. **52**, 01009 (2013), arXiv:1305.5281 [nucl-ex] .

[31] M. Unger (NA61/SHINE Collaboration), PoS **ICHEP2010**, 449 (2010), arXiv:1012.2604 [nucl-ex] .

[32] N. Abgrall, CERN-THESIS-2011-165 .

[33] R. Brun, F. Carminati, and S. Giani, (1994).

[34] M. Gorenstein, Phys.Rev. **C84**, 024902 (2011), arXiv:1106.4473 [nucl-th] .

[35] B. Baatar *et al.* (NA49 Collaboration), Eur.Phys.J. **C73**, 2364 (2013), arXiv:1207.6520 [hep-ex] .

[36] T. Anticic *et al.* (NA49 Collaboration), Eur.Phys.J. **C68**, 1 (2010), arXiv:1004.1889 [hep-ex] .

[37] C. Alt *et al.* (NA49 Collaboration), Eur.Phys.J. **C45**, 343 (2006), arXiv:hep-ex/0510009 [hep-ex] .

[38] T. Anticic *et al.* (NA49 Collaboration), Eur.Phys.J. **C65**, 9 (2010), arXiv:0904.2708 [hep-ex] .

[39] N. Abgrall *et al.* (NA61/SHINE), Eur.Phys.J. **C74**, 2794 (2014), arXiv:1310.2417 [hep-ex] .

[40] M. Gazdzicki and D. Rohrich, Z.Phys. **C71**, 55 (1996), arXiv:hep-ex/9607004 [hep-ex] .

[41] M. Gazdzicki and O. Hansen, Nucl.Phys. **A528**, 754 (1991).

[42] J. Bachler *et al.* (NA49 Collaboration), Nucl.Phys. **A661**, 45 (1999).

[43] F. Verbeure *et al.* (LEBC-EHS), Sov.J.Nucl.Phys. **54**, 585 (1991).

[44] A. Rossi, G. Vannini, A. Bussiere, E. Albini, D. D'Alessandro, *et al.*, Nucl.Phys. **B84**, 269 (1975).

[45] A. Golokhvastov, Phys.Atom.Nucl. **64**, 1841 (2001).

[46] F. Becattini and U. W. Heinz, Z.Phys. **C76**, 269 (1997), arXiv:hep-ph/9702274 [hep-ph] .

[47] B. Back *et al.* (PHOBOS), (2003), arXiv:nucl-ex/0301017 [nucl-ex] .

[48] M. Gazdzicki and D. Roehrich, Z.Phys. **C65**, 215 (1995).

[49] A. Wilczek, *PhD. thesis in preparetion*, Ph.D. thesis, University of Silesia (2015).

[50] C. Alt *et al.* (NA49 Collaboration), Phys.Rev. **C73**, 044910 (2006).

[51] C. Alt *et al.* (NA49 Collaboration), Phys.Rev. **C77**, 024903 (2008), arXiv:0710.0118 [nucl-ex] .

[52] S. Afanasiev *et al.* (NA49 Collaboration), Phys.Rev. **C66**, 054902 (2002), arXiv:nucl-ex/0205002 [nucl-ex] .

[53] E. Schnedermann, J. Sollfrank, and U. W. Heinz, Phys.Rev. **C48**, 2462 (1993), arXiv:nucl-th/9307020 [nucl-th] .

[54] L. Landau, Izv.Akad.Nauk Ser.Fiz. **17**, 51 (1953).

[55] E. V. Shuryak, IYF-75-4 (1974).

[56] J. Klay *et al.* (E-0895), Phys.Rev. **C68**, 054905 (2003), arXiv:nucl-ex/0306033 [nucl-ex] .

[57] E. Abbas *et al.* (ALICE Collaboration), Phys.Lett. **B726**, 610 (2013), arXiv:1304.0347 [nucl-ex] .

[58] S. Adler *et al.* (PHENIX), Phys.Rev. **C69**, 034909 (2004), arXiv:nucl-ex/0307022 [nucl-ex] .

[59] M. Gazdzicki, M. Gorenstein, and P. Seyboth, Acta Phys.Polon. **B42**, 307 (2011), arXiv:1006.1765 [hep-ph] .

[60] M. Kliemant, B. Lungwitz, and M. Gazdzicki, Phys.Rev. **C69**, 044903 (2004), arXiv:hep-ex/0308002 [hep-ex] .

[61] R. Hagedorn, Nuovo Cim.Suppl. **6**, 311 (1968).

[62] W. Broniowski, W. Florkowski, and L. Y. Glozman, Phys.Rev. **D70**, 117503 (2004), arXiv:hep-ph/0407290 [hep-ph] .

[63] B. Abelev *et al.* (STAR Collaboration), Phys.Rev. **C79**, 034909 (2009), arXiv:0808.2041 [nucl-ex] .

[64] B. B. Abelev *et al.* (ALICE Collaboration), Phys.Lett. **B736**, 196 (2014), arXiv:1401.1250 [nucl-ex] .

[65] K. Aamodt *et al.* (ALICE Collaboration), Eur.Phys.J. **C71**, 1655 (2011), arXiv:1101.4110 [hep-ex] .

[66] T. Pierog and K. Werner, Nucl.Phys.Proc.Suppl. **196**, 102 (2009), arXiv:0905.1198 [hep-ph] .

[67] I. Arsene *et al.* (BRAHMS Collaboration), Phys.Rev. **C72**, 014908 (2005), arXiv:nucl-ex/0503010 [nucl-ex] .

[68] B. Abelev *et al.* (ALICE Collaboration), Phys.Rev.Lett. **109**, 252301 (2012), arXiv:1208.1974 [hep-ex] .

[69] V. Y. Vovchenko, D. Anchishkin, and M. Gorenstein, Phys.Rev. **C90**, 024916 (2014), arXiv:1407.0629 [nucl-th] .

[70] T. Sjostrand, S. Ask, J. R. Christiansen, R. Corke, N. Desai, *et al.*, Comput.Phys.Commun. **191**, 159 (2015), arXiv:1410.3012 [hep-ph] .

[71] W. Ehehalt and W. Cassing, Nucl.Phys. **A602**, 449 (1996).

[72] R. Poberezhnyuk, M. Gazdzicki, and M. Gorenstein, (2015), arXiv:1502.05650 [nucl-th] .

[73] A. Rybicki, J.Phys. **G30**, S743 (2004).